



Cite this: *J. Mater. Chem. A*, 2024, **12**, 27932

## Advanced metal–organic frameworks for superior carbon capture, high-performance energy storage and environmental photocatalysis – a critical review<sup>†</sup>

Farooq Sher, <sup>\*a</sup> Anna Hayward, <sup>b</sup> Abdelqader El Guerraf, <sup>cd</sup> Bohong Wang, <sup>e</sup> Imane Ziani, <sup>df</sup> Harun Hrnjić, <sup>dg</sup> Emina Boškailo, <sup>dg</sup> Alexander Chupin <sup>h</sup> and Monica R. Nemtanu<sup>i</sup>

Metal–organic frameworks (MOFs) have emerged as a transformative class of materials, offering unprecedented versatility in applications ranging from energy storage to environmental remediation and photocatalysis. This groundbreaking review navigates the recent advancements in MOFs, positioning them against traditional materials to underscore their unique strength and potential drawbacks. In the context of energy storage, particularly within the realm of supercapacitors (SCs), MOF-based electrodes are evaluated for their superior specific capacitance (exceeding 1000 F/g), although these benefits are tempered by higher production cost. A comparative analysis with conventional activated carbon (AC) electrodes reveals MOFs' enhanced performance but also highlights cost as a significant barrier to widespread adoption. In carbon capture and storage (CCS), MOFs are contrasted with established liquid-amine technologies, with MOFs demonstrating environmental benefits, including the ability to achieve high-purity CO<sub>2</sub> collection (>99%), despite higher expenses. Similarly, in photocatalysis, while titanium dioxide remains dominant, MOFs are shown to offer competitive performance with a reduced environmental footprint, though cost considerations again play a decisive role. This review not only consolidates the current state of MOF research but also identifies critical gaps, particularly in cost-effectiveness, that must be addressed to enable broader application. The findings advocate for continued innovation in MOF synthesis and production, with an emphasis on achieving a balance between performance and affordability. In summary, this review highlights the pivotal role of MOFs in advancing materials science and underscores the need for holistic approaches in material selection, with a forward-looking perspective on sustainable and economical production methods.

Received 4th June 2024  
Accepted 11th September 2024

DOI: 10.1039/d4ta03877k  
[rsc.li/materials-a](http://rsc.li/materials-a)

## 1 Introduction

The dawn of the 21st century marked the emergence of metal–organic frameworks (MOFs), porous structures consisting of metal ions and organic linkers. Prior to MOFs, zeolites (aluminium silicate crystals) were the world's most porous

materials.<sup>1</sup> However, MOFs have overcome zeolites' surface area by more than 100% in some cases. In addition to that, the structure of the cavities and the size of the pore in MOFs can be tailored as a function of metal ions, organic ligands, and synthesis conditions, and hence are thus amenable to engineering for targeted applications,<sup>2</sup> which catalyses exponential growth in research on their applications.<sup>3</sup> Due to their unique

<sup>a</sup>Department of Engineering, School of Science and Technology, Nottingham Trent University, Nottingham NG11 8NS, UK. E-mail: Farooq.Sher@ntu.ac.uk; Tel: +44 (0)115 84 86679

<sup>b</sup>School of Mechanical, Aerospace and Automotive Engineering, Coventry University, Coventry CV1 5FB, UK

<sup>c</sup>Laboratory of Applied Chemistry and Environment, Faculty of Sciences and Technologies, Hassan First University, Settat 26002, Morocco

<sup>d</sup>International Society of Engineering Science and Technology, Nottingham, UK

<sup>e</sup>National and Local Joint Engineering Research Center of Harbor Oil and Gas Storage and Transportation Technology, Zhejiang Key Laboratory of Petrochemical Environmental Pollution Control, Zhejiang Ocean University, No. 1 Haida South Road, 316022, Zhoushan, P.R. China

<sup>f</sup>Department of Chemistry, Laboratory of Applied Chemistry and Environment, Faculty of Sciences, Mohammed First University, Oujda 60000, Morocco

<sup>g</sup>Department of Chemistry, Faculty of Science, University of Sarajevo, Sarajevo 71000, Bosnia and Herzegovina

<sup>h</sup>Peoples' Friendship University of Russia (RUDN University), Moscow 117198, Russia

<sup>i</sup>Electron Accelerators Laboratory, National Institute for Laser, Plasma and Radiation Physics, 409 Atomistilor Street, Bucharest-Măgurele, Romania

<sup>†</sup> Electronic supplementary information (ESI) available. See DOI: <https://doi.org/10.1039/d4ta03877k>

architecture and chemical or physicochemical properties, MOFs remain in a class apart, with a wide reach of applications. Metal-containing nodes (SBUs) and organic linkers are used to create very porous structures, which typically have surface areas greater than  $7000\text{ m}^2/\text{g}$ .<sup>4</sup> Control over topology, dimensionality, and stability can be achieved by selecting the right metal centers and organic ligands. For example, functional groups high in nitrogen can enhance  $\text{CO}_2$  absorption; certain MOFs can attain up to  $40\text{ cc/g}$ .<sup>5</sup>

On the other hand, sensitivity to humidity and thermal instability create practical problems, as illustrated by ZIF-8, which swells at low pressure but phase transitions at higher pressures.<sup>6</sup> Synthesis conditions and metal-organic coordination bonds are key to the chemical stability and reactivity of MOFs; high-throughput computational screenings have identified MOFs with high gas adsorption capacities, such as methane storage up to  $200\text{ cm}^3\text{ cm}^{-3}$ .<sup>4</sup> However, theoretical predictions do not often match real-world performance, suggesting that somehow models and real applications are detached from one another. It typically focuses on crystallinity and leaves out the other forms, such as amorphous or semi-crystalline forms, which might also hold special properties.<sup>7</sup> All this proves that there is a need to develop better characterization techniques and insight into structure-function interplay to further advance the application of MOFs in carbon capture, energy storage, and environmental remediation. The historical development of MOFs shows the huge progress made in materials science from exclusively inorganic or organic structures to hybrid systems possessing new properties.<sup>8</sup> The necessity of a material that shows high porosity but custom architecture of the material developed during the late twentieth century marked the starting point for the development of MOFs.<sup>9</sup> Early studies, and mostly those related to Prussian blue analogues, were the basis for the fast-growing interest in MOF research in the late 1980s.<sup>10</sup> The “node-and-spacer” approach, proposed by Richard Robson, enabled design of frameworks with well-defined coordination geometries and complex structures. MOFs, like HKUST-1 and MOF-5, developed in the late 1990s and early 2000s, represent advances in synthesizing large surface area materials that have high porosity and good crystallinity.<sup>11</sup>

In response to escalating energy demands and intensifying environmental challenges, the development of advanced materials has become increasingly critical.<sup>12</sup> MOFs have emerged as a highly versatile class of materials, offering exceptional properties that hold the potential to revolutionize energy storage, environmental remediation, and photocatalysis.<sup>13</sup> As the global population continues to grow and conventional energy sources dwindle, innovative approaches to sustainable energy generation and environmental restoration are urgently needed. MOFs present a promising solution due to their structural flexibility, large surface area, and tunable properties. Energy storage, environmental remediation, and photocatalysis are key areas where advanced materials have the potential to drive transformative change. Traditional materials, such as metals, semiconductors, and polymers have historically played significant roles in these applications. However, these materials often face challenges in efficiency, stability, and

versatility. MOFs, with their exceptional characteristics, offer a promising alternative that could overcome these limitations. While MOFs are very promising, there are several serious technological problems to be overcome. Their structural stability is the first and foremost problem. Such interactions of the proton and metal ion can result in degradation, and therefore most MOFs cannot be used for an extended period of time in these environments.<sup>14</sup> Improvement of stability includes high-valent metal ions and proper organic linkers, which generally decrease the diversity of possible MOFs. On the other hand, most MOFs require comparatively high temperature and pressure for synthesis and, therefore, are energy-consuming and expensive. In this regard, the search for alternative synthesis techniques, including the solvothermal and microwave methods, or recently mechanochemical methods, assumes the leading role among researchers to decrease the price of synthesis and increase scalability.<sup>15</sup>

Moreover, their generally low electrical conductivity limits the broad use of MOFs in electrochemical applications. Strategies to enhance conductivity include embedding conductive material carbon-based compounds or using highly conjugated organic linkers; however, these add complexity and are more expensive to synthesize. For example, MOF derivatives, such as TMCs, have been designed to enhance conductivity and improve structural stability.<sup>16</sup> One such example of improvement is the hybrid ZnS/MXene, which was reported to demonstrate improved electron transfer and ion adsorption capabilities due to uniform anchoring of ZnS nanodots onto the MXene nanosheets. The incorporation of a few metals into one MOF structure has also shown some bright prospects in enhancing electrochemical performance but adds more complications in terms of synthesis and scalability. For instance, sequential chemical etching and sulfurization in the preparation of Zn-Co-S rhombic dodecahedral cages showed enhanced specific capacitance because they have a double-shelled structure.<sup>17</sup> Environmental degradation stands as one of the foremost challenges of the 21st century. Increased awareness of global warming, coupled with concerted efforts by governments and societies, is driving research into environmental pollution mitigation. The United Nations has specified a series of sustainable development goals, showcasing this assertion.<sup>18</sup> Recent research suggests that MOFs demonstrate tremendous potential in capturing and detoxifying environmental toxins across various media, such as water, air, and soil.<sup>19</sup> The increasing concentration of atmospheric  $\text{CO}_2$ , primarily driven by the combustion of fossil fuels since the industrial revolution, has been a major contributor to anthropogenic global warming.<sup>18</sup> The atmospheric concentration of  $\text{CO}_2$  has increased from 280 ppm in 1962 to 400 ppm in 2015,<sup>20</sup> a concerning trend due to its links to global warming and associated environmental degradation, as well as potential adverse health effects.<sup>19</sup> MOFs have shown significant potential in this regard, particularly in carbon capture and storage (CCS) technologies. Their ability to selectively adsorb  $\text{CO}_2$  from the atmosphere makes them a viable candidate for reducing greenhouse gas emissions.<sup>21</sup>



In the realm of energy storage, MOFs are being explored for their application in both supercapacitors (SCs) and metal-ion batteries. MOFs can serve two main roles in these energy storage devices: primarily, they can function as direct electrode materials with modifiable particle and pore dimensions. Secondly, they can serve as templates and precursors for producing porous carbons and metal oxides. The resulting porous carbons and metal oxides maintain the extensive surface area and highly porous structure of the MOF precursors, making them ideal for implementation in electrical double-layer supercapacitors (EDLCs) and pseudocapacitors.<sup>22</sup> Moreover, MOFs have garnered attention in photocatalysis owing to their distinctive properties. Photocatalysis entails harnessing light energy to propel chemical reactions,<sup>23</sup> and MOFs' extensive surface area and porosity provide numerous active sites for catalytic reactions. Researchers have incorporated various photocatalytic components, such as metal nanoparticles or organic dyes, into MOF structures to enhance their photocatalytic performance. MOFs can serve as photocatalysts themselves or as platforms to support other catalytic materials. The tunable nature of MOFs allows researchers to modify their electronic and optical properties, influencing their efficiency in light absorption and charge separation critical factors in photocatalytic processes.

In this comprehensive and groundbreaking review, the report embarks on a pioneering journey to assess the comparative advantages of MOFs over conventional materials. Delving into the realm of energy storage, it investigates how MOFs can potentially revolutionize energy storage technologies, including

supercapacitors and metal-ion batteries, due to their exceptionally high surface area, tunable electronic properties, and facile ion diffusion pathways. This new approach to energy storage could enable previously unattainable levels of efficiency and performance to be achieved. In the context of environmental challenges, the exploration focuses on a remarkable novelty, namely the way MOFs display an unprecedented affinity for carbon dioxide capture. This discovery offers a compelling and revolutionary alternative to conventional adsorbents, with the potential to significantly mitigate greenhouse gas emissions. Furthermore, in the domain of photocatalysis, MOFs have showcased a transformative capacity to harness solar energy for driving chemical reactions with unmatched efficiency, representing a major leap forward in sustainable energy conversion technologies.

This review tackles these issues by providing an in-depth analysis of case studies, experimental results, and theoretical insights to illuminate the merits and limitations of MOFs compared to conventional materials across three key applications: energy storage, carbon capture, and photocatalysis. Tables summarizing the advantages and disadvantages of both conventional and MOF materials are presented for each application, with a focus on performance, environmental impact, and cost-effectiveness. Each broad factor receives a relative percentage weighting based on importance, with the most critical factor assigned the highest percentage. Sub-factors within each category are also identified based on the literature, assigning them scores out of 3 (3 correlating to high importance). After determining the weightings, both materials

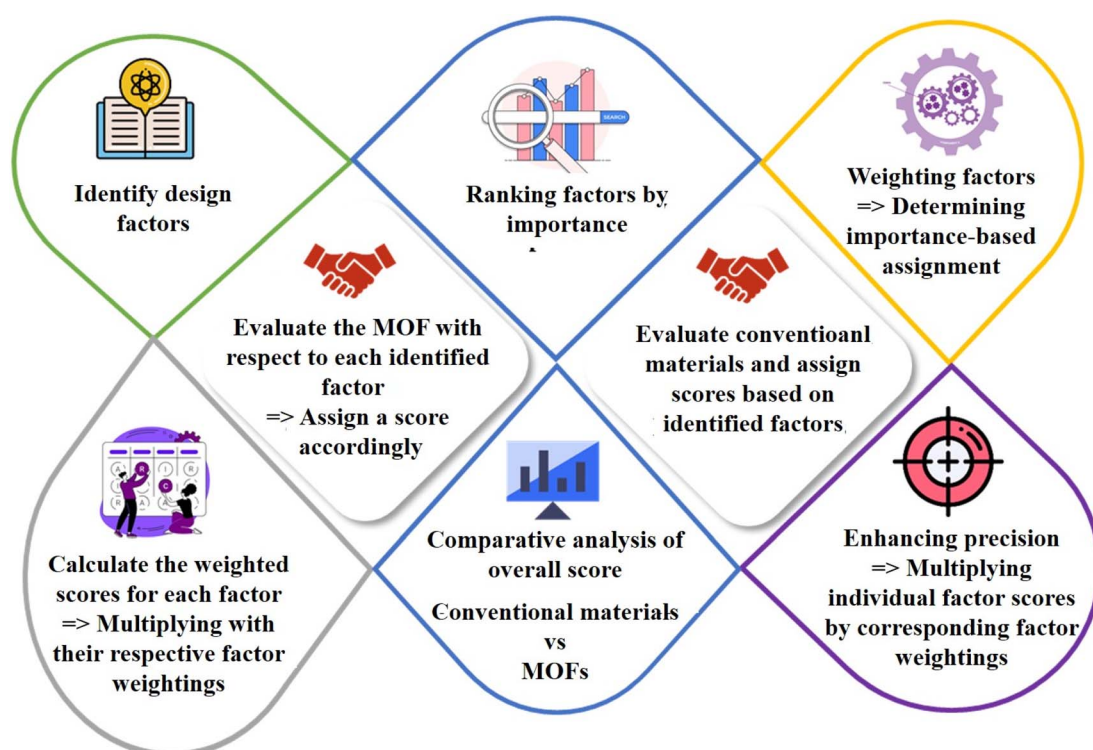


Fig. 1 Diagram explaining the adopted methodology for the present literature review. A systematic comparison matrix is employed to assess the relative benefits of MOFs, offering clear, actionable insights into their potential as a transformative material in critical fields.



are evaluated using a comparison matrix for each factor, using a scale of 1 to 5 (1 very bad, 2 bad, 3 suitable, 4 good, and 5 very good). The resulting scores allow a comparison of MOFs and conventional materials for each of the three applications, helping identify which material offers the most benefits based on the identified factors. Such a systematic approach will ensure that all aspects are covered and that clear, actionable insights into practical benefits of MOFs in addressing technological challenges in energy storage, carbon capture, and photocatalysis are delivered. Fig. 1 summarizes the methodology followed throughout this groundbreaking literature review.

## 2 Porous MOFs and conventional materials for carbon capture

The argument presented by Mukherjee *et al.*<sup>18</sup> emphasizes humanity's reliance on gas as a critical component of energy and industrial processes. They contend that liquid fuels and feedstocks in the chemical industry have been largely replaced by gases. However, this viewpoint is challenged by the research conducted by Furukawa *et al.*<sup>24</sup> which shows a steady increase in all fossil fuels, both sources agree on the general trend of increasing CO<sub>2</sub> levels and their contribution to global warming and consequential environmental degradation. A sorbent's CO<sub>2</sub> selectivity is determined by comparing how much CO<sub>2</sub> it can absorb to another gas while meeting certain predetermined parameters.<sup>18</sup> In the examination of a sorbent employed for post-combustion carbon capture, selectivity *versus* nitrogen (SCN) holds significant relevance. Selectivity is crucial as it impacts both the purity of the captured CO<sub>2</sub> and the concentration of CO<sub>2</sub> in the effluent gas discharged into the atmosphere. Mukherjee and colleagues<sup>18</sup> also suggest that increasing the SCN of a sorbent by five-fold could significantly reduce the cost of C-capture. Other important factors that influence sorbent selection for C-capture include stability, working capacity, regenerability and feasibility of scale-up.

### 2.1 Conventional liquid alkanolamine in carbon capture

For over half a century, liquid amine technology has remained at the forefront of carbon capture and storage (CCS) technologies.<sup>18</sup> This method of bulk-scale carbon capture operates through chemisorption, involving chemical reactions between CO<sub>2</sub> and the sorbent material. Originating in the 1930s, these processes were initially developed, and since the 1950s, they have been employed by gas-treating plants for the removal of acid gases like CO<sub>2</sub> and H<sub>2</sub>S.<sup>19,25</sup> Consequently, liquid amine processes are frequently recognized as the most mature CCS method and boast a high Technology Readiness Level (TRL) of 9.<sup>25,26</sup> In two commercial-scale facilities housed within coal-fired power plants, post-combustion liquid amine CCS technology had been successfully installed as of 2018.<sup>26</sup> The post-combustion liquid-amine CCS process (Fig. 2a) involves exposing the flue gas stream to an aqueous amine solution, commonly a member of the alkanolamine class, typically a 20–30 wt% aqueous monoethanolamine (MEA).<sup>29</sup> Subsequently, the amine undergoes a reaction with CO<sub>2</sub> in the flue gases, resulting

in the formation of carbamates or bicarbonate products, which can then be separated and removed. The utilization of liquid amines is based on their capacity to achieve significant levels of purification and separation through the chemisorption process.<sup>18</sup>

Monoethanolamine (MEA) offers several advantages, such as a substantial CO<sub>2</sub>-carrying capacity, biodegradability, and rapid adsorption rates.<sup>26,29</sup> Additionally, it is well-suited for carbon capture applications with low CO<sub>2</sub> partial pressures. Because of this, MEA has become the industry standard for carbon capture amines despite having modest degrees of toxicity and oxidative and thermal degradation.<sup>26</sup> In the context of standard post-combustion flue gas CO<sub>2</sub> separation, employing a 30 wt% MEA solution at pressures ranging from 10 to 15 kPa, a temperature of 40 °C, and targeting a 90% CO<sub>2</sub> removal rate, it is typically estimated that a reboiler would necessitate approximately 3.6–4.0 GJ per tonne of captured CO<sub>2</sub>.<sup>26</sup> This value has been verified by a number of small- and medium-sized pilot studies.<sup>30</sup> While it's important to acknowledge that reducing reboiler energy is just one of several performance considerations, it is often regarded as a primary focus in the realm of chemical sorbent research. Liquid amines offer a notable advantage for CCS due to their often-high selectivity. Liquid amine CCS technology does have several disadvantages, though. Chemisorbents form strong covalent connections, in contrast to physisorbents, which work through van der Waals interactions.<sup>18</sup> Consequently, the regeneration of sorbents in the case of chemisorbents demands more energy, resulting in a larger energy footprint. Furthermore, in situations with low CO<sub>2</sub> concentrations, the kinetics of the chemisorption process are likely to be sluggish, which is less than ideal for CCS.

In a study conducted by Li *et al.*,<sup>28</sup> a novel approach to advance CO<sub>2</sub> capture technology aims to reduce energy penalties and mitigate equipment corrosion simultaneously (Fig. 2b). A new biphasic solvent system was developed for carbon dioxide (CO<sub>2</sub>) capture, comprising monoethanolamine (MEA), 2-amino-2-methyl-1-propanol (AMP), dimethyl sulfoxide (DMSO), and *N,N,N',N'',N'''*-pentamethyldiethylenetriamine (PMDETA). Performance evaluation revealed that the optimized solvent achieved a high CO<sub>2</sub> loading of 0.88 mol/mol, with 95.3% of absorbed CO<sub>2</sub> stored in the rich phase, occupying only 56.8% of the total volume. Both MEA and AMP could absorb CO<sub>2</sub> to generate mostly carbamic acid species, according to <sup>13</sup>C nuclear magnetic resonance (NMR) studies and quantum chemical calculations. Sufficient mutual solubility was guaranteed by hydrogen bonding with the polar DMSO. Only the CO<sub>2</sub>-rich phase needed to regenerate since the less polar PMDETA remained isolated and caused phase separation. The M-A-D-P biphasic solvent dramatically reduced sensible heat and vaporisation heat by 63.1% and 94.8%, respectively, when compared to the MEA benchmark. Corrosion tests demonstrated that M-A-D-P exhibited virtually no corrosion to carbon steel, outperforming the MEA solution. Although liquid-amine technologies have proven effective as "wet scrubbers", their industrial-scale deployment has been hindered by several drawbacks. Grande *et al.*,<sup>31</sup> in their report, emphasize the need to advance CCS technology beyond liquid amine approaches to



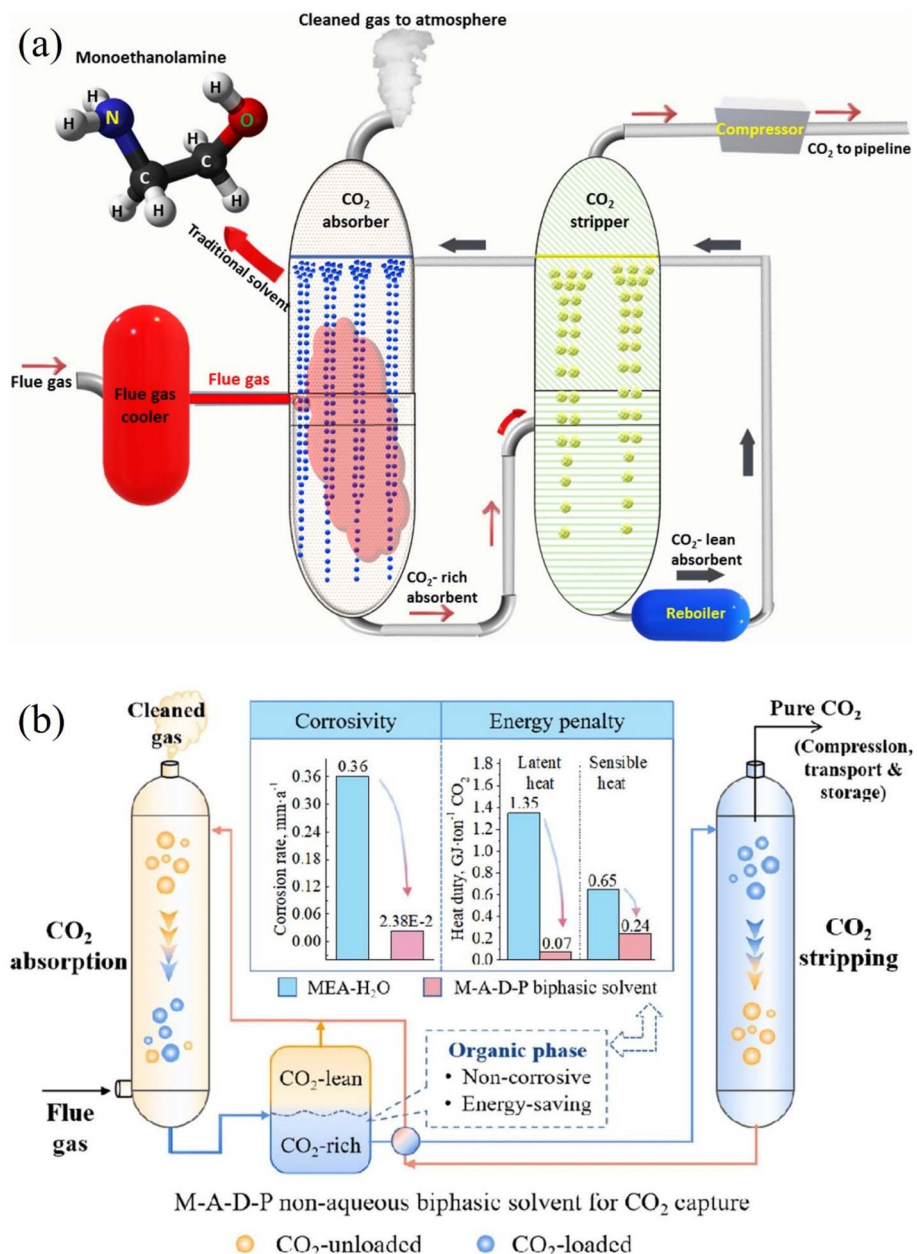


Fig. 2 (a) Post-combustion technology involves cooling hot flue gas before directing it to an absorber unit that typically contains a monoethanolamine solvent as the traditional sorbent. The CO<sub>2</sub>-rich absorbent is then sent to a stripper unit to release the CO<sub>2</sub> gas, while the CO<sub>2</sub>-lean absorbent is recycled back to the absorber unit. Finally, the pure CO<sub>2</sub> is compressed and dehydrated for transport via pipelines and for storage purposes. Adopted from ref. 27 with permission. (b) A schematic illustration of a reactor containing a nonaqueous monoethanolamine-based biphasic solvent for reduced energy penalty and corrosion of carbon dioxide capture. Adopted from ref. 28 with permission.

ensure sustainability, primarily due to the substantial regeneration energy requirements associated with liquid amine-based wet scrubbers, which can exceed 140 °C. The increased energy requirements result from the high stability of the carbamate/bicarbonate species generated during the amine-CO<sub>2</sub> reaction.<sup>32</sup> It is worth noting that the energy required to reverse an amine-CO<sub>2</sub> reaction varies depending on the specific amine used. Ghosh *et al.*<sup>19</sup> elucidate that this discrepancy is a consequence of bicarbonates demanding less energy compared to carbamates when regenerating the constituent amine.

Various additional drawbacks associated with liquid-amine technologies have also been highlighted.<sup>31</sup> Equipment requirements pose limitations as it is prone to corrosion over time, and retrofitting can prove challenging due to its substantial size. This perspective is substantiated by Vega *et al.*,<sup>25</sup> who propose a potential solution to mitigate equipment corrosion through the use of corrosion-resistant materials and inhibitors, albeit at an added cost. Vericella *et al.*<sup>27</sup> suggest an alternative approach by proposing the microencapsulation of the amine. This approach seeks to avoid direct contact between the amine and



the equipment, as well as effluent gases, potentially mitigating equipment corrosion and decreasing evaporative losses. Moreover, it has been reported by several sources that liquid amines are susceptible to deterioration and breakdown when they come into contact with dust, HCl, HF,  $\text{SO}_x$ ,  $\text{NO}_x$ , and oxygen, among other contaminants.<sup>25</sup> Concerns have been expressed regarding the elevated volatility and limited stability of liquid amines. As per the findings of Williams and their research team,<sup>33</sup> conducting multiple capture–release cycles leads to notable losses of amine sorbent, subsequently causing a decrease in efficiency and performance. The collective impact of these factors can also negatively affect the overall efficiency of a power plant utilizing post-combustion liquid amine carbon capture and storage technology. A recent report attributed a 30–40% reduction in the overall efficiency of power plants to the difficulties associated with implementing CCS technology.<sup>19</sup>

Furthermore, an associated cost was estimated to range from €70 to €100 per ton for this reduction in efficiency. Concerns have also been raised regarding the industrial scalability of liquid-amine technology, with certain publications questioning its suitability for large-scale implementation. Vega *et al.*<sup>25</sup> contend that, until the  $\text{CO}_2$  capacity can be expanded from its present 800 tons per day to the necessary 8000 tons per day, the technology may not be suitable for large-scale  $\text{CO}_2$  emission mitigation on an industrial level. Additionally, one of the most significant challenges associated with liquid-amine processes is their restricted scope for performance enhancement.<sup>18</sup> Much of the existing literature underscores the significance of creating novel technologies with enhanced capabilities to supplant current liquid-amine processes. Conversely, the Energy Technologies Institute (ETI) argues that liquid-amine technologies still offer opportunities for future advancements.<sup>34</sup> They cite the development progress of bi-phasic systems as evidence of this potential.

Moreover, the environmental impact of amines has raised significant concerns. Williams *et al.*<sup>33</sup> argue that, owing to their highly toxic nature, amines are unsuitable for direct air capture (DAC) applications and could potentially pose an environmental threat if employed in such contexts. Vericella *et al.*<sup>29</sup> corroborate this viewpoint, noting that the commonly used amine for CCS, monoethanolamine (MEA), generates toxic degradation byproducts. Furthermore, there are apprehensions that the decrease in power plant efficiency resulting from the presence of liquid-amine post-combustion technologies may partially offset the technology's advantages.<sup>18</sup> Another foremost issue with liquid-amine CCS is the high cost, with some sources claiming the capture of 1 ton of  $\text{CO}_2$  costs around 50–100 USD (as a conservative estimate).<sup>18</sup> In contrast, an earlier report from 2015 provided an estimate of the maximum cost of post-combustion amine CCS as \$110/t $\text{CO}_2$ .<sup>35</sup> As a result, numerous sources contend that the technology is not yet commercially feasible for widespread use. Another problem is the extra expense associated with the post-combustion C-capture system because it needs electricity to operate. Liquid-amine CCS (L-A CCS) technology typically causes a large rise in capital costs along with a decrease in power plant efficiency.<sup>34</sup>

There are indications that beyond 2030, continuous technological advancements may lead to cost reductions in liquid-amine technology, ultimately enhancing its viability for large-scale implementation. Developers in the US, Canada, and the UK have committed to sharing publicly all knowledge, data, and designs related to CCS technology, which should foster innovation. According to the ETI, larger projects will enable the exploitation of economies of scale, which will lead to additional cost reductions.<sup>34</sup> One recommended approach is the sequential deployment of existing C-capture technologies in 3 or more full-scale power plants. The ETI suggests that sequential deployments will result in a reduction in risk.<sup>34</sup> Reduced finance costs, larger scale, and infrastructure sharing all work together to potentially cut the cost of output energy by about 45%. Because it might result in more affordable financing solutions, risk minimisation reduces financing costs.

## 2.2 Metal-organic frameworks in carbon capture

**2.2.1 Performance and challenges.** Solid sorbents such as MOFs are exciting candidates for low-temperature C-capture.<sup>32</sup> Their intrinsic properties such as their high porosity and their customizable chemistry provide the potential to tune MOFs for improved  $\text{CO}_2$  uptake capacity and selectivity.<sup>26</sup> Despite their benefits, MOF sorbents face several hurdles. It is generally agreed that the thermal conductivity of sorbents affects the C-capture operation and regeneration process' cost and cycle time.<sup>36</sup> MOFs, however, tend to have poor thermal conductivities (at  $T = 25$  °C, the thermal conductivity of MOF-5 single crystal stands at a mere 0.32 W/m K).<sup>37</sup> The enhancement of MOFs' thermal conductivity is presently the subject of relatively few studies, thus perhaps more research in this field is warranted. Opt-Uio-66(Zr)–(OH)<sub>2</sub> (2.50 mmol/g) is one of the best-performing pristine MOFs.<sup>38</sup> This MOF is both water-stable and shows a  $\text{CO}_2$  uptake higher than that of MEA.<sup>38</sup> Based on their functional characteristics, modified metal oxide fragments (MOFs) for C-capture can be broadly categorised into three groups: MOFs with amine-functionalized sites (AFSs), unsaturated metal centres (UMCs), and saturated metal centres (SMCs).<sup>18</sup> Reports suggest that, while able to provide a significantly improved working capacity, the UMC-rich MOFs with the highest capacities suffer from modest selectivity *versus* nitrogen (SCN).<sup>18</sup> UMCs can be generated by removing the solvent molecules responsible for the partially coordinated metal atoms in some MOFs. This can be done through heating the material or vacuuming. These UMCs exhibit excellent  $\text{CO}_2$  affinity, and can therefore be used to enhance the capture capacity of a MOF at low pressures.<sup>39</sup>

A new bimetallic MOF, functionalized with pyrazine and used in combination with polysulfone (PSf), was employed to create a mixed matrix membrane (Fig. 3A).<sup>40</sup> This innovative membrane demonstrated adaptable interfaces facilitated by the incorporation of the interfacial plasticizer, polyethylene glycol (PEG). The inclusion of the MOF filler notably boosted the  $\text{CO}_2$  capture capacity of both pristine PSf membranes and PSf/PEG blend membranes. Specifically, with the PSf/PEG/Pyrazine-MOF membrane, the  $\text{CO}_2$  permeability rose dramatically from

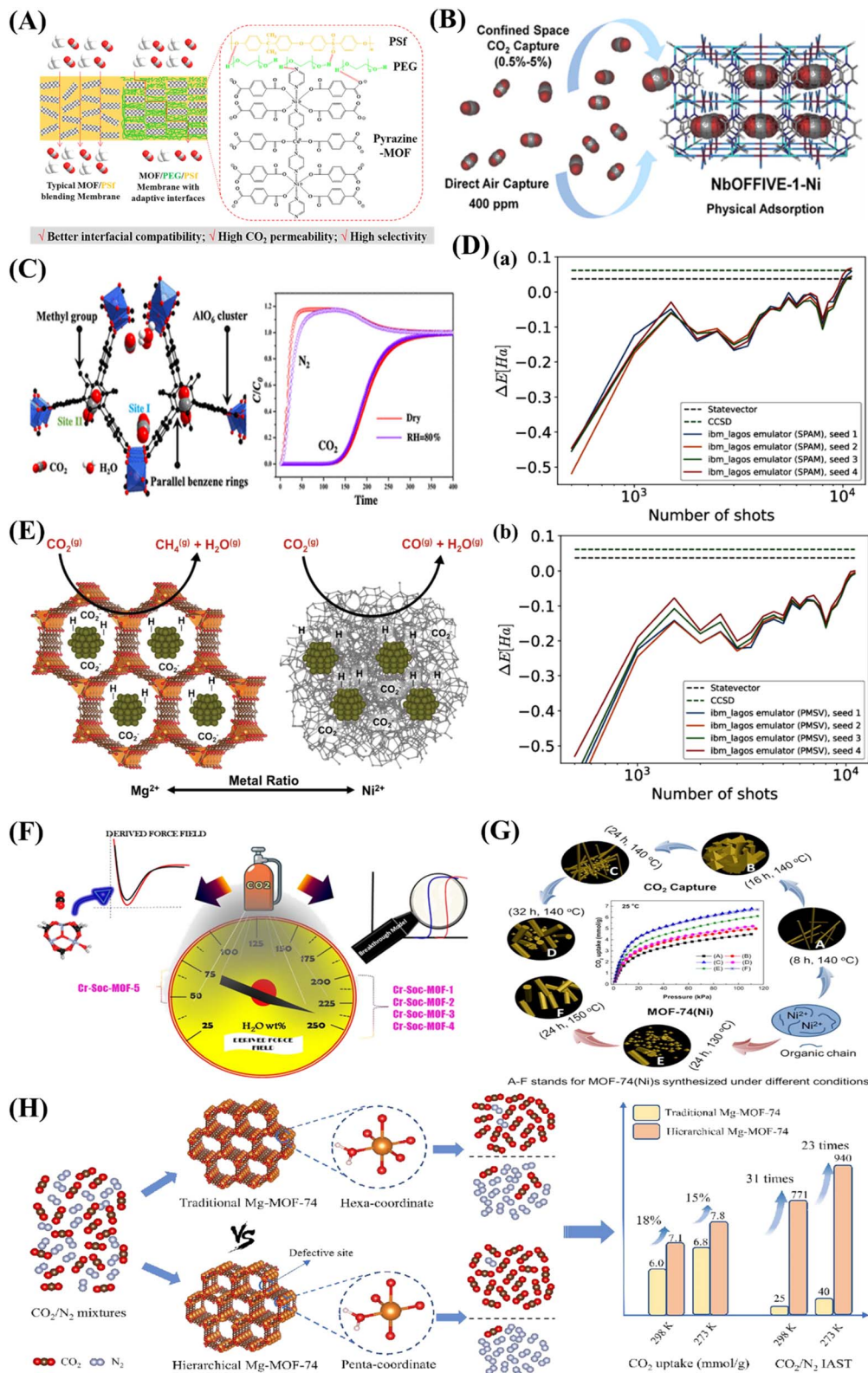


**Fig. 3** (A) An illustration of the interactions and interfacial structure of the PEG/PSf mixed matrix membrane with pyrazine-MOF incorporation for the separation of  $\text{CO}_2$  from  $\text{CH}_4$ . Adopted from ref. 40 with permission. (B) Fluorinated MOF, NbOFFIVE-1-Ni, for trace  $\text{CO}_2$  removal and air capture. Adopted from ref. 41 with permission. (C) Methyl-functionalized Al-based MOF ZJU-620(Al) for  $\text{CO}_2$  capture. The two main types of sites where  $\text{CO}_2$  molecules are adsorbed are site I, which is close to the  $\text{AlO}_6$  clusters, and site II, which is between two parallel benzene rings. Adopted from ref. 42 with permission. (D) Calculation of bond dissociation energy using noisy emulated hardware data for 2 noise rates. Demonstrating two error mitigation approaches: (a) state preparation and measurement (SPAM) error mitigation, and (b) post-measurement symmetry verification (PMSV). Both approaches use the same set of 4 randomization seed results in order of the number of measurement shots.



6.82 Barrer for the pure PSf membrane to 17.13 Barrer.<sup>40</sup> Bhatt *et al.*<sup>41</sup> detailed the development of a hydrolytically stable fluorinated metal-organic framework (MOF) referred to as NbOFFIVE-1-Ni. Remarkably, the synthesized MOF exhibits significant CO<sub>2</sub> adsorption capacities, measuring approximately 1.3 mmol/g gravimetrically and 51.4 cm<sup>3</sup> (STP) cm<sup>-3</sup> volumetrically when exposed to 400 ppm of CO<sub>2</sub> at 298 K (Fig. 3B). Furthermore, a methyl-functionalized aluminium-based MOF (ZJU-620(Al)) with remarkable chemical-thermal stability and a high specific surface area of 1347 m<sup>2</sup>/g has been recently developed.<sup>42</sup> This MOF has emerged as a highly promising candidate for CO<sub>2</sub> capture due to its exceptional recyclability and impressive capacity, reaching up to 4.25 mmol/g at 298 K and 1 atm. CO<sub>2</sub> molecules are primarily captured within two distinct sites. The first site (I) is situated in close proximity to the AlO<sub>6</sub> clusters, while the second site (II) is positioned between two parallel benzene rings, separated by a distance of 6.64 Å (Fig. 3C). While MOF technology has held great promise to date, the performance data from Fig. 3D raise some deeply troubling questions about realistic applicability.<sup>43</sup> Specifically, it constructs bond dissociation energy from the noise-prone measurements of emulated hardware under two error mitigation schemes: state preparation and measurement (SPAM) error mitigation and post-measurement symmetry verification (PMSV). A variational outcome of up to  $\pm 1$  mHa based on noise alone illustrates the practical challenges in reliably predicting MOF performance under more realistic conditions.<sup>43</sup>

Mg-MOF-74 is often used as a benchmark for other physisorbents, as it has an excellent CO<sub>2</sub> adsorption capacity under dry conditions at low pressures (5.5 mmol/g at 0.15 bar, 313 K (ref. 18 and 48) and up to 8 mmol/g at 1 bar and 298 K (ref. 39)). The high density of UMCs is largely responsible for the remarkable CO<sub>2</sub> uptake values. It is created by reacting 2,5-dihydroxyterephthalic acid with magnesium metal salts, which produces a large amount of UMCs within the MOF framework. Bahamon and associates compare a number of MOFs to zeolites in their report.<sup>49</sup> Because Mg-MOF-74 performs well in TSA operating settings, they present it as having good potential for TSA separation. According to their findings, Mg-MOF-74 outperformed zeolite 13X, a zeolite that is frequently utilised.<sup>49</sup> In the same context, a mixed-metal metal-organic framework (MOF) referred to as NiMg-MOF-74 was utilized as a template to achieve the even distribution of small nickel nanoclusters within the native MOF framework.<sup>44</sup> Through the adjustment of the Ni-to-Mg ratio within the initial MOF, it is possible to modulate both the available surface area and crystallinity after thermal treatment (Fig. 3E). This, in turn, has an impact on the capacity for CO<sub>2</sub> adsorption and the selectivity of hydrogenation.

On the other hand, critics have often pointed out the poor performance of MOFs in gas separation, particularly under humid conditions. Palakkal *et al.*<sup>45</sup> examined coordinatively unsaturated MOF (CUS-MOF) with square octahedral (Soc) topology. The research encompassed examinations of both co-adsorption (CO<sub>2</sub>/N<sub>2</sub>) and single-component (CO<sub>2</sub>, N<sub>2</sub>) adsorption with moisture at 298 K and pressures between 0 and 10 bar. The authors focused on five different Cr-Soc-MOFs, which exhibited experimentally established iso-structural topologies but differed in polynuclear aromatic ring size and *N*-heteroatom content within their pore walls (Fig. 3F). Remarkably, Cr-Soc-MOFs with larger pore volumes exhibited CO<sub>2</sub> uptake ranging from 23 to 35% by weight, with selectivity levels ranging from 20 to 50%, even up to 70% relative humidity (RH).<sup>45</sup> A Ni-based metal-organic framework, MOF-74(Ni), was synthesized using a straightforward condensation reflux method.<sup>46</sup> By adjusting the synthesis duration at different temperatures, both the structure and CO<sub>2</sub> adsorption isosteric heat of MOF-74(Ni) could be customized (Fig. 3G). After being produced at 140 °C for 24 hours, the optimised MOF-74(Ni)-24-140 demonstrated remarkable CO<sub>2</sub> adsorption capacity, attaining 8.29/6.61 mmol/g at 273/298 K with a pressure of 1 bar. This capacity surpassed that of previously reported MOF-74-Ni, UTSA-16, and DA-CMP-1 under similar conditions by factors of 2.0/2.1, 1.5/1.6, and 3.6/4.9, respectively. An *et al.*<sup>47</sup> reported the synthesis of a defect-rich hierarchical porous Mg-MOF-74 (Fig. 3H). The defect-rich hierarchical porous Mg-MOF-74 exhibits an increased adsorption enthalpy of CO<sub>2</sub> at zero load, rising from 36 to 46 kJ/mol compared to conventional Mg-MOF-74. Moreover, the saturated CO<sub>2</sub> adsorption capacity under ambient pressure has seen a significant improvement of 15%.

Despite the high performance of Mg-MOF-74, its application is hindered by several factors including its relatively poor CO<sub>2</sub> selectivity over other gases such as O<sub>2</sub>, N<sub>2</sub>, and CH<sub>4</sub> (all of which are abundant in the flue gas mixture).<sup>18</sup> Additionally, whereas CO<sub>2</sub> molecules are strongly attracted to UMCs, H<sub>2</sub>O molecules would preferentially occupy the open metal sites.<sup>50</sup> As a result, Mg-MOF-74 absorbs substantially less CO<sub>2</sub> when it is exposed to moisture. This is troublesome since there is a significant amount of H<sub>2</sub>O (g) (5–7%) in flue gases.<sup>50</sup> Hence, it's crucial to explore and devise methodologies for enhancing the selectivity over nitrogen of the MOF, particularly in the presence of water. An example of the ongoing research into this issue includes the introduction of amines into MOFs in an effort to emulate the chemisorption of CO<sub>2</sub> used by conventional liquid-amine technologies.<sup>51</sup> In a recent study conducted by Kim *et al.*<sup>52</sup> MOFs modified with diamines (nitrogen compounds) were investigated. The modified MOFs can capture and release CO<sub>2</sub> at lower temperatures than those used by existing carbon

Adopted from ref. 43 with permission. (E) Catalysts with MOF-74 templating comprising mixed metals for effective carbon dioxide capture and methanation. The resultant support material influences a qualitative CO<sub>2</sub> hydrogenation reaction pathway involving the reverse water-gas shift and Sabatier reactions. Adopted from ref. 44 with permission. (F) Coordinatively unsaturated MOF with square octahedral (Soc) topology (Cr-Soc-MOF) for super-adsorption of CO<sub>2</sub> under humid conditions. Adopted from ref. 45 with permission. (G) MOF-74(Ni) synthesized under different conditions for carbon capture and storage. Adopted from ref. 46 with permission. (H) A schematic diagram showing how defect-rich hierarchical porous Mg-MOF-74 and conventional Mg-MOF-74 are prepared differently and their application in CO<sub>2</sub> adsorption. Adopted from ref. 47 with permission.



Table 1  $\text{CO}_2$  adsorption data for a variety of functionalized MOFs under different experimental conditions

CO <sub>2</sub> uptake (mmol/g)							
Adsorbent	Functionality	Low pressure (mbar)	0.15 bar	1 bar	Temperature (K)	Selectivity (SCN)	References
Mg-MOF-74	UMC	NA	5.35	8.1	296	182 (IS) (15 : 85)	18
Mg <sub>2</sub> (dobpdc)	UMC	NA	4.85	6.42	298	NA	53
UiO-66-(CH <sub>3</sub> ) <sub>2</sub>	UMC	NA	1.3	4.01	293	58 (IS) (15 : 75)	54
UiO-66	UMC	NA	NA	1.8	298	23 (IAST) (14 : 57)	18
Co-MOF-74	UMC	NA	2.76	6.69	296	NA	18
mmen-Mg <sub>2</sub> (dobpdc)	Amine-modified	2.05 at 0.4 mbar	3.13	3.86	298	200 (IS) (15 : 75)	55
[Mg <sub>2</sub> (dobpdc) (N <sub>2</sub> H <sub>4</sub> ) <sub>1.8</sub> ]	Amine-modified	3.89 at 0.4 mbar	5.18	5.51	298	NA	56
UiO-66-NH <sub>2</sub>	Amine-modified	NA	1.15	2.6	298	32 (IS)	18
MOF-5	Pristine MOF	NA	NA	2.1	298	10.1 (IS)	57
MOF-505	Pristine MOF	NA	0.4	1.5	304	NA	18

capture materials.<sup>52</sup> As a result, the CCS process requires far less energy than it does with existing technology, which lowers the process' cost.<sup>52</sup> Amine-modified MOFs are produced by grafting amine functional groups onto MOFs.<sup>18</sup> This can improve the MOF's SCN and operating capacity, but regrettably, there is frequently a significant regeneration energy penalty.<sup>53</sup> Nonetheless, under capture conditions, some alkylamine-modified MOFs have good  $\text{CO}_2$  working capabilities, SCN, and moderate regeneration.<sup>39</sup> There have been successful reports of functionalizing Mg<sub>2</sub>(dobpdc) with *N,N'*-dimethylethylenediamine (mmen). Coordination bonds form between the amine groups and the unsaturated metal centers (UMCs) on Mg<sub>2</sub>(dobpdc). The resultant MOF, mmen-Mg<sub>2</sub>(dobpdc), boasts a high density of amine groups, leading to enhanced selectivity *versus* nitrogen (SCN) even in the presence of water. At 313.15 K and 0.15 bar, the  $\text{CO}_2$  adsorption capacity reaches 3.5 mmol/g. Moreover, this MOF effectively mitigates the substantial energy requirements for regeneration, further bolstering its potential for carbon capture applications.<sup>39</sup> Table 1 summarizes adsorption data for a variety of functionalized MOF sorbents at different pressures and temperatures.

**2.2.2 Manufacturability, stability and cost.** Mukherjee *et al.*<sup>18</sup> emphasize the importance of the industrial-scale production of candidate sorbents to meet the quantity demands of later-stage pilot-scale testing and wide-scale rollout. Most MOFs are not yet manufactured on a large scale, and the few that can be, are synthesized as powders.<sup>26</sup> MOFs need to be structured sorbents to be incorporated into the C-capture procedure. Therefore, it is necessary to look for ways to turn MOFs into pellets, beads, fibres, or monoliths. The absence of methods for transforming microcrystalline MOF powders into devices has given rise to numerous problems.<sup>18</sup> Some studies explore the incorporation of MOFs into support structures (monoliths or pellets) but these are still in the early development stages.<sup>58</sup> Generally, research into the pelletizing MOFs without binders has shown a reduction of approximately 5% in the MOF's  $\text{CO}_2$  uptake capacity.<sup>39</sup> Research conducted by Peterson *et al.*<sup>60</sup> employed octane adsorption experiments to investigate the effect of pelletization pressure on the properties of UiO-66. Results showed that pelletization at 68.94 bar led to

an 8% reduction in octane adsorption and pelletization at 689.5 bar led to a larger reduction of 16%. However, results for the pelletization of HKUST-1 reported by Asadi *et al.*<sup>61</sup> show a 20% decrease in  $\text{CO}_2$  uptake capacity. This suggests that sorbents may have varying uptake capacity responses to pelletization. Hu *et al.*<sup>62</sup> argue that, given the complexity of pelletization, an empirical approach involving practical investigations is necessary.

The current synthesis of MOF powders is typically done *via* solvothermal batch processes. These processes are time-consuming, require the use of expensive organic solvents, and involve complex purification methods.<sup>62</sup> These problems lead to high manufacturing costs, which may reduce their attractiveness as possible sorbents from an economic standpoint. Although more work needs to be done, some progress has been made recently, such as the utilisation of twin-screw extrusion (TSE) kg per hour-scale MOF synthesis without the use of ore-reduced solvents. When suggesting uses for newly created materials, a variety of considerations, including toxicity, life-cycle assessment studies, and economic implications, must be taken into account in addition to the previously mentioned concerns. On the other hand, one prominent drawback that has hampered the applicability of MOFs in this domain is their stability under the conditions of CCS operation, with many MOFs exhibiting poor hydrolytic stability.<sup>18</sup> This means that when MOFs are exposed to moisture, they are prone to decompose. There have been developments in the field to address this issue and recent research shows promise of progress. Investigated strategies include doping MOFs with alkyl amines (or other chemical functions) and improving the MOF's hydrophobicity.<sup>62</sup> Studies on doping MOFs with *N,N'*-dimethylethylenediamine, hydrazine (N<sub>2</sub>H<sub>4</sub>), and 2,2-dimethyl-1,3-diaminopropane (dmpn) have shown that the  $\text{CO}_2$  absorption capability is nearly entirely retained when there is moisture present.<sup>63</sup> However, it is important to note that doped MOFs may still struggle with poor chemical, mechanical, and thermal stability.<sup>53</sup> Research by Dalvi and Rossky<sup>64</sup> showed a marked improvement in hydrophobicity from MOFs decorated with fluoro or alkyl groups, suggesting this could be an alternative solution.



Another method of preparation that has been explored is wet granulation. This method, proposed by Chang and colleagues,<sup>65</sup> mixes the MOF with a mesoporous  $\gamma$ -alumina (MRA) binder to produce millimeter-scale spheres (Fig. 4a). Numerous MOFs, including MIL-101(Cr), UiO-66(Zr)-NH<sub>2</sub>, MIL-100(Fe), and UiO-66(Zr), have shown effectiveness with this strategy. After shape, the MOF's natural characteristics are preserved with the aid of a binder. Furthermore, tiny businesses like Mosaic Materials and NuMat are making a concerted effort to satisfy these needs.<sup>26</sup> In the research conducted by Das *et al.*,<sup>66</sup> the authors

detailed formation of a hydrogen-bonded three-dimensional (3D) framework involving a zinc(II) center, a partially fluorinated elongated dicarboxylate ligand, and an amine-rich melamine co-ligand (Fig. 4b). Notably, this framework exhibits two distinct types of 1D channels adorned with CO<sub>2</sub>-attractive ( $-\text{NH}_2$  and  $-\text{CF}_3$ ) groups that facilitate the framework's exceptional selectivity for CO<sub>2</sub> adsorption (uptake of 49.88 and 31.16 cm<sup>3</sup>/g at 273 and 298 K, respectively).<sup>66</sup> Furthermore, a straightforward and comprehensive room-temperature procedure has been established for the

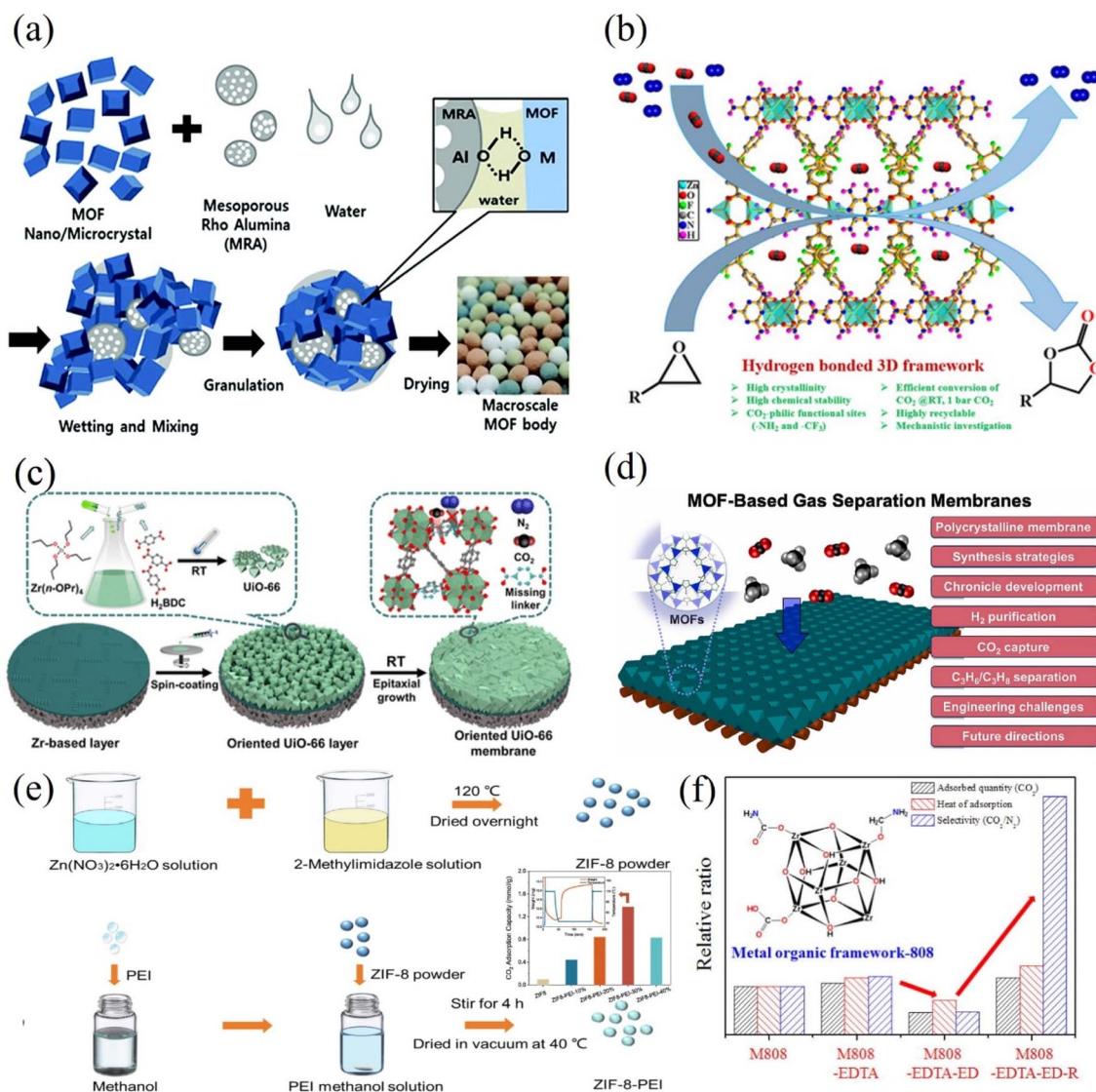


**Fig. 4** (a) Creating MOF granules or spheres via the wet granulation process by aggregating MOF and MRA particles. Adopted from ref. 65 with permission. (b) The rational design of a porous Zn(II)-MOF with several functional sites that can be used, under moderate conditions, for extremely effective CO<sub>2</sub> fixation with internal and terminal epoxides. Adopted from ref. 66 with permission. (c) A schematic diagram depicting the entire room temperature preparation process for defect-engineered (111)-oriented Uio-66 membranes. A higher CO<sub>2</sub>/N<sub>2</sub> adsorption selectivity was demonstrated and attributed to the stronger affinity interactions between CO<sub>2</sub> molecules and the defective sites in the Zr<sub>6</sub>-oxo cluster nodes. Adopted from ref. 67 with permission. (d) Diagram showing the *in situ* growth process for homochiral MOF membrane production on nickel net and its use for molecular separations. Adopted from ref. 68 with permission. (e) A synthesis process of unmodified and PEI-modified ZIF-8 and the corresponding adsorption capacity at different PEI loadings. Adopted from ref. 69 with permission. (f) Zr-based MOF functionalized with ethylenediaminetetraacetic acid (MOF-808-EDTA), ethylenediamine (MOF-808-EDTA-ED), and lithium aluminium hydride (MOF-808-EDTA-ED-R) for selective CO<sub>2</sub> adsorption. Adopted from ref. 70 with permission.



fabrication of (111)-oriented UiO-66 membranes.<sup>67</sup> This method utilizes a  $ZrO_2$  buffer layer-modified porous  $\alpha$ -Al<sub>2</sub>O<sub>3</sub> substrate and a Zr(*n*-OPr)<sub>4</sub> source (Fig. 4c). Experimental findings revealed that conducting the reaction at room temperature (RT) increased the number of missing linkers within the UiO-66 framework (1.5 per  $Zr_6$  formula unit). Consequently, this resulted in enhanced CO<sub>2</sub>/N<sub>2</sub> adsorption selectivity due to a stronger affinity interaction between CO<sub>2</sub> and the defective sites in the Zr<sub>6</sub>-oxo cluster nodes.<sup>67</sup>

Conversely, many research endeavours have focused on MOF-based gas separation membranes, with particular attention to ZIF-8 (ref. 68) (Fig. 4d). The exploration of MOF membranes for gas separation traces back to 2009,<sup>71</sup> with the milestone achievement of the first continuous MOF-5 membrane *via* an *in situ* growth method. This milestone marked the beginning of MOF membrane development for gas separations. Other methods include layer-by-layer growth, electrochemical synthesis, vapour phase synthesis, seeding and secondary growth, and contra-diffusion also appeared in the ensuing ten years. Particularly noteworthy is the considerable focus on ZIF-8 in MOF membrane research due to its exceptional C<sub>3</sub>H<sub>6</sub>/C<sub>3</sub>H<sub>8</sub> separation capabilities, straightforward synthesis, and the potential for producing high-quality membranes. A recent study involved the synthesis and characterization of ZIF-8 with varying weights of polyethyleneimine (PEI).<sup>69</sup> The results indicated that ZIF-8 with 30 wt% PEI achieved the highest CO<sub>2</sub> uptake of 1.4 mmol/g under dry conditions and demonstrated remarkable CO<sub>2</sub>/N<sub>2</sub> separation performance (Fig. 4e). The CO<sub>2</sub> adsorption capacity of ZIF-8-PEI30% notably rose to 1.7 mmol/g when exposed to humid flue gas with 50% relative humidity (RH). Furthermore, even after undergoing 50 adsorption/desorption cycles, only a slight decrease in adsorption capacity was observed. Park *et al.*<sup>70</sup> have directed their efforts towards improving the efficiency of a Zr-based metal-organic framework (MOF-808) for CO<sub>2</sub> capture by introducing various functional groups onto the MOF surface. Notably, reducing the MOF-808-EDTA-ED compound with lithium aluminium hydride (LAH) led to a significant enhancement in performance, including higher CO<sub>2</sub> adsorption capacity, CO<sub>2</sub>/N<sub>2</sub> selectivity, and isosteric heat of adsorption. For example, under conditions of 298 K and 1 atm, MOF-808, MOF-808-EDTA, MOF-808-EDTA-ED, and MOF-808-EDTA-ED-R demonstrated CO<sub>2</sub>/N<sub>2</sub> selectivity of 40, 48, 19, and 197, respectively (Fig. 4f). This significant enhancement is attributed to the contribution of functional groups and porosity. The introduction of amides during the reaction with ED resulted in decreased MOF porosity, negatively impacting CO<sub>2</sub> capture. However, subsequent reduction of amides to amines improved adsorption effectiveness.<sup>70</sup>

Regarding the cost, it can vary widely depending on several factors, including the specific MOF composition, synthesis method, scale of production, and market demand. Generally, MOFs are more expensive to produce compared to traditional adsorbents like activated carbon due to their complex synthesis processes and sometimes costly precursor materials. At present, the production of MOFs typically involves expensive starting materials and specialized synthesis techniques, which

contribute to higher production costs. Additionally, the purity and quality of MOF materials also affect their cost, with higher-purity MOFs often commanding a premium price. As was previously said, the creation of MOFs that require less temperature to absorb and release CO<sub>2</sub> will probably lead to lower process costs over time.<sup>52</sup> However, MOF sorbent costs are still considered the limiting factor for their commercial application.<sup>62</sup> Since MOF sorbents for post-combustion C-capture have not been subjected to real-world trials, prices can be estimated in part by considering the price of the substrates or raw sorbent utilised in the preparation.<sup>18</sup> The metal ions or clusters are often inexpensive, consequently, the main factor affecting the cost of a MOF sorbent is the linker cost. Whilst most sorbents use polycarboxylate ligands, there is a variety of inexpensive and commercially available ligands, for example, one of the most common ligands, 4,40-bipyridine (bipy).<sup>72</sup> Commercial MOF vendors still charge significantly more than more conventional porous materials like zeolites, even though MOFs are synthesised from comparatively cheap ingredients.<sup>62</sup> This is often attributed to high manufacturing costs which are the result of a shortfall in large-scale production methods.

### 3 Energy storage devices

Currently, supercapacitors (SCs) are among the most popular energy-storage devices,<sup>73</sup> which have already found applications in consumer electronics, memory backup systems as well as industrial-scale power and energy management devices.<sup>74</sup> Although conventional capacitors have a larger energy density, SCs are seen to be better because of their many benefits, including flexible packaging, low weight, minimal heating, and strong device stability.<sup>75</sup> Furthermore, SCs have proven to be both safe and reliable, as Sundriyal *et al.*<sup>74</sup> highlight in their recent application in the emergency doors of the Airbus A380. In addition, one of the most intriguing uses of SCs is in contemporary transportation systems like electric cars. The sales ban on internal combustion (IC) engines will be accelerated from 2040 to 2035 as a result of growing social and governmental pressure to reduce fossil fuel consumption. As a result, the electrical energy storage (EES) devices used in these transportation systems must be able to provide a high enough power density to expedite vehicle charging times.<sup>74</sup> SCs' high-power densities (up to 15 kW/kg) give them the ability to charge and discharge rapidly, which would enable fast charging of electric vehicles, and their good cycling stability would ensure that their performance wouldn't degrade significantly over time. However, their large-scale usage is hindered by low energy densities meaning that they are unable to hold large amounts of energy.<sup>75</sup>

In the same context, electrodes play a critical role in SC performance, therefore selecting an electrode design and material is key to ensuring effective energy storage. Sundriyal *et al.*<sup>74</sup> suggest several critical electrode parameters that determine the performance of the SC including specific capacitance, power and energy densities, cycle life, and stability in bending. Forse *et al.*<sup>76</sup> also offer a range of critical electrode material properties that require consideration, including a large specific surface area, good stability at high temperatures, pore



size and distribution, high corrosion resistance, high conductivity, and cost-effectiveness. Research by Huang *et al.*<sup>73</sup> supports this but summarises the performance criteria under the broad umbrella of material properties that allow for a short ion or charge transfer channel whilst also providing many active sites.

Many sources discuss the relationship between the specific surface area (SSA) and capacitance as though it were linear, with higher SSAs resulting in a higher capacitance.<sup>73</sup> Whilst this is true for certain SC electrodes, Wu and Cao,<sup>77</sup> highlight that in some instances, a higher SSA will not guarantee a greater capacitance. Effective surface area (ESA) is a surface area that is directly utilised for charge absorption and is associated with the distribution of pore sizes. As previously mentioned, the low energy density of SCs is currently impeding their practical deployment.<sup>78</sup> Energy density denotes the quantity of energy that a SC can store per unit volume of SC.<sup>74</sup> On the other hand, power density describes the amount of power transferred per SC volume. The difference between SSA and the attained specific capacitance is a topic covered in a number of studies. Some reports indicate that during charge storage, not all of the pores are used.<sup>75</sup> Consequently, Forouzandeh *et al.*<sup>75</sup> argue that while SSA is an important performance parameter for EDLC design, other factors such as pore size distribution and ESA will also influence the SC's electrochemical performance. In their research paper, Wu and Cao<sup>77</sup> state that the electrode surface area is the main influencer on the electrochemical properties of the SC.

Phiri *et al.*<sup>79</sup> highlight the important role played by ion-transport kinetics in SC electrode performance. According to their research, the material's surface area and pore structure affect the electrode's ion kinetics. Consequently, the authors suggest a material that combines a high SSA with a combination of micropores and mesopores (to raise the ESA) while thinking about ways to improve the electrochemical performance of electrodes. They suggest that the mesopores may serve as a quick pathway for the SC electrolyte to move, boosting the capacitance of the SC and that the micropores offer a sizable SA for quick ion adsorption. Wu and Cao<sup>77</sup> also propose other factors for consideration such as the electrical conductivity of the electrode material and the presence of surface functional groups. Overall, factors such as power and energy densities, cyclability, specific capacitance and morphology require consideration during the material selection process for SC electrode capacitors. Moreover, cyclability pertains to the count of charge and discharge cycles a supercapacitor can undergo before experiencing electrode degradation and notable performance decline.<sup>77</sup> Often, degradation only becomes evident after prolonged cycling. Consequently, estimating the cyclability can be difficult. Weinstein and Dash<sup>80</sup> warn that laboratory-based testing of cyclability often relies on "beaker tests". During these tests, the SC electrodes are placed in a beaker and submerged in the electrolyte. This kind of approach reduces the effect of contaminants on cyclability by allowing them to diffuse into the huge volume of electrolyte that causes errors. On the other hand, because of the device's real operating circumstances, there is minimal room for diffusion because the

electrolyte volume is rather tiny.<sup>80</sup> Therefore, the cycle life obtained through laboratory tests is likely to be different from values obtained from testing the real fabricated SC. Cyclability is an important factor for the assessment of both the performance and the environmental impact of the design. If the electrode degrades quickly, more material will be required over the lifetime of the device or the device will require replacing.

In another context, Forouzandeh *et al.*<sup>75</sup> highlight a series of considerations for assessing the environmental impact of an electrode including the toxicity, reusability (reformation prospects), and energy requirements for the primary manufacturing (processing raw materials). Furthermore, Weinstein and Dash<sup>80</sup> postulate that, because SCs are often relatively small compared to the device they power, there is little incentive to reduce the size and weight of the SC if it results in higher costs. Manufacturers of SCs are more concerned with controlling costs than with making incremental performance advances. Price is acknowledged as significant, but it is not given more weightage than the other factors.<sup>75</sup> In contrast to Weinstein and Dash, Pongprayoon and Chaimanatsakun<sup>81</sup> argue that the two most important design requirements for SCs are tuning the electrode material morphology (pore shape and size) to optimize the transportation of electrolyte ions and a high SSA to increase the availability of electrochemically active sites. Both are relevant for improving performance rather than reducing cost.

### 3.1 Porous carbonaceous materials for supercapacitors

Porous carbonaceous materials stand out as highly versatile materials for supercapacitor electrodes, particularly due to their diverse applications in various biomass sources. In recent scientific research, there has been a notable emphasis on synthesizing carbonaceous materials from biowaste, which produces a variety of morphologies and surface textures. The typical synthesis process involves carbonization and activation steps, leading to activated carbon with tunable pore sizes and exceptionally high specific surface area compared to other carbonaceous materials. This renders activated carbon a preferred choice for supercapacitor electrodes. Prior to the rise of MOFs, most studies on supercapacitor electrode materials were concentrated on carbon-based materials.<sup>82</sup> Activated carbon (AC) is used in almost all electrochemical capacitors (ECs), and many producers of SCs choose to use coconut shell AC as their active electrode material.<sup>80</sup> Phiri *et al.*<sup>79</sup> note that while graphene and carbon nanotubes (CNTs) are also common material choices for SC electrodes, their wide-scale deployment has been hindered by their high production costs and disposition to nanoparticle aggregation which limits their effective SSA.

**3.1.1 Performance and properties.** Carbon SC electrodes usually work *via* charge adsorption, resulting in large power densities and long cycle life.<sup>73</sup> In addition to this, carbon electrodes often present superb chemical stability and electrical conductivity. An AC fabricated electrode in a study by Li *et al.*<sup>83</sup> displayed a specific capacitance of 207.5 F/g and a cycle life of over 3000 cycles when tested at a current density of 0.5 A/g.



Another study reports an energy storage density of about 28 W h/kg, but it also mentions that the device's charge supply rate limits the amount of power that can be produced.<sup>84</sup> Research by Ajay and Dinesh<sup>85</sup> yielded a specific capacitance of 107.6 F/g for commercially available AC measured at a 5 mV/s scan rate. However, Phiri *et al.*<sup>79</sup> argue that biomass-derived ACs also have disadvantages, including discrepancies in the structures of the biomass sources. Because of this, the ideal circumstances for the synthesis of AC from one biomass source might not be appropriate for another. According to their studies, this can also apply to a single biomass source that is used intermittently. As a result, a biomass source needs to have a predictable and consistent structure to be taken into consideration for large-scale practical applications.

AC-based SC electrodes are well suited for this purpose, not only do they have a high thermal and electrochemical stability, but they also benefit from a large SSA. Available values of AC SSA vary with most papers agreeing on a value within the range of 1000–3000 m<sup>2</sup>/g.<sup>86,87</sup> Conversely, a study by Weinstein and Dash<sup>80</sup> suggests a theoretical maximum SSA of 2000 m<sup>2</sup>/g. Carbon materials have a high SSA in addition to being relatively simple to produce, modify, and optimise.<sup>87</sup> The premium-grade AC utilised for SC electrodes has been refined to guarantee that the ash level is less than 1% and the halogen and iron impurities are fewer than 100 ppm.<sup>80</sup> This purification helps to improve the cycle life of the electrode. Despite this, ACs are still comparatively cheap. ACs also benefit from high pore volumes in the range of 0.5–2 cm<sup>3</sup>/g.<sup>87</sup> As previously stated, other literature reports suggest that the SSA is not as important as the pore size and its impact on the effective specific surface area (ESSA).<sup>75</sup> Research by Arenillas *et al.*<sup>88</sup> supports this, suggesting that for AC electrodes, the whole SSA is not used for charge storage as the larger electrolyte ions are unable to enter the small micropores. The largest obtainable SSA for AC is estimated at 3000 m<sup>2</sup>/g, whilst the obtainable ESSA ranges from 1000 to 2000 m<sup>2</sup>/g.<sup>75</sup> Forouzandeh *et al.*<sup>75</sup> also examine the potential drawbacks associated with large specific surface areas (SSAs), noting in their report that, in some scenarios, augmenting the SSA can induce electrolyte decomposition and create dangling bond positions. Additionally, a high pore volume may arise from attempts to raise the SSA through excessive activation. Poor conductivity and low material density, which resulted in low energy and power densities, were among the effects of these huge pore volumes that were investigated.<sup>89</sup> The impact of various electrolytes on the obtained capacitance of AC electrodes has also been studied. It was shown that the capacitive performance of AC electrodes was enhanced when an aqueous electrolyte was used instead of an organic electrolyte.

The performance and characteristics of activated carbon as electrode materials for supercapacitors are very well presented in Fig. 5A(a and b). The latter presents the CV curves of the electrodes at a scan rate of 50 mV/s and gives an idea about their capacitive behaviour and electrochemical performance. The nearly rectangular shape of the CV curve indicates ideal capacitive properties; among them, better performance is obtained for the AC-HF sample.<sup>90</sup> Fig. 5A(b) shows the galvanostatic charge–discharge curves of the electrodes at a current density of 1.5 mA/

cm<sup>2</sup>, which provides the potential for energy storage. The GCD curves are overlapping linearly and symmetrically, which further testifies to the high reversibility and efficiency of the activated carbon electrodes, especially AC-HF, with the longest charging time and discharge time and thus indicative of higher energy storage capacity.<sup>90</sup> A recent breakthrough introduced a straightforward and cost-effective technique for producing high-performance cellulose-based activated carbon fibre papers (ACFPs), capable of serving as self-supporting supercapacitor electrodes without the need for binders.<sup>91</sup> This innovative approach combines wet papermaking, thermal carbonization, and double activation processes, enabling the on-site conversion of fibrillated pulp fibres into cellulose-derived activated carbon, seamlessly integrated with carbon fibres (CFs) (Fig. 5B). The electrochemical evaluations demonstrated that the ACFPs exhibited outstanding electric double-layer capacitive behaviour (Fig. 5C), with coulombic efficiency and capacity retention remaining at 98.58% and 100%, respectively, even after 10 000 cycles (Fig. 5D). The authors further elucidated the schematic representation of charge transfer and electrolyte ion transfer within ACFP.<sup>91</sup> The configuration presented in Fig. 5E demonstrates a stable three-dimensional conductive network structure through the close interweaving of CFs within the ACF matrix. This arrangement facilitated swift electron migration along the CFs and enhanced the adsorption of electrolyte ions by the ACFs.<sup>91</sup>

In the work of Li *et al.*,<sup>92</sup> a deliberately engineered self-supporting and flexible film composed of activated carbon, carbon nanotubes, and reduced graphene oxide (AC/CNTs/RGO) has been developed (Fig. 5F). The AC/CNTs/RGO electrode demonstrates an impressive specific capacitance of 101 F/g when operated at a current density of 0.2 A/g, resulting in a remarkable maximum energy density of 30 W h/kg. Conversely, three-dimensional porous carbon materials were synthesized by utilizing sakura petals as the source material and employing a combination of pre-carbonization and KOH activation techniques (Fig. 5G).<sup>93</sup> The synthesized porous material exhibited a high specific surface area (up to 1785.41 m<sup>2</sup>/g), leading to a maximum specific capacitance of 265.8 F/g at a current density of 0.2 A/g. Additionally, under continuous cycling for 2000 cycles, the capacitance retention rate remains excellent, reaching an impressive 90.2%, demonstrating outstanding cycling stability.<sup>93</sup> Recently, AC was prepared using biochar derived from date seeds *via* pyrolysis and activated with H<sub>2</sub>SO<sub>4</sub>.<sup>94</sup> The elaborated samples demonstrated a specific capacitance of 487.5 F/g at a current density of 1 A/g. Additionally, galvanic charge and discharge trends indicated a higher charge storage capacity with reduced discharge. Another study focuses on converting inexpensive Cilantro plants (*C. sativum*) into AC aiming to produce a cost-effective AC material that shows promise in supercapacitors for energy storage.<sup>95</sup> The material that was synthesised at 700 °C showed ideal specific surface area (SSA) and surface functionalities, which promoted surface redox processes, electrode wetting, and ion diffusion-induced pseudo-capacitance. At 1 A/g, its specific capacitance was 162.4 F/g. Particularly noteworthy is the remarkable performance of the activated carbon (AC) symmetric supercapacitor, delivering a high-power density of



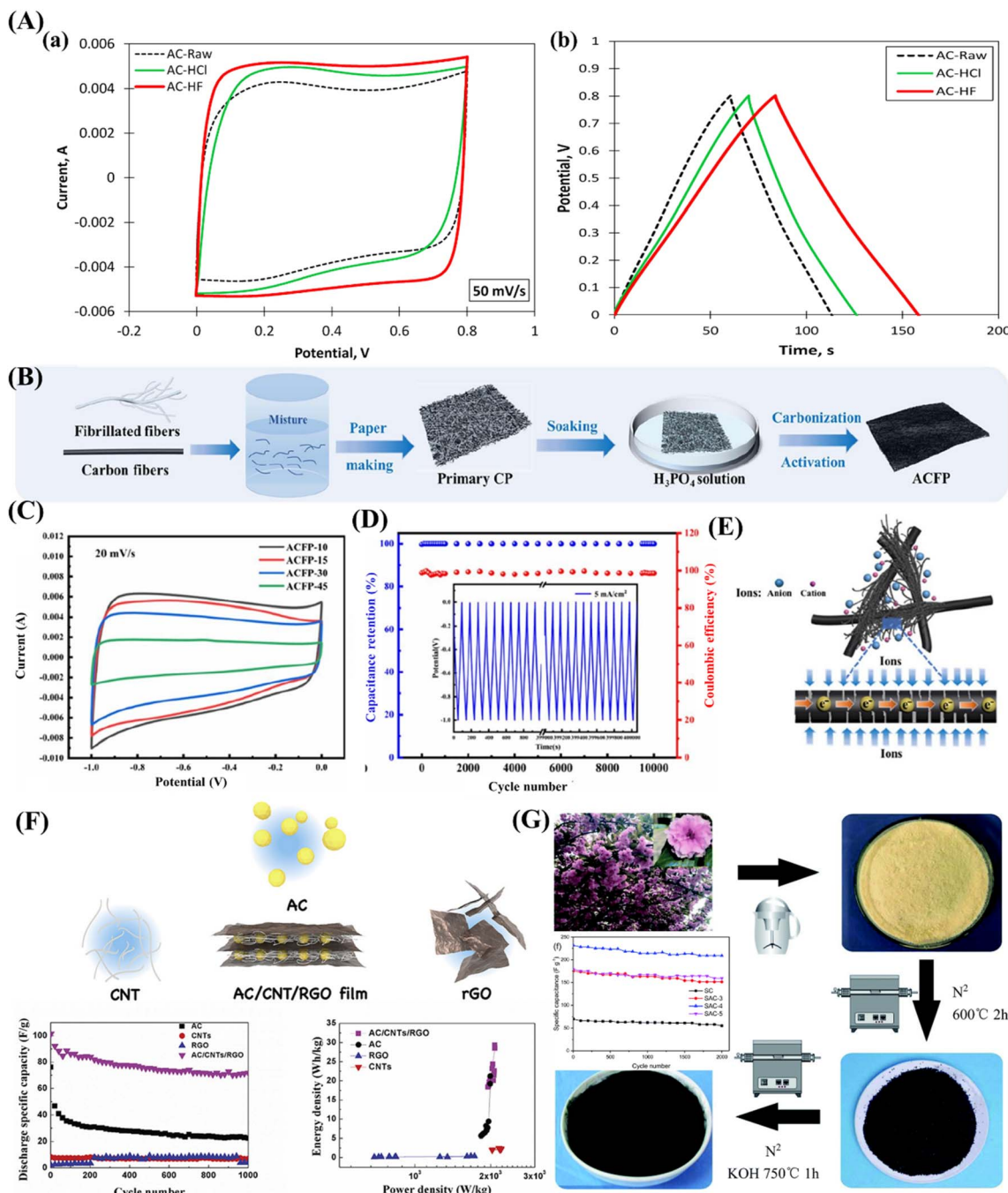


Fig. 5 (A) (a) Cyclic voltammetry curves measured at a scan rate of 50 mV/s; (b) galvanostatic charge discharge curves measured at a current density of 1.5 mA/cm<sup>2</sup>. Adopted from ref. 90 with permission. (B) Illustration depicting the production process of cellulose-based activated carbon fibre papers (ACFPs). (C) cyclic voltammetry curves recorded for ACFPs with varying CF content using a 20 mV/s scan rate, (D) retention of capacitance and coulombic efficiency measured at a current density of 5 mA/cm<sup>2</sup>, and (E) schematic diagram illustrating the charge transfer and electrolyte ion transfer within the conductive networks in ACFPs. Adopted from ref. 91 with permission. (F) A flexible electrode consisting of self-supporting activated carbon, carbon nanotubes, and reduced graphene oxide and its SC performance shows a high specific capacitance of 101 F/g at the current density of 0.2 A/g. Adopted from ref. 92 with permission. (G) Schematic representation illustrating the production process of porous carbon derived from sakura, along with its corresponding long-term cycling performances. Adopted from ref. 93 with permission.

243.94 W/kg and maintaining minimal capacitance loss over 5000 cycles at 10 A/g, indicative of excellent cycling stability.

**3.1.2 Environmental impact.** Numerous commercially available ACs are produced from precursors such as coal and

polymers, which are fossil fuel-based, making them both expensive and environmentally unfriendly.<sup>79</sup> However, ACs derived from biomass are still promising candidates for SC electrode materials.<sup>86</sup> Large pore volume and surface area



(which can surpass graphene's), ease of preparation, and a customised architecture that has been deemed feasible for commercial usage are some of their potential qualities. Gao *et al.*<sup>96</sup> also draw attention to the other environmental benefits of bio-mass-derived ACs including the renewability and abundance of raw materials that can be used to make ACs. Furthermore, AC-based electrodes show good potential for recyclability. The recycling process for activated carbon was investigated by Jiang and Pickering.<sup>97</sup> The recycling procedure is assumed to be capable of recovering 90% of the electrode's active materials.<sup>84</sup> The measured surface area of the AC that was recovered by this technique is only 95% of its original, pristine value. This indicates a little decline in the content's quality.<sup>97</sup>

Considering the environmental impact of recycling/recovering materials, Cossutta *et al.*<sup>84</sup> suggest using the substitution model. This model's underlying idea is that material recovery reduces the need to generate additional virgin material, which benefits the environment. The quality of the recycled product determines how much virgin material may be substituted (0.95 g of virgin AC can be replaced by 1 g of recovered material).<sup>84</sup> This is not a 1:1 substitution due to the degradation of material quality/properties. Research by Ke and Wang<sup>98</sup> provides a value for the theoretical specific capacitance for used AC as 200 F/g (this value is based on results for maximum actual SSA). Cossutta *et al.*<sup>84</sup> highlight that, while the production of AC requires energy, it is not as greenhouse gas (GHG) intensive as other electrode materials (such as graphene). AC production produces around 5 g CO<sub>2</sub> eq/g (compared to ~80 g CO<sub>2</sub> eq/g). Furthermore, since the emissions from the recycling process are lower than the emissions connected to the sourcing and initial production of ACs, recycling AC supercapacitors can result in a net reduction in GHG emissions. Research by Ntuli and Hapazari<sup>99</sup> also suggests that the use of agricultural by-products or lignocellulosic materials (such as coconut shells) as feedstocks for AC production would further reduce GHG emissions as processing would avoid the emission of GHGs when they rot or burn. However, the lifecycle analysis (LCA) of the AC as electrode materials for supercapacitors manifests a fundamental environmental performance. From here, it is observed that following the ISO framework, 1 kg of AC from coconut shells contains 34.4 MJ of energy use and 5.68 kg of CO<sub>2</sub>, char production and activation account for 86% of the CO<sub>2</sub> emissions at 97%.<sup>100</sup> New AC electrodes exhibit competitive environmental performance in comparison with coal-derived AC, reduced graphene oxide, and algae-derived biochar aerogel electrodes, though they have larger impacts on land and water use as a function of the agricultural intensity of coconut production. They have lower impacts in regard to terrestrial ecotoxicity and freshwater eutrophication.<sup>101</sup>

The AC production process involves high temperatures and activation agents such as potassium hydroxide, hence is highly energy-intensive with chemical wastes as by-products. The specific surface area for mesophase-derived AC, for example, is 2000 m<sup>2</sup>/g, reducing to 1600 m<sup>2</sup>/g when treated thermally but improving its stability by 99%.<sup>102</sup> During usage, AC-based supercapacitors show excellent performance, with thermally

treated AC (AC-1000) exhibiting only a 5% reduction in specific capacitance after 10 000 cycles, compared to untreated AC's reductions of 12% and 17%.<sup>103</sup> An asymmetric capacitor using AC and AC-1000 shows a capacitance decrease from 220 F/g to 210 F/g after 10 000 cycles, and to 198 F/g after 20 000 cycles.<sup>104</sup> These efficiencies translate into reduced energy losses and extended lifetimes for devices. However, some of the challenges are in disposal and recycling, wherein exposure to residual chemicals from AC materials may contaminate the environment. Overall, AC materials enjoy huge technical advantages, but their lifecycle environmental impact implores that the production methods used should be as clean and green as possible, the usage as efficient as can be, and the disposable or recyclable end-of-life-time processes as innocuous as can be to avoid adverse impacts on the environment.

**3.1.3 Recent developments in AC electrodes.** Recent literature provides a range of strategies for the improvement of AC electrochemical performance. In their 2020 research paper, Grishchenko and colleagues<sup>105</sup> explored modifying the surface of the AC electrodes through oxidation, and while there was a significant reduction in the SSA of oxidized material, they achieved a 1.4 times higher specific capacitance in a symmetric SC electrode compared to a pure AC electrode. Another example of the continuing improvement of AC electrodes can be seen in the work by Cheng *et al.*<sup>106</sup> To create a new class of nanocomposite electrodes, the scientists examined the synergistic effects of combining ACs and carbon black (CB) with other species such as carbon nanofibers (CNFs) and carbon nanotubes (CNTs). The study demonstrated that, in comparison to pure AC electrodes, the electrochemical performance was significantly improved by mixing the species employed in the SC electrode. The weight percentage composition of the optimised nanocomposite electrode was 1.25% CB, 3.75% CNTs, 1.25% CNF, and 88.75% AC. The completed SC demonstrated good cyclability (capacitance retention of 91.4% over 30 000 cycles) and volumetric performance (high capacitance of 66.1 F/cm<sup>3</sup>, power density of 101.7 kW/L, and energy density of 29.6 W h/L).

The improved performance is the result of the obtained morphology, as the added CB particles fit into the voids between AC particles and it was found that the flexible CNTs wrap tightly and uniformly around the AC particles. The CNFs were added, which helped to lessen the CB particles' tendency to aggregate. By acting as a bridge between CB and CNT-wrapped AC particles, CNFs' relative stiffness (as compared to CNTs) enhances the structural stability of the nanocomposite. The final electrode featured a three-dimensional electrical conduction network that enhanced capacitive behaviour and packing density. Furthermore, the nanocompositing approach employed by Cheng *et al.*<sup>106</sup> utilizes readily available materials to synthesize the nanocomposites. These can then be used to mass-produce large-scale high-performance SC electrodes *via* the cost-effective industrial slurry process. A recent study focuses on synthesizing graphene oxide (GO) using a modified version of Hummers' method.<sup>107</sup> The produced GO is then incorporated into an activated carbon slurry to create electrodes for supercapacitors. The addition of an appropriate amount of



graphene oxide (GO) into the electrode renders it hydrophilic, thereby enhancing the interfacial contact between the electrode and the hydrogel electrolyte. The oxygen-containing functional groups present on GO attract cations and facilitate ion dissociation, thereby improving ion mobility. However, as an insulator, GO affects electrode conductivity. Remarkably, utilizing GO with weight ratios of 5% achieves a balance, providing a sufficient free ion ratio for good ion conductivity while maintaining acceptable electronic conductivity. Supercapacitors incorporating GO5 exhibit minimal equivalent series resistance (ESR) of  $4\ \Omega$  and a maximum specific capacitance of 117.7 F/g. In a similar context, biowaste from litchi seeds was utilized to synthesize 3D activated carbon (3D-AC), which was further combined with reduced graphene oxide (rGO) and multi-walled carbon nanotubes (MWCNTs) to create a multidimensional carbonaceous material.<sup>108</sup> This composite exhibited a specific capacitance of 320 F/g at 1 A/g. Additionally, 3D-AC served as a supporting matrix for the growth of zinc cobalt sulfide nanoparticles, leading to promising electrochemical performance in both asymmetric and symmetric devices.

Other recently explored strategies include using ultrasonic radiation for Fermi-level position modification of the activated carbon,<sup>109</sup> sulphur and oxygen functionality doping of the porous AC,<sup>110</sup> and the formation of composite electrodes *via* the insertion of polymers into the AC substrate.<sup>111</sup> The price of AC has decreased dramatically over time, and this has been ascribed to the SC carbon market's strong price sensitivity relative to performance. Suppliers such as Kuraray, whose prices have dropped from \$150 to \$200 USD per kilogramme to \$15 USD per kg, are an example of this price reduction.<sup>80</sup> More recent studies provide a lower value of \$4.15 USD per kg and also emphasize the manufacturing economic benefits of coconut shell AC by highlighting their abundant supply.<sup>87,112</sup> Activated carbon, while a popular material in supercapacitors,

has several limitations that impact its performance. One of the main issues is its broad and irregular pore size distribution that is predominantly microporous ( $<2\text{ nm}$ ). These small pores can limit the accessibility of electrolyte ions, particularly larger ions in organic electrolytes, resulting in reduced capacitance and inefficient ion transport. Despite its high surface area, activated carbon often exhibits low specific capacitance because not all of its surface area is effectively utilized due to the presence of micropores that are too small for ion penetration. Additionally, the properties of activated carbon are less tuneable compared to MOFs. This lack of tunability restricts the ability to optimize its surface chemistry, pore structure, and functional groups for specific applications.

### 3.2 Metal organic frameworks as supercapacitors

Table 2 presents a selection of functionalized MOFs investigated for their suitability as supercapacitor electrodes and compared to activated carbon. The table demonstrates a wide range of potential specific capacitances, with some MOFs showing values higher than those of AC, indicated at the bottom of the table. Additionally, MOFs exhibit the potential for enhanced cyclability compared to ACs, highlighting their promise for supercapacitor applications.

**3.2.1 Pristine MOFs and their composites.** From the available literature, it can be observed that the use of pristine MOFs for electrochemical applications, such as SC electrodes, is rare.<sup>118</sup> As previously mentioned, this is predominantly due to their inherent insulating properties which result in low capacitance, often regarded as insufficient for most electrochemical applications.<sup>119</sup> One report explores the use of Fe-MOF and its variants (MIL-88B, MIL100, and MIL-53) as SC electrodes coupled with an aqueous and neutral electrolyte.<sup>120</sup> The device's performance is significantly impacted by the material

Table 2 Supercapacitor's performance of functionalized MOF compared to AC electrodes

Electrode material	Cycle life	Specific surface area m <sup>2</sup> /g	Current density/scan rate	Specific capacitance F/g	Reference
ZIF-8 (HNC) MOF derived porous carbon	20 000	1215	536 mA h/g 1 mV/s	253.6	73
ZIF-8 (NPCF) MOF derived porous carbon	5000	NA	1 mV/s (rate)	332	22
ZIF-8 (NCF) MOF derived porous carbon	10 000	NA	5 mV/s (rate)	264	22
Co-MOF MOF directly used	NA	2900	0.6 A/g	206.76	74
Zr-MOF (1) MOF directly used	NA	1047	5 mV/s	1144	22
ZIF-8 (NPC) MOF derived porous carbon	NA	1523	5 mV/s	251	22
MOF-5 (NPC) MOF derived porous carbon	NA	2872	1 mV/s	312	22
Ni-MOF	49.1% (5000)	295.7	1 A/g	1024.4	74
NiO <sub>x</sub> @NP 3-electrode system	91.5% retention after 5000 cycles	1523	5 mV/s	581.30	113
From waste PET					
3D Ni-MOF	5000	NA	1 A/g	2150	114
Fe-MOF@AC	10 000	180.7	1 A/g 1 mV/s	470.05	115
NiO@Ni-MOF	3000	433	1 A/g 1 mA/cm <sup>2</sup>	144	116
Cu-MOF and Co-MOF	1000	NA	3 mV/s	451 and 103 C/g	117
Activated carbon	>3000	NA	0.5 A/g	207.5	83



properties of the electrode, such as the size of the pellet and the pore diameters. Using an aqueous 0.1 M  $\text{Na}_2\text{SO}_4$  electrolyte, it was discovered that the MIL-100 sample only produced a specific capacitance of 34 F/g. The irritating nature of the Fe-MOF and insufficient mixing between the conductive and non-conductive phases of the Fe metal centres were the authors' explanations for this very low specific capacitance. This stops the material's electrons from moving through it in the best possible way when the iron centre is being reduced or oxidised. The Fe-MOF was deemed unsuitable for use as an electrode due to the limited quantity of redox-active Fe ions in the structure. The use of bare Fe-MOF electrodes has also proven problematic, as experiments have shown that during the reduction cycle, the electrode is subject to some degree of dissolution.

Despite their limitations, MOFs exhibit a rapid diffusion of electrolyte ions into the pores of electrode materials. Consequently, research into utilizing pristine MOFs as SC electrodes has experienced a noticeable uptick. These MOFs often work as pseudocapacitors *via* faradaic redox reactions between the electrodes and the electrolyte. As the work by Wang *et al.*<sup>121</sup> shows, these fabricated electrodes yield theoretical values for capacitance as high as 2000 F/g.<sup>121</sup> However, Ramachandran *et al.*<sup>122</sup> argue that these benefits come at the cost of the electrode's cycle life. In their investigation, they discovered that the cycling stability of pseudocapacitive MOFs was weakened by frequent charging and discharging cycles. This results from the occasional dissolving of the MOF electrode material during the reduction reactions, as well as incompatibility between the electrode and electrolyte. A prominent example of the use of pristine MOFs as SC electrodes is the work done by Lee *et al.*<sup>123</sup> in their paper. During their experiments with a Co-based MOF electrode in an aqueous electrolyte of 1 M  $\text{LiOH}$ , the authors were able to achieve a specific capacitance of 206.76 F/g with a current density of 0.6 A/g. After the electrode's cycle life was examined, it was discovered that, after 1000 cycles of testing, its capacitance retention could reach 98.5%. However, the Co-based MOF electrode's performance significantly decreased and was ultimately declared unsatisfactory when tested in different electrolytes (such as KOH and KCl). An investigation was conducted into how the temperature of the synthesis reaction affected the performance, degree of crystallisation, and particle size of a zirconium-based MOF (UiO-66).<sup>124</sup> It was observed that a sample with the smallest particle size and a synthesis reaction temperature of 50 °C achieved the highest specific capacitance (1144 F/g at a 5 mV/s scan rate). However, the cost may prove to be a limiting factor as 1 kg of UiO-66 has been priced at around \$25000 USD.<sup>125</sup>

Other research into altering MOF morphology to improve SC performance includes the synthesis of a superstructure electrode from "accordion-like Ni-MOF".<sup>126</sup> Whilst being tested at current densities of 1.4 and 7 A/g, the electrode achieved enhanced specific capacitances (988 F/g and 823 F/g respectively). Additionally, after 5000 cycles, the capacitance retention was 96.5%, which was a respectable retention rate. Highly elevated specific capacitances have also been seen with Ni-MOF electrodes in combination with a 6 M aqueous KOH electrolyte. Yang *et al.*<sup>127</sup> report that, with current densities of 0.5 A/g and 10

A/g, specific capacitances of 1127 F/g and 668 F/g respectively could be achieved. The high specific capacitances were explained by the authors as the result of the electrode's pseudocapacitive nature. Additionally, it was discovered that this electrode had improved cycling stability, demonstrating 90% after 3000 cycles. The MOF's layered structure and sizable open facets were both credited with its cycling stability and quick surface redox reactions.

Rahmanifar *et al.*<sup>128</sup> reported a one-pot co-synthesis method for creating a novel, water-stable Ni-MOF in combination with a Co-MOF. They also developed a dual Ni/Co-MOF-reduced graphene oxide (rGO) nanocomposite (Fig. 6a). The asymmetric device comprising activated carbon/Ni/Co-MOF-rGO demonstrated impressive performance, delivering a specific energy of 72.8 W h/kg at 850 W/kg and maintaining a capacity of 15.1 W h/kg even under the high specific power of 42.5 kW/kg. Furthermore, it exhibited exceptional cycle life, retaining 91.6% capacitance after 6000 charge–discharge cycles at 1 A/g.<sup>128</sup> In the work of Li *et al.*,<sup>129</sup> a controlled and straightforward two-step method was introduced for cultivating Ni-MOF arrays on the surface of  $\text{NiCo}_2\text{O}_4$  nanowires by regulating the MOFs' formation reaction (Fig. 6b). The  $\text{NiCo}_2\text{O}_4$ @Ni-MOF hybrid electrode, after optimization, demonstrates improved electrochemical performance. It presents a notable specific capacity of 208.8 mA h/g at a current density of 2 mA/cm<sup>2</sup>, alongside exceptional rate capability.<sup>129</sup>

Recent research focused also on the potential of using waste polyethylene terephthalate (PET) derived Ni-MOFs in the synthesis of the  $\text{NiO}_x$ @NPC nanocomposite (NiO<sub>x</sub> nanoparticles with nitrogenous porous carbon).<sup>113</sup> The simple solvothermal route used to synthesize this porous carbon composite has been described as cost-efficient. A schematic of the process can be seen in Fig. 6c. The BDC (benzene-1,4-dicarboxylic acid) utilised in this report's synthesis of the  $\text{NiO}_x$ @NPC came from discarded PET bottles. The final product showed good specific capacitance, cycling stability, and a high specific surface area (1523 m<sup>2</sup>/g). But nothing about whether it's appropriate for widespread implementation is mentioned.<sup>113</sup> In another context, a novel electrode material comprising MOFs (Zr-TAA, where TAA stands for *trans*-aconitic acid) and multi-walled carbon nanotubes (MWCNTs) was easily synthesized using a one-pot reflux method and subsequently employed in a high-performance supercapacitor (Fig. 6d). Due to its improved conductivity and even distribution of pore sizes, this composite material exhibits outstanding electrochemical performance, achieving a specific capacitance of 562.06 F/g. Moreover, it retains nearly all of its initial capacitance even after undergoing 1000 cycles of testing with a 6 M KOH electrolyte.<sup>130</sup>

A recent study has concentrated on developing a 3D Ni-MOF with an outstanding capacitance of 2150 F/g at a current density of 1 A/g.<sup>114</sup> Subsequently, the synthesized Ni-MOF and reduced graphene oxide were utilized as the anode and cathode electrode materials, respectively, in a two-electrode asymmetric supercapacitor device (ASC) setup (Fig. 6e). This ASC manifested a specific capacitance of 125 F/g (at 0.2 A/g) and showcased a high energy density of 50.17 W h/kg at a power density of 335.1 W/kg. Furthermore, the ASC demonstrated excellent reversibility (97.9% coulombic efficiency) and cycling stability



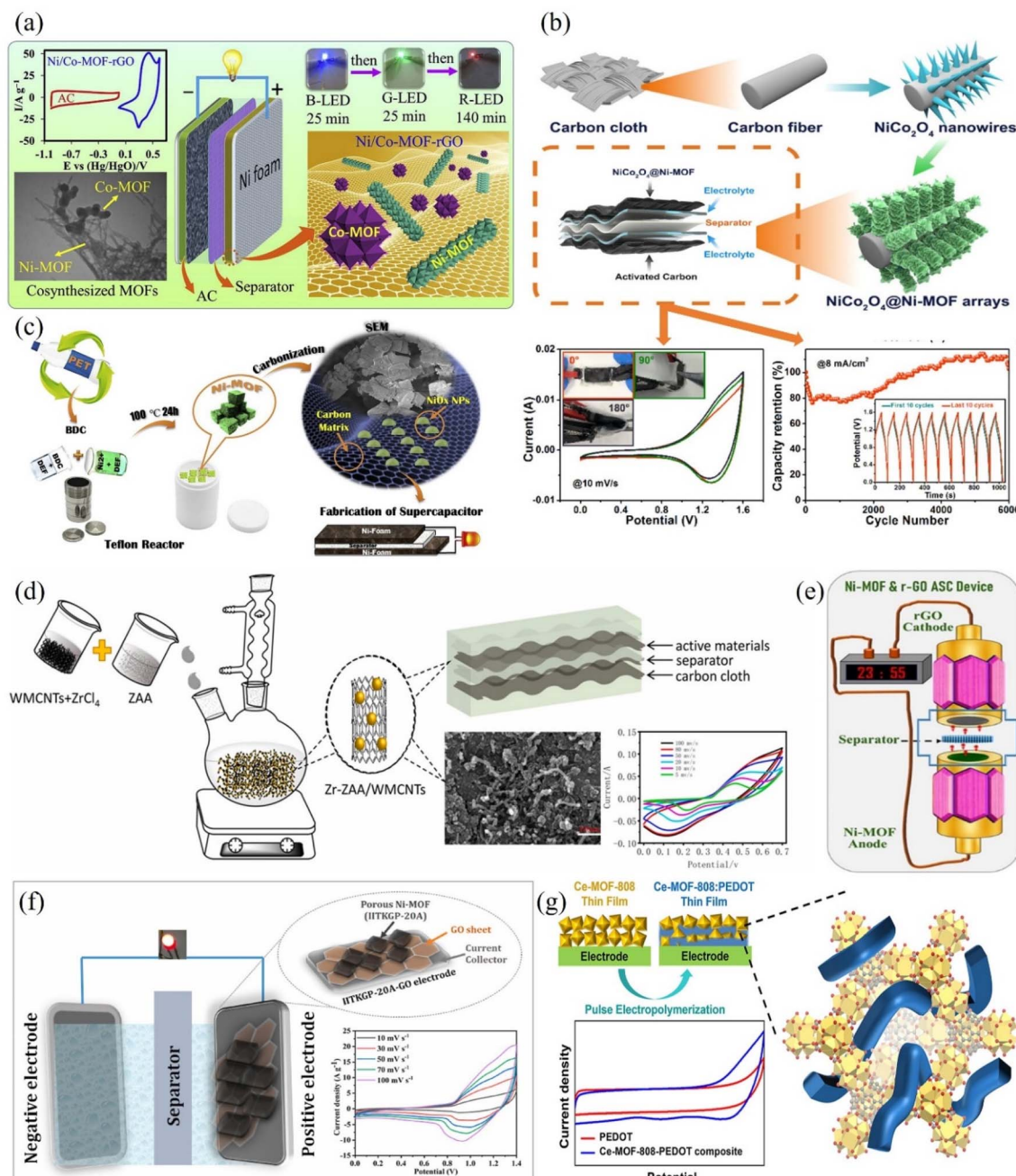


**Fig. 6** (a) An asymmetric AC//Ni/Co-MOF-rGO device showing a capacitance of 860 F/g@1.0 A/g in a 3E cell setup. Adopted from ref. 128 with permission. (b) A schematic depiction of the synthetic method employed to create core/shell hybrid arrays of  $\text{NiCo}_2\text{O}_4@\text{Ni-MOF}$  on a carbon cloth substrate and the corresponding CV curves, and cycling stability tested at 8 mA/cm<sup>2</sup>. Adopted from ref. 129 with permission. (c) Schematic diagram of the proposed method of synthesizing  $\text{NiO}_x@\text{NPC}$  nanocomposites using waste PET with enhanced electrical conductivity and stability and improved charge relocation operation for a better performance of supercapacitor devices. Adopted from ref. 113 with permission. (d) A novel electrode material, composed of MOFs (Zr-TAA, where TAA is *trans*-aconitic acid) and MWCNTs synthesized using a simple one-pot reflux method and applied to high-performance supercapacitors. Adopted from ref. 130 with permission. (e) A three-dimensional Ni-MOF used as an anode electrode in a two-electrode asymmetric supercapacitor device setup. Adopted from ref. 114 with permission. (f) Highly scalable and pH stable 2D Ni-MOF-based composites (ITKGP-20A-GO) for high-performance supercapacitors exhibiting a specific capacitance of ~840 F/g at 2 A/g current density. Adopted from ref. 131 with permission. (g) A cerium-based MOF@conducting polymer (PEDOT) nanocomposites for supercapacitors. Adopted from ref. 132 with permission.

(94%) after 5000 constant charge–discharge cycles. In the investigation by Sahoo *et al.*,<sup>131</sup> a microporous 2D Ni-MOF was elaborated, demonstrating high scalability and thermodynamic

stability across a wide pH range (2–10). Upon introducing GO with a weight percentage of 3%, a specific capacitance value of approximately 840 F/g at 2 A/g was achieved, ranking among the

highest within the category of bare MOFs and their composites/derived materials. Subsequently, when used as the electrode material in an asymmetric supercapacitor (Fig. 6f), it displayed a specific capacitance of 111.4 F/g at a current density of 2 A/g and exhibited excellent retention of 84% cycle life over 7000 cycles.<sup>131</sup>

The study by Wechsler *et al.*<sup>133</sup> reported the fabrication of supercapacitor electrodes using pristine nickel hexaaminobenzene ( $\text{Ni}_3(\text{HAB})_2$ ) metal–organic framework (MOF) *via* electrophoretic deposition (EPD). The symmetric supercapacitor employing the MOF showcases remarkable electrochemical capacitive performance within a potential range of 0–1 V, demonstrating an areal capacitance of  $13.64 \text{ mF/cm}^2$  and exceptional ultra-high cycling stability, maintaining 81% of its capacity over 50 000 cycles. The superior performance of the supercapacitor is attributed to the binder-free electrophoretic deposition (EPD) process and the distinctive structure of 2D MOF nanosheets, which promote ion diffusion throughout the electrodes. Additionally, the literature review explored the utilization of a combination of MOFs and conducting polymers. Nanocomposites were fabricated by combining a cerium-based MOF (Ce-MOF-808) with poly(3,4-ethylene dioxythiophene) (PEDOT) through pulse electrodeposition of PEDOT within thin films of Ce-MOF-808.<sup>132</sup> The highly porous Ce-MOF-808 displays reversible electrochemical reactivity, offering pseudocapacitance, while electronically conducting PEDOT contributes to a notable double-layer capacitance and enhances electronic conduction between the redox-active cerium sites in the MOF (Fig. 6g). As a result, the composite demonstrates superior performance compared to both pristine MOF and pristine electrodeposited PEDOT as active materials for supercapacitors.<sup>132</sup>

**3.2.2 Nanocrystalline MOFs.** Research has also advanced in the field of nanocrystalline MOFs (nMOFs) and coin-type cell SCs, this is another example of altering the morphologies of pristine MOFs to enhance their supercapacitive properties. Gu

*et al.*<sup>119</sup> posit that decreasing the particle size of MOFs into nanometre dimensions is an effective method for increasing their achievable capacitance. Particle size reduction improves the material's electrochemical performance significantly by lowering the electrolyte ion diffusion distance and raising the material's ESA.<sup>134</sup> These nMOFs were not commonly reported until recently. Only a few well-known MOFs, like MOF-5, ZIF-8, and ZIF-67, attracted attention because of their composition, which made downscaling simple. A variety of brand-new nMOFs have been developed and tested as part of recent research. Gu *et al.*<sup>119</sup> begin by synthesizing two MOF crystals *via* the adoption of the redox-organic linker from 3,30,5,50-oxybenzobenzenetetracarboxylic acid ( $\text{H}_4\text{L}$ ) and metal centres of  $\text{Ni}^{2+}/\text{Cu}^{2+}$  (Fig. 7a). An *in situ* solvothermal procedure was used in a single step to obtain the appropriate nanomaterials. One significant finding was that, with careful choice of solvent and surfactant, the different morphologies attained during material production could be efficiently controlled. When evaluated at current densities of 1 A/g and 5 A/g, respectively, one sample of the as-synthesized nano-NiMOF electrode produced capacitances of 1024.4 F/g and 648.9 F/g, demonstrating exceptional SC performance.<sup>119</sup>

Work by Choi *et al.*<sup>135</sup> explores the synthesis of a range of nMOF structures including HKUST-1, Zr-MOF, nMOF-867, and MOF-5. The nMOF-867 sample exhibited very good supercapacitive behaviour, achieving a capacitance of  $5.085 \text{ mF/cm}^2$ , almost 6 times higher than the achievable capacitance from a fabricated electrode using commercially available AC (Fig. 7b). After 10 000 charge–discharge cycles, the nMOF-867 electrode continued to show exceptionally good cycling stability, with a retention of over 90%. With a capacitance of  $5.085 \text{ mF/cm}^2$ , the Zr-MOF sample under evaluation demonstrated exceptional supercapacitive qualities. This is nearly a 6-fold increase above the capacitance provided by an AC electrode made from commercially available AC. Additionally, the Zr-MOF electrode

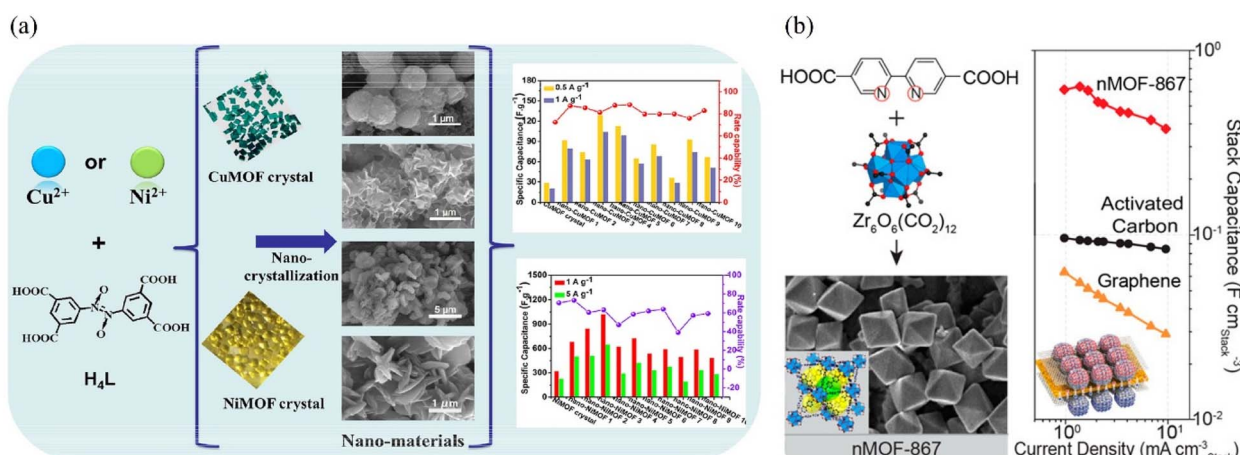


Fig. 7 (a) *In situ* solvothermal synthesis of nanoscale CuMOF and NiMOF crystals and their specific capacitance (1024.44 F/g and 128.82 F/g for nano-NiMOF and nano-CuMOF respectively) and rate capacitance. Adopted from ref. 119 with permission. (b) Nanocrystals nMOF-867 with exceptionally high capacitance showing a stack and areal capacitance of 0.64 and  $5.09 \text{ mF cm}^{-2}$ , respectively, with performance maintained over at least 10 000 charge/discharge cycles. Adopted from ref. 135 with permission.



demonstrated exceptionally high cycling stability (greater than 90%, which is considered ultrahigh) even after 10 000 cycles.<sup>135</sup>

Some 2-dimensional (2D) MOFs with a high SSA and tunable porosity have been discovered recently. In their pure state, these MOFs can give sufficiently high electrical conductivity for SC applications.<sup>136</sup> Charge delocalisation inside the material's planes and prolonged pi-conjugation provide this electrical conductivity.<sup>137</sup> Sheberla *et al.*<sup>136</sup> observed MOF Ni<sub>3</sub>(HITP)<sub>2</sub>'s high bulk electrical conductivity (over 5000 S/m), a value that exceeds those achieved by AC and porous graphite. The first non-carbon-based EDLC symmetric SC was fabricated using Ni<sub>3</sub>(HITP)<sub>2</sub> electrodes after this discovery. After 10 000 cycles, the supercapacitor showed an extremely high areal capacitance of 18 mF/cm<sup>2</sup>, and 90% capacity retention.<sup>136</sup> Another 2D MOF that has been investigated for high-performing SC electrodes is hexaaminobenzene (HAB)-derived MOF. Feng *et al.*<sup>138</sup> reported both a high volumetric and areal capacitance (760 F/cm<sup>3</sup> and 20 F/cm<sup>2</sup> respectively). The cycle life data were similarly encouraging, demonstrating that capacitance retention could only be increased by a factor of 10 after 12 000 charging-discharging cycles. Research indicates that selecting the right electrolyte is essential for optimal SC performance. In one experiment, a 1 M LiOH aqueous electrolyte and a Co-based MOF electrode operated at a current density of 0.6 A/g produced a specific capacitance of 206.76 F/g.<sup>123</sup> Furthermore, retention of this capacitance was good (up to 98.5%) over 1000 test cycles. However, when the electrolyte was changed to KCl or KOH, the performance of the electrode was not satisfactory.

**3.2.3 Environmental impacts.** Literature focusing on MOF toxicity is limited, and the topic is generally poorly understood.<sup>125</sup> If a MOF is toxic, this is likely the result of the organic ligand metal ions or functional groups.<sup>139</sup> The metal ions in MOFs are in the form of nanoparticles that are nonbiodegradable.<sup>125</sup> Kumar *et al.*<sup>125</sup> have suggested that out of the most common metal ions in MOFs, zinc and iron are likely to be the least toxic as they are used in the human body. While the toxicity of MOFs may not be fully known, some sources suggest that when MOFs decompose, they may exhibit the same toxicity levels as constituent raw materials from which they are generated. In summary, when considering the environmental impact of MOFs, several factors come into play. (1) Synthesis process: the synthesis of MOFs often involves solvents and energy-intensive processes. Depending on the specific synthesis route, this could contribute to environmental impacts such as greenhouse gas emissions and resource depletion. However, efforts are being made to develop more sustainable synthesis methods, such as using green solvents or employing energy-efficient techniques. (2) Resource utilization: the materials used in MOF synthesis, such as metal ions and organic ligands, can have environmental implications depending on their sources and extraction methods. For example, if the extraction of metal ions involves environmentally damaging processes or if rare or toxic elements are used, it could pose environmental concerns. (3) End-of-life disposal: consideration should be given to the disposal of MOF-based supercapacitors at the end of their lifespan. While MOFs themselves are generally stable materials, the electrodes and other components of supercapacitors may contain metals or other materials that could

pose environmental risks if not properly managed through recycling or safe disposal methods. (4) Performance and durability are key considerations for MOF-based supercapacitors. These devices have inherent advantages such as high surface area and customizable pore structures, which can significantly improve their performance. If MOFs can facilitate the development of supercapacitors with greater energy density and prolonged cycle life compared to conventional materials, it could have a positive impact on the environment. By extending the lifespan of electronic devices and minimizing the frequency of replacements, this advancement has the potential to reduce environmental impacts. (5) Scale of production: as with any technology, the environmental impact of MOF-based supercapacitors will depend on the scale of production and deployment. Large-scale production could lead to increased energy consumption, waste generation, and resource depletion if not managed properly. The environmental impact and sustainability of Metal–Organic Frameworks (MOFs) used in supercapacitors necessitate a thorough examination, particularly when compared to traditional materials. MOFs like nMOF-867 exhibit superior electrochemical properties, with a stack capacitance of 0.644 F cm<sup>3</sup> and an areal capacitance of 5.085 mF cm<sup>2</sup>, far surpassing commercial activated carbon supercapacitors.<sup>140</sup>

However, most of the methods for MOF synthesis incorporate eco-toxic solvents, such as *N,N*-dimethylformamide, coupled with high energy requirements, which may pose a serious environmental impact. Therefore, an in-depth LCA is needed in estimating these materials. For instance, high carbon footprint and energy use can be associated with the production of MOFs; for instance, nMOF-867 is associated with high environmental cost despite its high performance and long lifetime, maintaining activity beyond 10 000 cycles.<sup>141</sup> Moreover, the environmental advantages of MOFs like UiO-66-NH<sub>2</sub>, which can be synthesized using aqueous methods reducing environmental impacts by up to 91%, must be weighed against challenges such as degradation and scalability. These methods yield a cradle-to-gate carbon footprint of 43 kg CO<sub>2</sub> eq/kg and a lower production cost of \$15.8 per kg compared to solvothermal processes.<sup>142</sup> On the long-term sustainability front, MOFs still hold much promise because green synthesis methods using either water or ethanol as solvents have already been developed, and biodegradable MOFs that can minimize their impact on the environment are under construction. Although this might be the case, there is a clear lack of long-term data relating to MOF recyclability and degradation, and their high initial production costs underline the necessity for performing holistic LCA with respect to end-of-life disposal and possible environmental release to make such next-generation materials more environmentally and economically feasible against traditional ones.<sup>143</sup>

### 3.3 Metal–organic frameworks for battery technologies

MOFs and their derivatives have garnered much interest and proved rather promising to improve sodium-ion battery (SIB), and lithium-ion battery (LIB) performance. The work by Zhao *et al.*<sup>144</sup> proved the potential of Prussian blue analogues (PBAs) as SIB cathode materials through effective etching. Specifically,



etching  $\text{Na}_2\text{NiFe}(\text{CN})_6$  ( $\text{NaNiHCF}$ ) into a dice shape increased its specific surface area, enhancing sodium storage sites and accelerating  $\text{Na}^+$  diffusion. The etched  $\text{NaNiHCF-3}$  showed a large reversible capacity of 83.5 mA h/g that accounted for about 98.2% relative to the theoretical capacity, while the unetched counterpart precursor only delivered 76.8 mA h/g. Moreover,  $\text{NaNiHCF-3}$  exhibited 71.2 mA h/g at 10C with a rate capability far beyond that of other electrodes and maintained a very stable life with 94% capacity retention over 1000 cycles at 1C. These results further underline the role of morphological control in the electrochemical performance of MOFs with respect to capacity use and cycling stability. Indeed, the tunable porosity and high surface area of MOFs enable theoretically improved ion transport and storage capabilities. For example, nitrogen-doped amorphous Zn-carbon multichannel fibers have exhibited a coulombic efficiency above 99% for more than 500 cycles at current densities from 1 to 5 mA cm<sup>2</sup>, demonstrating major improvements in lithium metal anode performance. Symmetric cells based on these materials achieve stable cycling for over 2000 hours, which is the potential for long-term applications.<sup>145</sup> However, the synthesis process is complex due to electrospinning and MOF coating, and this complicates large-scale production. The specific capacity of 104 mA h/g during the high rate of 5C in the full-cell tests with  $\text{LiFePO}_4$  cathodes is quite encouraging, but its broader compatibility with various cathode materials remains to be explored. While these MOF-derived materials could effectively reduce dendrite formation and issues regarding local current density, the long-term stability in a range of environmental conditions remains to be evaluated.

Always in the context of LIBs, the study of Du *et al.*<sup>146</sup> presents an efficient synthesis of 2D layered Mo-MOF@PPy via reflux heating and coating methods, aimed at improving the performance of anode materials in LIBs. Serving as a precursor during the electrochemical reaction, the high-valence Mo within the Mo-MOF effectively binds with  $\text{Li}^+$ , thereby contributing to the superior electrochemical performance of the material. Additionally, the polypyrrole (PPy) coating significantly enhances the electrical conductivity of the composite by promoting electron transfer. As a result of these synergistic effects, Mo-MOF@ppy achieves a specific capacity of 930 mA h/g at a current density of 100 mA/g and retains a capacity of 750 mA h/g at 500 mA/g after 200 cycles. In a similar study, Zhao *et al.*<sup>147</sup> utilized stannous sulfate ( $\text{SnSO}_4$ ) and graphene to synthesize Sn-MOFs/G nanorods, which were evaluated as anode materials for LIBs. The resulting material exhibited a high specific capacity of 462 mA h/g after 500 cycles at 1 A/g and demonstrated remarkable rate performance, achieving 265 mA h/g at 2 A/g.

In detail, the recent progress involving MOFs and MOF-derived materials has unveiled their huge potential towards enhancing the performance of batteries. For example, the synthesis of copper-substituted  $\text{CoS}_2@\text{Cu}_x\text{S}$  DSNBs by a multi-step MOF-based templating strategy resulted in very impressive electrochemical properties, such as high capacity (535 mA h/g at 0.1 A/g), better rate capability (333 mA h/g at 5 A/g), and extended cycling stability (76% capacity retention over 300

cycles).<sup>148</sup> The improvements may be attributed to their complex nanostructure, which provided enhanced ionic and electronic conductivity, improved electrochemical reactivity, and mechanical stability. In this respect, this approach can overcome the poor conductivity and fast capacity fading of sulfur metal through the combination of different active materials with hierarchical hollow structures, which can reduce ion diffusion paths and strain accommodation during cycling. Rational design and controlled composition, as emphasized in the present work, are preliminary steps for the development of high-performance anode materials, and this work further confirms the bright application of MOF-derived materials in next-generation batteries. Although these results are very promising, problems like intrinsic instability of MOFs in electrolyte environments and scalability issues, coupled with generally low electrical conductivity, have to be resolved before their full potential is tapped. Therefore, future studies should address the issues of scalability and stability if the full potential of MOFs in battery applications is to be exploited, ensuring technological advancement with sustainability.

The main advantage of MOFs over activated carbon in energy storage devices lies in their highly tunable structure and functional versatility. MOFs are composed of metal nodes connected by organic linkers, allowing precise control over pore size, shape, and surface chemistry. This tunability enables the design of materials with optimized ion transport and storage, potentially leading to higher capacitance and energy density. Unlike activated carbon, which often has a broad and irregular pore size distribution, MOFs can be synthesized with uniform and well-defined pores, ensuring consistent ion diffusion and reducing resistance during charge-discharge cycles. Additionally, the organic linkers in MOFs can be chemically modified to introduce specific functional groups that enhance interactions with electrolyte ions, while the metal centers can be selected or doped to introduce redox activity, contributing additional pseudocapacitance. MOFs can also encapsulate or host other functional materials, further enhancing their electrochemical performance by providing additional active sites or improving electrical conductivity. This versatility in synthesis and integration with conductive materials makes MOFs a promising material for next-generation supercapacitors, offering the potential for higher energy densities, improved ion transport, and customizable electrochemical properties. However, challenges such as low conductivity, stability, and cost still need to be addressed for MOFs to become a widely adopted alternative in commercial applications.

### 3.4 MOF metal nodes, ligand architecture and synthesis strategies

In MOFs, the metal nodes, also known as metal clusters or secondary building units (SBUs), play a pivotal role in determining the structure and properties of these materials. These nodes form the inorganic backbone of the MOF and are interconnected by organic ligands to create an extended porous network. The composition of these nodes can vary widely, ranging from simple single metal ions like  $\text{Zn}^{2+}$ ,  $\text{Cu}^{2+}$ , or  $\text{Fe}^{3+}$ ,



which can coordinate with multiple ligands, to more complex metal clusters such as  $\text{Zr}_6\text{O}_4(\text{OH})_4$  or  $\text{Cr}_3\text{O}$ , which involve multiple metal ions linked together, contributing to the stability and diversity of the MOF structure.<sup>149</sup> The coordination environment of the metal nodes, defined by the number of ligands or atoms bonded to the metal ion, is crucial in determining the geometry of the node, which in turn influences the overall topology and dimensionality of the MOF. For example, a metal node with a high coordination number can lead to the formation of highly connected, three-dimensional frameworks, whereas lower coordination numbers might result in simpler, two-dimensional or even one-dimensional structures.

The metal nodes not only shape the structural framework but also impart distinct chemical properties to the MOF. The choice of metal can significantly influence attributes such as thermal stability, chemical reactivity, and catalytic activity. Transition metals like chromium (Cr), zirconium (Zr), or titanium (Ti) are known for imparting higher stability and robustness to the MOF, making them suitable for applications that require durability. On the other hand, metals like copper (Cu) or zinc (Zn) offer tunable reactivity, which can be advantageous in catalytic processes. Metal nodes also play a critical role in the functionality of MOFs. For instance, they can act as active sites for catalysis, with MOFs containing iron (Fe) or cobalt (Co) nodes being explored for oxidation reactions.<sup>150,151</sup> Additionally, the type of metal used in the nodes affects the adsorption characteristics of the MOF, particularly in gas adsorption applications. MOFs with unsaturated metal sites, such as those with open metal sites, can strongly adsorb gases like  $\text{CO}_2$  or  $\text{H}_2$ , making them valuable for gas storage and separation technologies.

Moreover, the electrical properties of MOFs are influenced by the metal nodes, which is particularly important in applications such as supercapacitors and batteries, where conductivity is essential. Metal nodes can also be tuned through post-synthetic modifications, allowing for the enhancement or alteration of the MOF's properties. This can be achieved through metal exchange or doping, introducing new functionalities or improving stability. For example, in MOFs like HKUST-1, which utilizes  $\text{Cu}^{2+}$  ions as the metal node, the resulting structure is a robust three-dimensional framework that has been widely studied for gas storage.<sup>152</sup> Similarly, MIL-101, which contains  $\text{Cr}^{3+}$  ions, is renowned for its exceptional thermal and chemical stability, making it suitable for various industrial applications.<sup>153</sup> Another notable example is UiO-66, where  $\text{Zr}^{4+}$  ions provide high stability, making it a popular choice for gas storage and separation.<sup>154</sup> Overall, metal nodes are a crucial design element in MOFs, as they not only determine the structural framework but also significantly influence the functional properties, making them central to the development of advanced materials for a wide range of applications.

On the other hand, ligand architecture in MOFs is a crucial determinant of their structural integrity, topology, and functional properties. Organic ligands, or linkers, connect metal nodes or clusters to form the extended porous networks characteristic of MOFs. The size and shape of these ligands significantly influence the MOF's pore dimensions and overall

framework.<sup>155,156</sup> For instance, longer ligands typically create larger pores, which can be advantageous for applications like gas storage or catalysis, while the geometric arrangement of the ligands whether linear, angular, or branched affects the dimensionality and complexity of the MOF structure. Functional groups on the ligands, such as carboxylates, phosphonates, imidazolates, or sulfonates, play a pivotal role in determining the strength and nature of the coordination bonds with metal nodes, impacting the MOF's stability and reactivity. For example, carboxylate groups form strong bonds with metal ions, leading to highly stable frameworks like those in UiO-66, while functional groups such as amines or hydroxyls can enhance adsorption properties by introducing sites for hydrogen bonding.<sup>154</sup> The connectivity of the ligands and how many coordination sites they offer affect the density of the network and the robustness of the resulting MOF. Ligands with higher connectivity can create more intricate and stable 3D frameworks, as seen in HKUST-1, where the bidentate trimesic acid ligand coordinates with multiple metal ions.<sup>157</sup> Additionally, the coordination mode of the ligand, whether monodentate, bidentate, or multidentate, influences the rigidity and stability of the framework. Ligand architecture can also be tuned through post-synthetic modifications, allowing for the introduction of new functionalities or enhancements, such as improved  $\text{CO}_2$  capture capacities through the addition of amine groups. Examples of MOFs that showcase the importance of ligand architecture include the IRMOF series, which utilizes terephthalic acid ligands to form various frameworks with different properties, and ZIFs (Zeolitic Imidazolate Frameworks), where the imidazolate ligands create highly stable, zeolite-like structures.<sup>158,159</sup>

Regarding the synthesis of MOFs, it encompasses a variety of methods, each tailored to achieve specific structural, compositional, and functional characteristics in the final material.<sup>160</sup> Hydrothermal synthesis involves dissolving metal salts and organic ligands in water, followed by heating the solution in a sealed container under high temperature and pressure. This method, widely used for its simplicity, produces high-quality MOF crystals, as seen in the synthesis of UiO-66, where zirconium chloride reacts with terephthalic acid.<sup>161</sup> Solvothermal synthesis, a variant that uses organic solvents instead of water, allows for the formation of MOFs that are sensitive to water or require particular solvents for solubility, such as HKUST-1, which is synthesized using a solvent system involving alcohols and acetic acid.<sup>162</sup> Ligand-assisted synthesis leverages pre-formed metal-organic complexes to guide the growth of MOFs, enhancing uniformity and control over the final product's properties.

Microwave-assisted synthesis of MOFs is grounded in the principle of using electromagnetic radiation to interact with removable electronic components, such as electrons, ions, or polar molecules in solids, or ions and electrons in liquids. This method typically operates at temperatures above 100 °C and within reaction times of no more than 60 minutes. Improvements in reaction conditions can be achieved by optimizing various factors, including the choice of solvent, duration of radiation exposure, temperature, intensity of microwave



radiation, and the quantities of reactants. Adjusting these variables helps to enhance the efficiency and quality of the MOF synthesis process.<sup>163</sup> Electrochemical synthesis utilizes an electric current to drive the formation of MOFs from metal salts and ligands, allowing precise control and the creation of MOFs with unique properties, including thin films or coatings on conductive substrates. Moreover, solvothermal–hydrothermal hybrid synthesis combines aspects of both methods, using a solvent system that interacts with both water and organic components, useful for synthesizing MOFs with specific property balances. Post-synthetic modification, though not a primary synthesis method, involves altering the MOF framework after its initial formation through techniques like ligand exchange or metal ion substitution, tuning the MOF's functionality and stability for specialized applications. Direct synthesis from metal oxides uses metal oxides or salts directly to form MOFs in the presence of organic ligands under controlled conditions, advantageous for creating highly stable frameworks. Each of these methods offers unique advantages depending on the desired MOF properties, such as crystal size, pore structure, stability, and functional capabilities, making them crucial for tailoring MOFs to specific applications.<sup>164,165</sup>

## 4 Photocatalysis

In 1972, Fujishima and Honda's pioneering work saw the creation of the first photocatalytic system using  $\text{TiO}_2$  and ultraviolet light irradiation.<sup>166</sup> Since then, a variety of materials have been investigated for photocatalysis applications. As noted by Djurišić *et al.*,<sup>167</sup> there have been few advancements or breakthroughs in photocatalyst concepts and designs. The majority of current research shows only modest advancements, and if photocatalytic technologies are to ever be used on an industrial scale, a significant amount of research and development will be needed. The standards for an effective photocatalyst are generally agreed upon in the literature. The material's characteristics should, in general, permit well-visible light absorption, sufficient degree of resistance to photo corrosion and ideally should inhibit the recombination of electron–hole pairs.<sup>168</sup> Work by Dhakshinamoorthy *et al.*<sup>169</sup> further stresses the importance of responsiveness to visible light to ensure the efficient use of solar energy, by emphasizing that visible light makes up 43% of total solar energy. Shanmugham *et al.*<sup>168</sup> provide a range of ideal photocatalyst material properties to help achieve these goals, including a high surface area, narrow band gap, and thermal stability. In addition, several papers agree on the importance of photocatalyst morphology and structure for performance as it influences the surface area and the availability of active sites.

### 4.1 Conventional photocatalytic materials

Photocatalysis is a transformative technology that leverages light to drive chemical reactions, offering innovative solutions in various fields including environmental remediation, energy production, and chemical synthesis. At the heart of this technology are photocatalyst materials, which absorb photons and

use this energy to facilitate or accelerate chemical processes. Among conventional photocatalyst materials are titanium dioxide ( $\text{TiO}_2$ ), zinc oxide ( $\text{ZnO}$ ), and carbon-based materials such as graphene oxide (GO), and reduced graphene oxide (rGO). Each of these materials has its strengths and limitations, so the choice of photocatalyst often depends on the specific application and the desired properties. Pawar *et al.*<sup>170</sup> hail titanium dioxide ( $\text{TiO}_2$ ) nanoparticles as being among the most promising photocatalyst materials for commercial use. This is due to their superb optical and electronic characteristics, excellent chemical stability, high photoactivity, low cost, and reusability. Various morphologies of titania photocatalysts, spanning from nano to macrostructures, have been documented in the literature.<sup>171</sup> These encompass spherical particles, rod-like structures, tubular forms, fibrous configurations, and sheet-like arrangements at the nanoscale (Fig. 8a). These diverse morphologies have been meticulously designed to achieve distinct photocatalytic capabilities by fine-tuning factors such as particle size, specific surface area, pore structure and volume.<sup>171</sup> Research by Zhao *et al.*,<sup>177</sup> however, emphasizes the disadvantages of semiconductor nanoparticles (NPs) such as  $\text{TiO}_2$  including a complex separation process from reaction systems, and a high rate of recombination of photogenerated electron–hole pairs.  $\text{TiO}_2$  is also prone to aggregation in reactions which reduces its effective surface area and therefore performance.

In their work, Moma and Baloyi<sup>178</sup> postulate that the main issue with  $\text{TiO}_2$  photocatalysts is the bandgap (3.2 eV). As a result, only 5% of the solar spectrum of the UV light region can be used for photocatalysis.  $\text{TiO}_2$  has a low photocatalytic efficiency as a result. Research by Zhao *et al.*<sup>177</sup> supports this view, by arguing that this disadvantage is the primary hindrance preventing the use of  $\text{TiO}_2$  in isolation for photocatalysis. To increase  $\text{TiO}_2$ 's efficiency, current research also attempts to enhance its photocatalytic activity under visible light irradiation.<sup>179</sup> One method investigated is nitrogen-doped  $\text{TiO}_2$ , results of such studies show enhanced photocatalytic activity compared to pure  $\text{TiO}_2$ .<sup>178</sup> Recent studies also suggest that modifying the defects in  $\text{TiO}_2$  can expand the range of light absorption and enhance the efficiency of charge separation. Various methods, including hydrogenation, plasma treatment, chemical reduction, electrochemical reduction, and oxidation (Fig. 8b),<sup>172</sup> are employed to produce defective  $\text{TiO}_2$  photocatalysts. These catalysts exhibit different types of defects, encompassing bulk and surface defects, and their relevance in photocatalytic applications is documented.<sup>172</sup> Notably, oxygen vacancies and  $\text{Ti}^{3+}$  defects are identified as pivotal factors in augmenting photocatalytic performance.

Due to the wide band gap of  $\text{TiO}_2$ , its application in visible photocatalysis is limited. To address this issue, several studies propose introducing oxygen vacancies and carbon quantum dots (CQDs) with up-conversion properties to enhance photocatalytic activity. Li *et al.*<sup>173</sup> prepared various configurations, including one-dimensional  $\text{TiO}_2$  nanotubes (TNs), TNs with oxygen vacancies (OVTNs), TNs embedded with composite CQDs (CQD-TNs), and OVTNs embedded with composite CQDs (CQD-OVTNs). The impact of oxygen vacancies and CQDs on



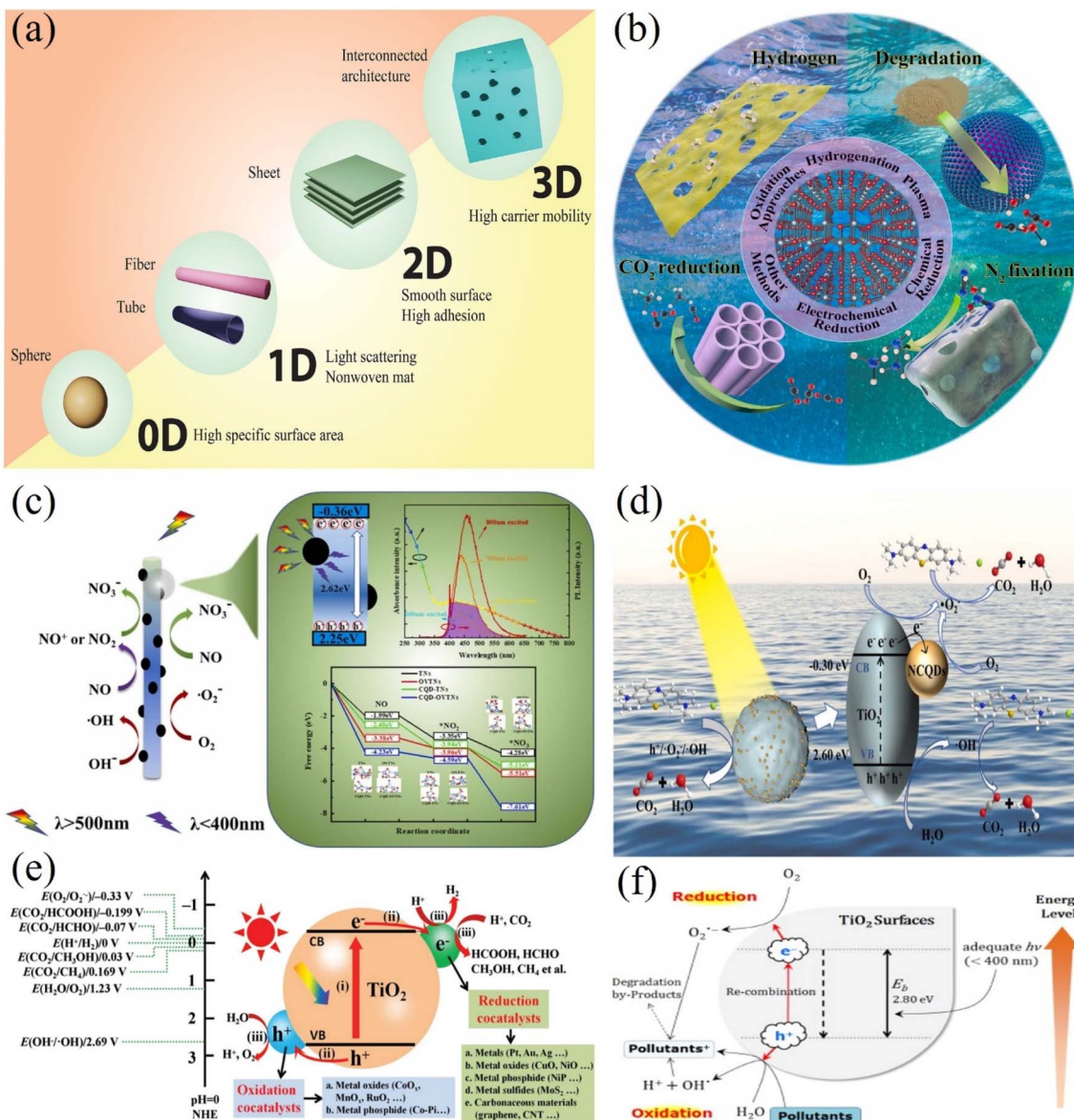


Fig. 8 (a) Various structural configurations of  $\text{TiO}_2$  at both the nano and macro scales. Adopted from ref. 171 with permission. (b) A schematic diagram depicting the utilization of defective  $\text{TiO}_2$  materials in photocatalytic applications.  $\text{TiO}_2$  photocatalysts are fabricated using various methods such as hydrogenation, plasma treatment, chemical reduction, electrochemical reduction, and oxidation. Adopted from ref. 172 with permission. (c) Oxygen vacancies and carbon quantum dots (CQDs) with up-conversion properties for enhanced photocatalytic activity of  $\text{TiO}_2$  for NO removal under visible light irradiation. Adopted from ref. 173 with permission. (d) Mechanism for the degradation of methylene blue using NCQDs/ $\text{TiO}_2$  under solar irradiation. Adopted from ref. 174 with permission. (e) Illustration of the photocatalytic reactions occurring on  $\text{TiO}_2$ -based photocatalysts, enhanced with reduction and oxidation cocatalysts. The redox potentials of various species at pH = 0, referenced to the NHE, are also depicted. Adopted from ref. 175 with permission. (f) Pollutant removal through the generation of photoinduced charge carriers ( $e^-/h^+$ ) on the surfaces of semiconductor  $\text{TiO}_2$  particles. Adopted from ref. 176 with permission.

$\text{NO}_x$  removal through photocatalysis was investigated. Results show that CQD-OVTNs exhibit a significant synergistic effect between CQDs and oxygen vacancies, enhancing visible photocatalytic NO removal efficiency by approximately 12, 2, and 2.6 times compared to TNs, OVTNs, and CQD-TNs, respectively (Fig. 8c).<sup>173</sup> Similarly, nitrogen-doped carbon quantum dots (NCQDs) were utilized to enhance  $\text{TiO}_2$  through a simple hydrothermal–calcination synthesis method.<sup>174</sup> The incorporation of NCQDs enhances visible light absorption and facilitates

electron transfer, thereby improving the separation of photo-generated electron–hole pairs. Even with a low NCQD content of 3 wt%, the photodegradation rate for methylene blue was 2.25 times faster compared to pristine  $\text{TiO}_2$ .

A plausible mechanism for the photocatalytic degradation of methylene blue (MB) by NCQDs/ $\text{TiO}_2$  is depicted in Fig. 8d.<sup>174</sup> When exposed to sunlight, electrons within the valence band (VB) of  $\text{TiO}_2$  absorb photon energy from solar radiation, generating electron ( $e^-$ ) hole ( $h^+$ ) pairs in the conduction band

(CB) and VB, respectively. The  $e^-$  can readily combine with dissolved oxygen in water to form  $\cdot O_2^-$ . Furthermore, the  $h^+$  can oxidize  $OH^-$  and  $H_2O$  molecules adsorbed on the  $TiO_2$  surface to produce  $\cdot OH$  radicals. However,  $e^-$  and  $h^+$  often recombine with low efficiency, limiting photocatalytic activity. The introduction of nitrogen-doped carbon quantum dots (NCQDs) serves to enhance visible light absorption and promote charge transfer. Consequently, more photocarriers are generated, and their recombination is substantially suppressed, resulting in a notable increase in efficient active radicals. Consequently, with the combined action of  $h^+$ ,  $\cdot O_2^-$ , and  $\cdot OH$  radicals, methylene blue (MB) molecules undergo mineralization to yield  $CO_2$  and  $H_2O$ .<sup>174</sup>

In a comprehensive photocatalytic process employing a  $TiO_2$ -based photocatalyst, three primary stages are involved: (1) absorption of light and the generation of photogenerated electron-hole pairs by  $TiO_2$ , (2) separation and transfer of these photogenerated electron-hole pairs, and (3) redox reactions occurring on the surface of  $TiO_2$  and cocatalysts (as depicted in Fig. 8e). These consecutive steps collectively govern the overall photocatalytic effectiveness of  $TiO_2$ -based photocatalysts.<sup>175</sup> On the other hand, to utilize semiconductor photocatalysts for water treatment, several requirements must be met: the process should be feasible at room temperature and pressure, ensuring complete mineralization without generating secondary pollution.<sup>176</sup> In addition, it should enable repetitive cycles and maintain low operational costs.  $TiO_2$  photocatalysis embodies a photo-induced charge separation process occurring on the  $TiO_2$  surface, which generates highly reactive oxygen species capable of microbial inactivation and organic mineralization without producing secondary pollutants.

The schematic representation depicted in Fig. 8f illustrates the elimination of pollutants through the generation of photo-induced charge carriers ( $e^-/h^+$ ) on the surfaces of semiconductor  $TiO_2$  particles.<sup>176</sup> Upon exposure to UV light, the surface of  $TiO_2$  catalysts suspended in water triggers photo-induced electrons in the conduction band to participate actively in reduction processes. Typically, they interact with dissolved oxygen in the air, resulting in the generation of superoxide radical anions. Meanwhile, the photo-induced holes in the valence band migrate to the surface of  $TiO_2$  and react with adsorbed water molecules, leading to the formation of hydroxyl radicals.<sup>176</sup> It is worth noting that hydroxyl radicals ( $OH^\cdot$ ) play a crucial role as primary active species in the photocatalytic oxidation reaction.

Regarding the environmental impact,  $TiO_2$  has been described as eco-friendly as not only is it reusable (for photocatalysis) but it is also non-toxic,<sup>170,180</sup> with Chen *et al.*<sup>181</sup> claiming it's "the most efficient and environmentally benign photocatalyst". However, there is concern over the potential effects of  $TiO_2$  nanoparticles on humans and animals.<sup>182</sup> Although the shape and magnitude of  $TiO_2$  nanoparticles are mostly determined by the physical and chemical properties of the particles, research on the mechanistic toxicology of these particles indicates that they may induce genotoxicity, inflammation, and cell destruction.  $TiO_2$  nanoparticles have been identified by the National Institute for Occupational Safety and

Health as potentially carcinogenic to humans as a result.<sup>182</sup> In their life cycle assessment (LCA), Wu *et al.*<sup>183</sup> evaluated the impact of nano- $TiO_2$  based on a range of synthesis routes. They discovered that physical synthesis approaches produced a greater environmental impact since they needed large amounts of supporting gas and substantial energy inputs. Chemical routes have a fair amount of impact, with upstream precursor production accounting for a large share of that impact. Because of the bacteria culture media utilised, biological channels also posed a significant environmental impact. Because organic precursors required large amounts of organic solvents, they performed especially poorly. The LCA model included a freshwater ecotoxicity evaluation factor to account for the possibility of nano- $TiO_2$  leakage into water sources. It is crucial to remember that while appropriate modelling assumptions have been made and some  $TiO_2$  production pathways are not covered by this LCA, total correctness cannot be guaranteed.<sup>183</sup>

On the other hand,  $TiO_2$  is generally considered cost-effective for photocatalytic uses.<sup>180</sup> Furthermore, novel cost-effective production methods are still being developed. An example is the facile sequential calcination and ball milling strategy.<sup>184</sup> It was stated that a post-treatment procedure was developed for less expensive  $TiO_2$  photocatalysts with lower photocatalytic activity. The straightforward and affordable method seeks to raise the less expensive  $TiO_2$  photocatalysts' photocatalytic activity to the same degree as more expensive commercial counterparts with higher photoactivities. This procedure about ninety-fold improves the performance of inexpensive KA100 in lab testing. In addition to  $TiO_2$ , zinc oxide ( $ZnO$ ) and carbon-based materials have garnered significant attention as photocatalysts due to their excellent transport properties, affordability, and versatile morphological structures. In the work of Sansenya *et al.*,<sup>185</sup> photocatalysts based on  $ZnO$  with a specific surface area of about  $10.6\text{ m}^2/\text{g}$  were prepared. The materials have demonstrated the high photodegradation capacity of reactive red 141 (R141), Congo red (CR), and Ofloxacin after 20, 60, and 180 minutes of solar light irradiation, respectively. The stability of the photocatalyst was confirmed after three cycles of use, maintaining high performance even after the third cycle, indicating its promising reusability. In a similar context, silver was incorporated into  $ZnO$  photocatalysts at varying concentrations, exhibited a hexagonal phase with notable performance under visible light and improved anti-photocorrosion properties.<sup>186</sup> Complete removal of reactive red dye and ofloxacin antibiotic was achieved after 25 and 80 minutes of irradiation, respectively. The enhanced photocatalytic activity is attributed to the efficient separation of electron-hole pairs at the photocatalyst interface. The introduction of metallic silver onto the  $ZnO$  photocatalyst creates a Schottky barrier at the silver/ $ZnO$  interface, which enhances quantum efficiency and photocatalytic activity.

Kim *et al.*<sup>187</sup> introduced a novel, high-efficiency catalyst based on a boron-doped  $C_3N_4/ZnO$  composite. This composite demonstrated a significantly enhanced photocatalytic hydrogen evolution rate, approximately 2.9 times greater than that of undoped  $C_3N_4/ZnO$ . This is a straightforward and effective



approach for designing highly efficient heterojunction photocatalysts by utilizing charge transfer switching *via* doping. Recently, it has been found that decorating the Rh co-catalyst of the benchmark GaN-ZnO photocatalyst with  $\text{Al}_2\text{O}_3$  species *via* atomic layer deposition significantly mitigates reverse reactions.<sup>188</sup> This modification enhances photocatalytic oxygen water splitting (OWS) activity by more than an order of magnitude, with an apparent quantum efficiency increase from 0.3 to 7.1% at 420 nm. The partial coverage of Rh surface sites with inert  $\text{Al}_2\text{O}_3$  effectively suppresses reverse reactions by obstructing the reduction/oxidation cycle of Rh atoms during the photocatalytic OWS process. Moreover, combining ZnO with carbon-based materials, such as graphene oxide, can further enhance its photocatalytic properties. Indeed, an efficient photocatalyst was successfully synthesized using GO/ZnO nanocomposites with embedded metal nanoparticles through a simple one-pot method.<sup>189</sup> A catalytic activity of 84% for the degradation of methylene blue (MB) dyes was achieved with a nanocomposite containing 3.125% GO after 90 minutes of sunlight irradiation. Thus, the GO-ZnO-Ag nanocomposite demonstrates significant potential as an efficient and adaptable photocatalyst for the photodegradation of organic dyes in industrial wastewater. In another study, the photocatalytic degradation of Rhodamine B (RhB) and MB by a material comprising sol-gel synthesized ZnO nanochips, GO and RGO was discussed.<sup>190</sup> Results indicated that ZnO nanochips integrated onto graphene sheets exhibited enhanced photocatalytic activity, achieving approximately 76.5–98.9% degradation of RhB and MB within 90 minutes of visible light irradiation. Furthermore, ZnO@RGO demonstrated superior photocatalytic performance compared to ZnO@GO, with approximately 2.4 and 2 times higher kinetic rates for the removal of RhB and MB, respectively.

Common materials like  $\text{TiO}_2$ , ZnO, and GO are popular photocatalysts, but they have notable limitations.  $\text{TiO}_2$  and ZnO both have wide band gaps (~3.0–3.2 eV and ~3.2 eV, respectively), restricting their activity to UV light, which limits their effectiveness under visible light. Both materials also suffer from rapid recombination of electron-hole pairs, reducing their photocatalytic efficiency. Additionally,  $\text{TiO}_2$  and ZnO have lower surface areas, limiting the number of active sites, and ZnO is further hampered by photo corrosion under UV light. GO, while possessing a high surface area, offers limited photocatalytic activity on its own and primarily functions as a support material. Its variable band gap and the complexity of reducing GO to rGO for enhanced activity also pose challenges. In contrast, MOFs offer greater flexibility with tunable band gaps, higher surface areas, and versatile functionalization options, making them superior photocatalysts for a wide range of applications.

## 4.2 Metal organic frameworks as photocatalysts

Heterogeneous photocatalysis (HP) stands as an advanced oxidation method that has surfaced as a promising alternative with a broad spectrum of applications. These applications include treating effluents for decontamination and disinfection, addressing environmental challenges related to pollutants

like  $\text{CO}_2$  and  $\text{NO}_x$  in the atmosphere, and facilitating energy conversion. These are among the most prevalent and widespread uses of this technology. In this context, metal-organic frameworks (MOFs) have been developed to enhance the characteristics and photocatalytic capabilities of conventional semiconductors. MOFs have emerged as innovative photocatalysts due to their intrinsic structural features, which include vast surface area, organised porous structure, and structural diversity. This application is especially well-suited for MOFs since they can combine photosensitiser and catalytic functions into a single structure.<sup>191</sup> The high porosity of MOFs (macropores larger than 50 nm in some cases) enables rapid substrate and product transport/diffusion from the catalytic sites.<sup>22</sup> Additionally, organic ligands have the ability to absorb photons and transfer electrons from the ligand to the metal centre, thereby generating an excited state in the process. Thus, the utilization of MOFs as photocatalysts encompasses a diverse and extensive range of applications (Fig. 9a).<sup>192</sup>

Regarding the elimination of Cr(vi) from water, Gao *et al.*<sup>193</sup> have synthesized a high-throughput MOF composed of bi-benzene-1,4-dicarboxylic acid (Bi-BDC) and featuring a consistent rod-like structure using a microwave-assisted technique (Fig. 9b). This MOF demonstrated the capability to achieve a complete photocatalytic reduction of Cr(vi) in just 6.0 minutes when exposed to low-power LED UV light.<sup>193</sup> Furthermore, the degradation of the contaminant was also reported using a MOF photocatalyst. Jing *et al.*<sup>194</sup> constructed a binary CdS-Cd-MOF nanocomposite by an *in situ* sulfurization of Cd-MOF. When exposed to simulated sunlight, the degradation rate of methylene blue using 10 mg of the material reached 91.9% within 100 minutes.<sup>194</sup> The mechanism of the photocatalytic degradation is described based on the difference in the band gap between the CdS (2.29 eV) and Cd-MOF (2.8 eV) (Fig. 9c). In a similar context, a recent study investigates the photocatalytic degradation of ofloxacin using UiO/MIL/CN.<sup>195</sup> In this work, the synthesis involved growing UiO-66 on the surface of  $\text{NH}_2$ -MIL-125 using the solvothermal method to create MOF-on-MOF architecture. Following that, the authors achieved the successful deposition of  $\text{g-C}_3\text{N}_4$  nanosheets onto the surface of UiO-66/ $\text{NH}_2$ -MIL-125, resulting in the development of a novel double Z-scheme heterojunction photocatalyst (Fig. 9d). When exposed to visible light, this double Z-scheme heterojunction serves as an exceptionally efficient photocatalyst for the degradation of ofloxacin, exhibiting a rate constant of  $0.07 \text{ min}^{-1}$ .<sup>195</sup>

Furthermore, the photocatalytic reduction of carbon dioxide into valuable chemicals stands as an appealing technique, addressing both environmental concerns and energy scarcity simultaneously. Interestingly, MOFs have garnered significant interest in this field due to their remarkable chemical and structural diversity. Wang *et al.*<sup>196</sup> employed an *in situ* hydrothermal process to combine  $\text{TiO}_2$  nanoparticles with a mixed ligand-based MOF structure consisting of CuTCPP and BDC (CTU). This integration resulted in the formation of CTU/ $\text{TiO}_2$  nanocomposites, which effectively merge MOFs with inorganic semiconductors (Fig. 9e). When employed as photocatalysts for  $\text{CO}_2$  conversion under simulated solar light ( $\lambda > 300 \text{ nm}$ ), the optimized CTU/ $\text{TiO}_2$  heterostructure demonstrated



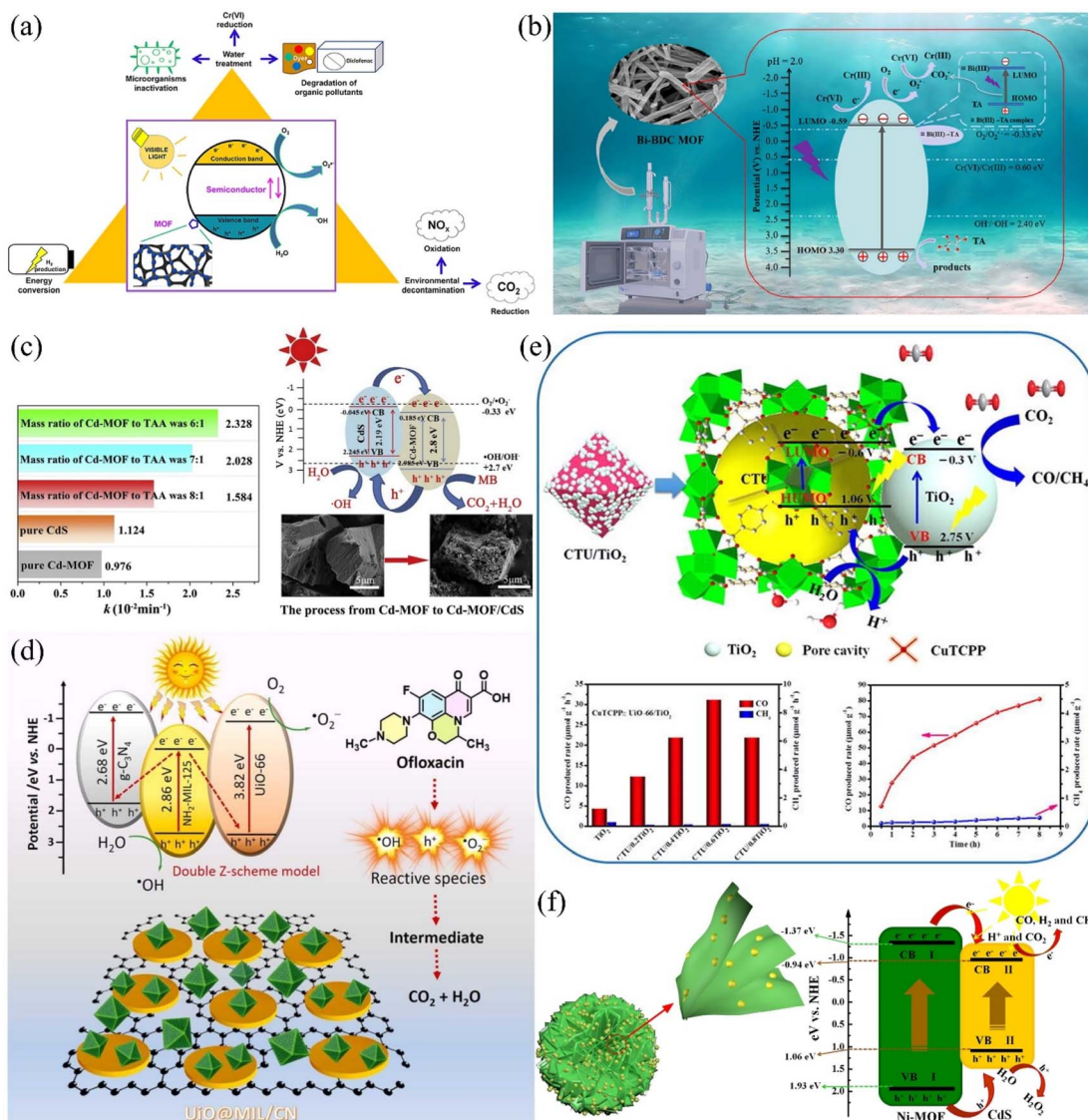


Fig. 9 (a) Composite materials featuring metal–organic frameworks for heterogeneous photocatalysis driven by visible light. MOF-based composites have potential applications in the degradation of organic compounds, reduction of Cr(vi), inactivation of microorganisms, oxidation of NO<sub>x</sub>, reduction of CO<sub>2</sub>, and production of H<sub>2</sub>. Adopted from ref. 192 with permission. (b) Microwave-assisted synthesis of the Bi-BDC MOF photocatalyst and its efficient reduction of Cr(vi) within 6.0 min under a low-power LED UV light. Adopted from ref. 193 with permission. (c) Visible light CdS/Cd-MOF photocatalyst with enhanced photodegradation of methylene blue (91.9% in 100 minutes under simulated sunlight irradiation). Adopted from ref. 194 with permission. (d) Double Z-scheme heterojunction based on Uio@MIL/CN for the photocatalytic degradation of ofloxacin under visible light irradiation. Adopted from ref. 195 with permission. (e) CuTCPP-functionalized zirconium MOF and TiO<sub>2</sub> for photocatalytic CO<sub>2</sub> reduction to CO under simulated solar illumination. The figure shows the dependence of total CO/CH<sub>4</sub> evolution on the amount of TiO<sub>2</sub> and various CTU/TiO<sub>2</sub> ratios under Xe lamp irradiation (λ > 300 nm) within 1 hour, total CO/CH<sub>4</sub> evolution amount produced by CTU/0.6TiO<sub>2</sub> under Xe lamp irradiation within 8 hours, and a proposed photocatalytic CO<sub>2</sub> reduction pathway over CTU/TiO<sub>2</sub>. Adopted from ref. 196 with permission. (f) 3D hierarchical structure of CdS/Ni-MOF and schematic diagram illustrating the electron transfer process and photocatalytic mechanism involved in the reduction of CO<sub>2</sub>. Adopted from ref. 197 with permission.

significantly enhanced performance.<sup>196</sup> The rate of CO<sub>2</sub> reduction into CO reached 31.32  $\mu\text{mol/g h}$ , approximately seven times higher than that achieved with bare TiO<sub>2</sub>. In another study conducted by Xu *et al.*,<sup>197</sup> they explored the development of 3D hierarchical CdS/Ni-MOF photocatalysts. These photocatalysts exhibited a notable CO yield, surpassing the yields achieved by both Ni-MOF and CdS individually by 16 and 7 times, respectively. The researchers proposed a preliminary mechanism for

the CO<sub>2</sub> conversion process (Fig. 9f). Upon exposure to UV-Vis light, both Ni-MOF and CdS become excited, generating electrons (e<sup>-</sup>) and holes (h<sup>+</sup>). Their intimate interface facilitates the efficient transfer of excited electrons from Ni-MOF to CdS, which boasts a more positive conduction band.<sup>197</sup> Consequently, CdS, acting as the active site, proficiently reduces CO<sub>2</sub> to CO. Concurrently, the holes in the valence bands of Ni-MOF and CdS engage in oxidation reactions, yielding oxygen and



hydrogen peroxide, effectively eliminating the holes. This well-coordinated charge separation and electron–hole pair transfer contribute to the enhanced photocatalytic activity of the system.

Because the careful selection of linkers/metal clusters or the addition of catalysts can significantly increase light adsorption, reactant adsorption, charge separation, and reactant activation, the modification of MOF elements is especially crucial for photocatalyst applications.<sup>23</sup> As a result, photocatalytic performance will be enhanced. Sensitiser addition is one example of modulating ligand and metal clusters. MOFs can incorporate sensitisers (metal complexes or organic dyes) to increase the amount of visible-light-driven photocatalysis.<sup>167</sup> In their study, Furukawa *et al.*<sup>24</sup> successfully introduced dyes and encapsulated precious metals into a series of MOF photocatalysts, producing an enhanced photocatalytic performance for almost all MOFs tested as well as a slightly increased spectral region for photoactivity. In a similar vein, Pt/NH<sub>2</sub>-MIL-125(Ti) was used in visible light for CO<sub>2</sub> reduction.<sup>23</sup> The results of this were also positive with the material showing an improvement in photocatalytic performance when compared to the plain NH<sub>2</sub>-MIL-125(Ti). Pt/NH<sub>2</sub>-MIL-125(Ti) exhibited a remarkable boost in its photocatalytic efficiency for CO<sub>2</sub> reduction into formate. Over the course of 8 hours of irradiation, Pt/NH<sub>2</sub>-MIL-125(Ti) yielded approximately 12.96 mmol of formate, representing a notable 21% increase in activity when compared to the performance of pure NH<sub>2</sub>-MIL-125(Ti). These experiments suggest that the use of precious metals in MOFs to improve photocatalytic behaviour has great potential.

Furthermore, studies indicate that MOFs' thermal and chemical stabilities are a bonus and contribute to their appeal as catalysts and catalytic hosts. Zhao *et al.*<sup>22</sup> posit that MOF photocatalysts should be stable under service conditions, including water. In addition to this, MOF photocatalysts have shown resistance to moderately acidic and basic solutions.<sup>22</sup> An example of an aquatically stable MOF can be found in the report of Drache *et al.*<sup>198</sup> in which they investigated a series of Zr-based MOFs and found they exhibited excellent stability in water. The authors suggest that this is a result of the strong coordination between the organic ligands and the Zr nodes. Howarth *et al.*<sup>199</sup> recommend another method to improve the stability of MOFs in water, involving decorating the MOF organic linkers with sulphonate, fluorinated, or phosphonate substituents. Metal oxide encapsulation within MOF photocatalysts is an additional line of inquiry. POMs, or polyoxometalates, have attracted a lot of interest because of their exceptional redox capacity, highly negative charges, and structural characteristics.<sup>22</sup> When POM [(PW<sub>9</sub>O<sub>34</sub>)<sub>2</sub>Co<sub>4</sub>(H<sub>2</sub>O)<sub>2</sub>] was encapsulated in MOF-545 the product was able to endure reversible electron transfer reactions with negligible structural degradation.<sup>200</sup> This material was also successfully used for water oxidation under visible light. As demonstrated, recent advancements have introduced numerous new MOFs and MOF-based composites specifically designed for the photocatalytic reduction of CO<sub>2</sub>. MOFs are recognized as state-of-the-art photocatalysts due to their exceptional coordination between active metal centers and organic linkers. Their unique structural features such as vast surface areas, well-ordered frameworks, high porosity, and

significant structural tunability contribute to their effectiveness.<sup>201</sup> Compared to traditional catalysts, MOF-based photocatalysts present several advantages, including ultra-high specific surface areas, adjustable pore structures that enhance CO<sub>2</sub> adsorption and reduction and unlike homogeneous photocatalysts, they are easily separated from the reaction products and can therefore be reused many times.<sup>22</sup> As such, MOF photocatalysts will have a longer lifetime, contributing to a decrease in waste, end-of-life process costs, and pollution. Additionally, the metal nodes and organic ligands in MOFs can be selectively functionalized, and the abundant pores allow for the accommodation of various functional guest substances.

Despite these benefits, challenges persist in the use of MOF composites as photocatalysts. These include low visible light utilization efficiency, poor stability with rapid loss of activity and structural integrity after several cycles, and reliance on organic sacrificial reagents and solvents that pose environmental concerns. Furthermore, not much research has been done on how MOFs employed in photocatalytic applications affect the environment. An LCA could be performed to more accurately assess the possible impact of MOF photocatalysts. On the other hand, as previously noted, the synthesised MOFs continue to be costly because of the intricate synthesis procedures and the absence of mass production processes, even though the component linkers and ions are frequently quite affordable.<sup>18</sup> However, MOFs' improved efficiency compared to TiO<sub>2</sub> photocatalysts and their potential for an extended lifetime will likely reduce their long-term costs.

## 5 Evaluation and comparison

Investigating potential MOFs as sorbents, SC electrodes or photocatalysts is a difficult endeavour due to the vast number available, with over 90 000 synthesized MOFs in the public domain.<sup>202</sup> However, the creation of software with these capabilities is yet to be achieved.<sup>35</sup> To increase the TRL level of MOF sorbents, pilot-scale MOF production needs to be investigated. Methods of bulk-producing structured MOFs are imperative if they are to be used for industrial use. Table 3 shows a summary of the advantages and disadvantages of MOFs, liquid amine, activated carbon, as well as titanium dioxide for application in various technologies identified from a review of the recent literature.

### 5.1 Carbon capture

Metal-organic frameworks (MOFs) present numerous advantages over non-MOF materials for applications in carbon capture. MOFs such as MOF-5 and HKUST-1 exhibit exceptional surface areas and porosity, exceeding 1000 m<sup>2</sup>/g, which translates to higher CO<sub>2</sub> adsorption capacities up to 33.5 wt% and 31.0 wt% respectively under standard conditions.<sup>203</sup> This is significantly better than traditional materials like zeolites and activated carbons, which have lower surface areas and CO<sub>2</sub> adsorption capacities. The tunability of MOFs allows for precise control over pore size and functionality, enhancing selectivity towards CO<sub>2</sub>, as demonstrated by ZIF-8's CO<sub>2</sub>/N<sub>2</sub> selectivity of 25

**Table 3** Advantages and disadvantages of MOFs, liquid-amine, activated carbon, and  $\text{TiO}_2$  technologies for uses in CCS, SC electrodes and photocatalysis

	Advantages	Disadvantages
MOFs	<ul style="list-style-type: none"> <li>Controllable morphology (pore size)</li> <li>MOFs are used for CCS at lower temperatures compared to amines<sup>52</sup></li> <li><math>\text{CO}_2</math> capture capacity <math>\geq</math> amine scrubber under the same dry working conditions<sup>32</sup></li> <li>Solid sorbents have a much lower heat capacity compared to liquid-amine solutions<sup>32</sup></li> <li>Suitable for DAC processes<sup>33</sup></li> <li>Some MOFs can provide a greater <math>\text{CO}_2</math> uptake capacity, good SCN, and acceptable regeneration energy requirements<sup>50</sup></li> <li>Reduced effect on power plant efficiencies<sup>203</sup></li> <li>High capacitance compared to ACs</li> <li>Some MOFs show exceptional cycling stability<sup>22</sup></li> <li>High power densities</li> <li>Possibility of using waste PET for production<sup>113</sup></li> <li>Light harvesting range can be extended to include visible/NIR light through the inclusion of long-wavelength-light-responsive units within the MOF</li> <li>Can reduce recombination of the photogenerated electrons and holes</li> <li>Some MOFs have shown improved photocatalytic behaviour</li> <li>Reported successful application under mild conditions</li> <li>Proven success in bulk scale CCS<sup>18</sup></li> </ul>	<ul style="list-style-type: none"> <li>Still in early developmental stages – further research is required<sup>191</sup></li> <li>Poor stability under CCS operational conditions<sup>18</sup></li> <li>Prone to decompose when exposed to moisture<sup>18</sup></li> <li>Poor thermal conductivity (leading to higher regeneration costs and slower regeneration processes)<sup>36</sup></li> <li><math>\text{CO}_2</math> capture capacity can be reduced in the presence of moisture<sup>18</sup></li> <li>Lack of processes to convert MOF powders into devices<sup>18</sup></li> <li>Low <math>\text{CO}_2</math> capacity in the presence of water<sup>29</sup></li> <li>Reports of poor stability over multiple cycles of absorption/desorption<sup>29</sup></li> <li>Can have high production costs<sup>29</sup></li> <li>All the feasible methods to modify MOFs for DAC currently rely on amine doping<sup>62</sup></li> <li>Little known about MOF toxicity</li> <li>Suitability for widespread deployment not well established</li> <li>Comparatively complex synthesis process</li> <li>The stability of MOFs under photocatalytic reaction conditions requires more research – some reports of low stability</li> <li>Energy intensive – high solvent regeneration energies (<math>&gt;140\text{ }^\circ\text{C}</math>)<sup>31</sup></li> <li>Requires large equipment.<sup>31</sup></li> <li>Prone to equipment corrosion and requires inhibitors to prevent it<sup>31</sup></li> <li>Prone to degradation<sup>25</sup></li> <li>Can reduce the overall efficiency of a powerplant<sup>18</sup></li> <li>Limited potential for performance improvement<sup>19</sup></li> <li>High cost, and levels of sorbent loss<sup>33,35</sup></li> <li>Highly toxic and environmentally harmful, not suitable for DAC<sup>33</sup></li> <li>Insufficient <math>\text{CO}_2</math> capacity for the mitigation of industrial-scale emissions<sup>25</sup></li> <li>Low power densities</li> <li>Capacitive performance is not as high as that offered by some MOFs</li> <li>Low specific capacitance<sup>83</sup></li> </ul>
Liquid amines	<ul style="list-style-type: none"> <li>The most developed method of CCS<sup>25</sup></li> <li>MEA has a high <math>\text{CO}_2</math>-carrying capacity<sup>29</sup></li> <li>MEA has a fast absorption rate<sup>29</sup></li> <li>Amines can provide high separation/purification performance<sup>18</sup></li> <li>Some liquid amines like MEA are low-cost<sup>26</sup></li> <li>MEA is readily biodegradable<sup>26</sup></li> </ul>	<ul style="list-style-type: none"> <li>Complex separation process<sup>205</sup></li> <li>Prone to aggregation<sup>205</sup></li> <li>Rapid rate recombination of the photogenerated electron-hole pairs<sup>205</sup></li> <li>Photocatalytic activity is restricted to the UV region (low photocatalytic efficiency)<sup>207</sup></li> </ul>
Coconut shell activated carbon	<ul style="list-style-type: none"> <li>Low cost<sup>80</sup></li> <li>Raw material readily available<sup>80</sup></li> <li>High thermal and electrochemical stability<sup>204</sup></li> <li>Renewable and non-toxic<sup>204</sup></li> <li>Low net GHG emissions over the lifespan<sup>96</sup></li> <li>Showed great promise for commercial use<sup>170</sup></li> <li>Non-toxic<sup>170</sup></li> <li>Environmentally benign<sup>181</sup></li> <li>Suitably efficient photoactivity<sup>206</sup></li> <li>High stability<sup>206</sup></li> <li>Low cost<sup>206</sup></li> </ul>	<ul style="list-style-type: none"> <li>Capacitive performance is not as high as that offered by some MOFs</li> <li>Low specific capacitance<sup>83</sup></li> </ul>
Titanium dioxide		<ul style="list-style-type: none"> <li>Complex separation process<sup>205</sup></li> <li>Prone to aggregation<sup>205</sup></li> <li>Rapid rate recombination of the photogenerated electron-hole pairs<sup>205</sup></li> <li>Photocatalytic activity is restricted to the UV region (low photocatalytic efficiency)<sup>207</sup></li> </ul>

at room temperature. However, MOFs generally show high sensitivity toward moisture and high structural degradation, such as MOF-5, which can lose as much as 90% of its  $\text{CO}_2$  adsorption capacity under humid conditions. Moreover, high

synthesis and processing costs, along with difficulties in the production of defect-free membranes, are of vital importance against scalability. Carbon capture performance metrics are important. Although MOFs showed an upper  $\text{CO}_2$ -carrying



capacity compared to liquid amines in the laboratory tests, both materials showed a suitable level of CO<sub>2</sub> selectivity with excellent selectivity shown by MOFs doped with amines. MOFs doped with amine dopants also had lower regeneration energies compared to liquid amines. The possibility of development is higher for MOFs due to their tunable structure and number of available MOFs. While MOFs are under development, liquid amines find industrial applications. Both materials have stability problems under CCS conditions, and as far as reported there was no problem of corrosion observed with MOF, unlike liquid amines which in addition to being corrosive are volatile. On performance, MOF scores 128 against liquid amine's 93. The three broad factors were further allocated relative weightings based on the findings of the literature review and summed up to 100. For C-capture, the weights were distributed as performance 34/100, environmental impact 25/100 and cost implications 41/100. The factors, along with weightings for the evaluation of carbon capture materials, are shown in Table 4, and the comparison matrix showing the scoring of liquid-amine and

MOF-based materials against these factors is presented in Table 5.

Carbon capture technology stands as one of the most important strategies for mitigating climate change through the reduction of CO<sub>2</sub> emissions from industrial sources. There are three major parameters used that express a comparison among the different carbon capture methods: their cost, efficiency, and environmental impact. Cost means the financial expenditure incurred to capture, transport, and store CO<sub>2</sub>, including capital, operational, and maintenance costs. Advanced carbon capture methods using MOFs reduce this cost to a large extent. For example, conventional amine-based capture processes may range between \$40 and \$100 per ton of CO<sub>2</sub> captured while advanced materials, such as MOFs, are expected to drop these costs down to \$20–\$50 per ton by the increase in efficiency and reduction in energy requirements.<sup>209</sup> Efficiency is the percentage of CO<sub>2</sub> that can be captured from the sources of emission relative to the total amount of emissions produced. Traditional methods have efficiencies of 85–90%, while MOFs

Table 4 C-capture factors and corresponding suggested weighting along with the justifications

Subject	Factor	Weighting	Justification
Performance	CO <sub>2</sub> -carrying capacity	3	This affects the efficiency of the material and influences the amount of sorbent required for a CCS application <sup>18</sup>
	CO <sub>2</sub> selectivity	3	This affects the purity of adsorbed CO <sub>2</sub> and the concentration of CO <sub>2</sub> in the emitted flue gases <sup>18</sup>
	Regenerability	3	This affects the energy efficiency of the C-capture process <sup>31</sup>
	Potential for development	1	All current technologies (both liquid amine and MOF sorbents) require further improvement before they can be deployed on an industrial scale. Therefore, the material must offer sufficient scope/potential for these changes <sup>31</sup>
	Current successful application	2	CCS technology takes a considerable period of time to test and validate, very few materials make it to trials and even fewer are successful in reaching real-world applications. <sup>19</sup> Successful small-scale trials or real-world trials are good indications of the material's suitability
	Stability under service conditions	3	The material used in CCS applications must be able to withstand the operating conditions and regeneration conditions to perform well
	Corrosivity and volatility	2	Ideally, materials used should not be volatile as that can lead to high levels of sorbent loss and reduced levels of performance over time. <sup>33</sup> Corrosive materials can also cause performance issues as they may damage the equipment, thus reducing its efficiency <sup>33</sup>
	Material recyclability	3	For the technology to be "future-proof" it needs to be sustainable
	Toxicity	2	A toxic material is detrimental to the environment, it can also result in higher costs for disposal at the end of the product's life
	Production methods	2	Energy-intensive production methods may negate some of the benefits of the technology use
Environmental impact	Functional energy requirements	3	Literature suggests that the application of post-combustion CCS can lead to an overall reduction of a power plant's efficiency <sup>19</sup>
	Raw material cost	2	Influences the overall cost of a material. It is also important to consider the likelihood of a significant change in the price of a material
	Usage costs (equipment, temperature/pressure requirements)	3	If a technology is excessively expensive then it will likely never be suitable for wide-scale deployment. Furthermore, if the costs of using the technology outweigh the benefits then it is likely the technology will fail or be superseded and become obsolete
	Synthesis/manufacturing costs	3	High production costs can act as a barrier to wide-scale technology deployment. It is also important to consider if the production costs are likely to reduce when the technology develops further/becomes more mainstream



Table 5 Comparison matrix between liquid amines and MOFs for C-capture applications<sup>a</sup>

Factor	Weighting	Material score		Justification
		Liquid-amines	MOFs	
CO <sub>2</sub> -carrying capacity	6	3	5	MOFs have shown higher CO <sub>2</sub> -carrying capacities in laboratory tests <sup>52</sup>
CO <sub>2</sub> selectivity	5	3	3	Both materials have shown suitable levels of CO <sub>2</sub> selectivity. <sup>52</sup> While pristine MOF sorbents have shown SCN values below those of liquid-amine sorbents, amine-doped MOF sorbents have shown excellent SCN values exceeding those of liquid-amine sorbents <sup>18</sup>
Regenerability	5	3	4	While both materials have shown acceptable (albeit high) results for the required regenerability energy, some amine-doped MOF sorbents have exhibited lower regeneration energies <sup>18,31</sup>
Potential for development	4	1	5	Liquid amine technology provides little potential for further development whereas MOF sorbents provide vast potential due to their customisable structure and the number of available MOFs. <sup>19,25</sup> Furthermore, MOFs have shown potential for DAC <sup>62</sup>
Current successful application	5	4	2	Liquid amines are already used in industry but are yet to be rolled out on a wide scale. <sup>25</sup> MOFs for CCS are still in their developmental stages and are a long way from real-world trials <sup>52</sup>
Stability under service conditions	6	3	3	Both pristine MOF sorbents and liquid-amine sorbents have issues with stability under CCS conditions. <sup>18,25</sup> Whilst amine-doped MOFs have shown improved stability under regeneration and service conditions, they are still mildly affected by the presence of moisture <sup>18</sup>
Corrosivity and volatility	3	1	5	Liquid amines are shown to be very corrosive and can cause damage to equipment if it has not been given a protective coating. <sup>25</sup> Liquid amines are also very volatile and therefore the process can be subject to high levels of sorbent loss. <sup>33</sup> There are currently no reported issues with MOF sorbents and corrosion
Performance score		93	128	
Recyclability	4	3	3	Recycling prospects for both materials are reasonably poor <sup>18,26</sup>
Toxicity	8	1	4	Liquid amines are toxic. <sup>33</sup> There is limited research into the toxicity of MOFs, however, the literature suggests that some may be toxic when they start to decompose <sup>125</sup>
Production methods	7	3	3	The production of both materials is both complex and reasonably energy-intensive
Functional energy requirements	6	3	4	MOFs have shown potential for CCS at a lower temperature than those used for liquid-amine CCS. <sup>52</sup> Furthermore, amine-doped MOF sorbents have a lower regeneration energy requirement compared to liquid-amine sorbents <sup>18</sup>
Environmental impact score		59	89	
Raw material cost	14	3	2	The cost of the MOF constituent linkers and metal clusters is relatively cheap. <sup>18</sup> However, pre-synthesised MOFs are expensive due to complex production processes. <sup>18</sup> Some liquid-amines like MEA are relatively low-cost <sup>26</sup>
Usage costs (equipment, temperature/pressure requirements)	15	3	4	MOFs have demonstrated the potential for CCS at lower temperatures. <sup>52</sup> Liquid-amine scrubbers have also been shown to reduce the overall efficiency of a power plant to a greater degree than the predicted effects of MOF sorbents <sup>18,203</sup>
Production costs	12	3	2	As previously discussed, MOFs are expensive due to complex production processes. Liquid-amine technology is comparatively well-developed, and processing costs are cheaper <sup>26</sup>
Cost score		123	112	
Overall scores		275	329	

<sup>a</sup> Note: all materials were evaluated for each factor using a scale ranging from 1 to 5 (where 1 corresponds to "very bad," 2 to "bad," 3 to "suitable," 4 to "good," and 5 to "very good").

and other advanced materials could theoretically be as high as 95–99% according to the study on 2D MOFs for the reduction of CO<sub>2</sub>, where Cu<sub>3</sub>(C<sub>12</sub>N<sub>6</sub>S<sub>6</sub>)<sub>2</sub> demonstrated very high activity with small overpotentials, which reflects high efficiency in the

processes of capture and conversion of CO<sub>2</sub>.<sup>210</sup> Environmental impact looks at the bigger picture of how carbon capture affects the environment in general, such as the probable risks associated with the leakage of CO<sub>2</sub> during storage, the energy used by



capture and sequestration, and the net reduction of GHG emissions. While traditional methods may leave room for a capture process that is 10–20% more energy-intensive, advanced MOF-based methods can reduce this extra energy requirement to under 10%, making the process more sustainable. Moreover, according to the researchers in this study, 2D MOFs showed improved selectivity toward CO<sub>2</sub> reduction relative to competing reactions, such as hydrogen evolution, which further minimizes unwanted environmental impacts. The utilization of 2D MOF as an advanced material in carbon capture technology shows a very promising avenue toward cost-effective, efficient, and environmentally sustainable processes.

## 5.2 Photocatalysis

Given the very high porosity of the MOFs, the surface area can reach more than 3000 m<sup>2</sup>/g. Such high values raise the adsorption and reduction rates of CO<sub>2</sub> in photocatalysis. Furthermore, their tunable structure provides conditions for the introduction of different metals, increasing active sites, and enhancing photocatalytic properties. Also, the MOFs exhibit enhanced light harvesting and photostability, which is very critical in efficient photocatalysis.<sup>211</sup> However, these materials have low stability in an aqueous/high-temperature environment and poor light absorption, thereby mostly limiting their application to only the ultraviolet regime, with the added need for sophisticated and

expensive synthesis methods. MOFs demonstrated lower recombination rates and higher resistance to aggregation compared to titanium dioxide, which, although highly stable, is prone to aggregation. While titanium dioxide is restricted to UV light, MOFs can be active in a broader spectrum that includes visible light. Moreover, the MOFs provide larger surface areas with increased resistance to photo-corrosion. MOFs score 176 while titanium dioxide scores 116, hence superior efficiency for performance evaluation. The evaluation parameters are weighted as performance, which is efficiency, at 45/100, environmental impact at 18/100 and cost implications at 37/100. Performance factors include photostability, the extent of light absorption and recombination rates 180. Environmental impact factors include stability of materials in various environments and resistance to photo-corrosion. These are, among others, the complexity and cost of the synthesis methods. Table 6 presents the evaluation criteria in the case of photocatalysis, and Table 7 presents a detailed comparison between titanium dioxide and MOFs in photocatalytic applications.

## 5.3 Supercapacitors

Supercapacitors, being next-generation energy storage devices, are assessed based on the metrics of specific capacitance, energy density, power density, and cycling stability. The presence of high specific surface areas and porosity contributes to

Table 6 Photocatalysis factors and the corresponding suggested weighting along with the justifications

Subject	Factor	Weighting	Justification
Performance	Recombination rate	3	Low recombination rates are desirable as it directly effects the efficiency of the photocatalyst
	Stability under photocatalytic conditions	3	The photocatalytic material must be able to withstand the operating conditions to perform well
	Level of current development	2	Successful small-scale trials or real-world trials are good indications of the material's suitability
	Resistance to aggregation	2	Material aggregation can block the active sites of a material and therefore reduce the effective surface area of the material and consequently reduce its efficiency
	Photocatalytic activity under visible light	3	In order to maximise the efficiency of a photocatalyst, ideally it should be photoactive in a wide region of the light spectrum. Most current photocatalysts are only active in the UV region of the spectrum
	Material morphology	3	This has been shown to greatly influence the efficiency of photocatalysts <sup>205</sup>
	Resistance to photo corrosion	2	High resistance to photo corrosion is desirable as photo corrosion can lead to a reduction in performance over time
	Toxicity	3	A toxic material is detrimental to the environment, it can also result in higher costs for disposal at the end of the product's life
	Energy requirements for processing raw materials	2	Energy-intensive processing methods can be detrimental to the environment. This is an important consideration for technologies with a wide-scale deployment aim
	End of life outlook	2	For the technology to be "future-proof" it needs to be sustainable. Consequently, the option for recycling or safe disposal is very important
Cost	Raw material cost	3	This greatly influences the overall cost of a material. It is also important to consider the likelihood of a significant change in the price of a material
	Production costs	3	High production costs can act as a barrier to wide-scale technology deployment. It is also important to consider if the production costs are likely to reduce when the technology develops further or becomes more mainstream



Table 7 Comparison matrix for titanium dioxide and MOFs for photocatalytic applications<sup>a</sup>

Factor	Weighting	Material score		Justification
		TiO <sub>2</sub>	MOFs	
Recombination rate	7	2	4	MOFs have shown reduced recombination rates
Stability under photocatalytic conditions	8	4	3	Titanium dioxide has shown high stability under photocatalytic conditions. <sup>206</sup> MOFs however, have shown some degradation under these conditions <sup>23</sup>
Level of current development	4	5	4	Titanium dioxide has shown issues with aggregation <sup>205</sup> unlike MOFs
Resistance to aggregation	5	1	3	ACs are prone to aggregation and therefore often have to be used as a gel suspension, this often limits the reduction of the device size
Photocatalytic activity under visible light	9	1	5	Titanium dioxide's photoactivity is restricted to the UV region of the light spectrum (only 5% of available light). <sup>205</sup> However, some MOFs have shown photoactivity in an extended region of the spectrum
Material morphology	7	3	4	MOFs can provide a significantly larger surface area. <sup>121</sup> Furthermore, titanium dioxide is prone to aggregation which reduces its effective surface area <sup>205</sup>
Resistance to photo corrosion	5	3	4	MOFs have shown increased resistance to photo corrosion. <sup>205</sup>
Performance score		116	176	Titanium dioxide has mild difficulty with photo corrosion <sup>170</sup>
Toxicity	6	5	4	Some MOFs used for this application (such as MILMIL-100(Fe)) are non-toxic. <sup>121</sup> Titanium dioxide is non-toxic <sup>170</sup>
Processing raw materials	6	3	4	The production of both materials is both complex and reasonably energy-intensive. However, due to the novelty of MOFs, their production costs remain prohibitively high <sup>205</sup>
End of life outlook	6	2	2	Methods for recycling both materials remain largely unsearched
Environmental impact score		60	54	Titanium dioxide is a low-cost material whereas MOFs for this application are high-cost <sup>206</sup>
Raw material costs	17	5	2	MOFs have a significantly higher processing cost <sup>191</sup>
Processing costs	20	3	3	
Cost score		145	94	
Overall scores		341	304	

<sup>a</sup> Note: all materials were evaluated for each factor using a scale ranging from 1 to 5 (where 1 corresponds to "very bad," 2 to "bad," 3 to "suitable," 4 to "good," and 5 to "very good").

really good electrochemical performance in metal-organic framework materials such as Cu-MOF, Zr-MOF, and Ti-MOF. For example, Cu-MOF showed a specific capacitance of 104.8 F/g with an energy density of 18.2 W h/kg, greatly outperforming all other materials because of increased ionic transport and charge storage capabilities.<sup>212</sup> Moreover, Ni-DMOF-ADC gave a specific capacitance of 552 F/g and over 98% retention after 16 000 cycles, indicating its excellent cycling stability. Similarly, Ni<sub>3</sub>(HITP)<sub>2</sub> tends to be 117 F/g and 90% after 10 000 cycles. For instance, MnO<sub>x</sub>-MHCF has reached as high as 1200 F/g with 94.7% retention after 10 000 cycles in composite materials, whereas rGO/ZIF-8 has reached 336 F/g with 96% retention.<sup>213</sup> While these methods could enhance the capacity, the poor intrinsic conductivity of pristine MOFs remains a large problem and needs conductive additives or hybridization with conductive materials like graphene and conductive polymers. Although this composite approach has improved the conductivity and overall performance, it adds complexities in synthesis and possible trade-offs in mechanical stability.<sup>214</sup> Therefore, innovation in design and optimization of electrode materials remains the key to unlocking the full potential of supercapacitors so that high power and long-life energy storage applications are fully satisfied.

However, the complex and rather pricey synthesis processes of MOFs, combined with the fact that long-term stability and durability under real conditions is still a topic of research, represent major handicaps. On the other hand, non-MOF materials are normally much more stable and less expensive but do not offer such high tunability and selectivity as MOFs do. For overall performance, MOFs score 173, while activated carbon scores 126. The supercapacitors could therefore have evaluation parameters that are weighted at 40/100 for performance, 15/100 for environmental impact, and 45/100 for cost implications. Parameters for performance include those for cycling stability, capacitance, energy and power densities; parameters in environmental impact include the stability of the materials and their impact on the environment; those in cost implication involve the complexity of the methods of synthesis and expenses incurred. The evaluation criteria for supercapacitors are summarized in Table 8, while Table 9 presents the comparison matrix between AC and MOFs as electrodes of supercapacitors.

Overall, MOFs score higher than liquid amines for CCS applications despite their poor cost score (52 compared to 60 for liquid amines) and the high weighting assigned to cost factors. As the radar graph (Fig. 10a) shows, the MOFs score considerably



Table 8 Supercapacitor factors and corresponding suggested weighting along with justifications

Subject	Factor	Weighting	Justification
Performance	Cycle life	3	The electrode's lifespan is very important as it affects which applications the electrode can be used for as well as the level of performance over its lifespan <sup>74</sup>
	Capacitance	3	A poor capacitance can limit an SC's potential applications. A high capacitance is desirable
	Current successful application	2	Successful laboratory results or real-world trials are good indications of the material's suitability
	Size and weight	2	Literature suggests that for most applications, weight and size are not a key consideration, as the systems they would be used in are already very large and packaging space will likely not be an issue <sup>80</sup>
	Integrity under service conditions (e.g., thermal stability)	3	This is important as it affects the lifespan of the electrode as well as its performance (including issues with charge leakage) and overall suitability for this application <sup>119</sup>
	Energy and power densities	3	High energy and power densities are desirable for SCs. High power density would optimise their charging speeds and therefore make the SC an attractive option for electric vehicle charging equipment. A high energy density would increase the number of potential applications of the SC (as it would be able to hold more energy)
	Raw material renewability	3	For the technology to be "future-proof" it needs to be environmentally sustainable
Environmental impact	Toxicity	3	A toxic material is detrimental to the environment, it can also result in higher costs for disposal at the end of the product's life
	Recyclability	2	For the technology to be "future-proof" it needs to be sustainable
	Production impacts (e.g., energy use)	2	Energy-intensive processing methods can be detrimental to the environment. This is an important consideration for technologies with a wide-scale deployment aim
Cost	Material cost	3	Manufacturers want to keep costs low even at the expense of performance. Literature suggests that price is one of the key factors for the material choice of SC electrodes <sup>80</sup>
	Ease of production/production cost	2	Simple, low-energy production processes are often cheaper. If the production method can be used for bulk production, it also means the cost of the product is likely going to be lower

better for environmental impact due to liquid-amine toxicity and environmental harmfulness. Notwithstanding their relatively modest stage of development, MOFs have a high-performance grade because they also have the potential to provide considerable performance improvements over liquid amines. According to the graph, MOFs' performance score gives them the greatest advantage over liquid amines. In contrast, ACs receive a slightly better rating for SC electrode applications than MOFs. However, the radar graph (Fig. 10b) shows that MOFs score considerably better for performance and their score for environmental impact is only slightly less than that of AC. It is apparent from Fig. 10 that this evaluation suggests that the factor preventing the wide-scale use of MOF electrodes is cost. Literature suggests that the incredibly low price of AC is acting as a barrier to the entrance of any other material to the SC electrode market,<sup>80</sup> despite the potential for improved performance. Consequently, further research into the cost-effective synthesis of MOF electrodes may be beneficial. Regarding photocatalytic application, titanium dioxide achieved the highest overall score, suggesting that, based on these factors, it provides the most benefits despite MOFs achieving a considerably higher performance score of 70 (as seen

in Fig. 10c). Because of the high weighting of the cost elements, MOFs' cost score was significantly lower than titanium dioxide's, which is probably what prevents MOFs from being used in this application. In summary, the cost of MOFs can vary considerably, influenced by factors such as the specific MOF material, the synthesis method, the production scale, and the purity of the final product. It's important to note that while some MOFs may be relatively expensive to produce, they can offer unique properties and advantages in various applications, which can justify their cost in certain contexts. As research and development in MOFs continue to advance, there may be efforts to optimize synthesis methods and reduce production costs, making MOFs more accessible for a broader range of applications.

## 6 Limitations and future research directions

### 6.1 Current MOF technologies

Probably the most stressed limitation of the existing technologies behind MOFs is their poor thermal stability. The span in the thermal decomposition temperatures ( $T_d$ ) of MOFs is very



Table 9 Comparison matrix for AC and MOFs as SC electrodes<sup>a</sup>

Factor	Weighting	Material score		Justification
		Activated carbon	MOFs	
Cycle life	8	3	4	MOFs have exhibited higher cycling stabilities in both beakers and constructed SC laboratory tests. <sup>75</sup> ACs have shown suitable performances for this application <sup>80</sup>
Capacitance	9	3	5	Secondary data suggest that MOFs are able to achieve higher values for capacitance compared to ACs <sup>106</sup>
Current successful application	6	4	3	ACs have proven to be successful and are currently used by electrode manufacturers. <sup>80</sup> While MOFs have shown success in laboratory tests, there have been no extensive real-life application trials
Size and weight	7	3	4	ACs are prone to aggregation and therefore often have to be used as a gel suspension, this often limits the reduction of the device size
Energy and power densities	10	3	5	AC electrodes have shown limited power output due to the device's charge delivery rate. <sup>84</sup> Laboratory testing of MOFs has shown improved power densities <sup>119</sup>
Performance score		126	173	
Raw material renewability	3	4	3	While ACs can be produced from renewable sources, the majority of commercially available ACs are produced from non-renewable precursors. <sup>79</sup>
Non-toxicity	4	5	3	Many MOFs used for this application involved non-renewable materials for their synthesis <sup>75</sup>
Recyclability	5	4	3	AC electrodes show great recycling potential, with research suggesting processes and promising results from laboratory tests. <sup>97</sup> While there is little research available on the recycling of MOF SC electrodes, there is research focused on the synthesis of MOFs using waste PET plastics <sup>113</sup>
Production impacts (e.g., energy use)	3	3	4	AC production is simple and chemical activation requires relatively little energy. <sup>80</sup> It is important to note that bulk production of MOFs is largely unresearched and consequently an accurate assessment of this factor is difficult
Environmental impact score		61	48	
Material cost	35	4	2	AC is very cheap. <sup>80</sup> MOFs are prohibitively expensive <sup>74</sup>
Ease of production/ production cost	10	5	4	ACs' production process is well-developed and relatively inexpensive. <sup>80</sup> Bulk production of MOFs requires further research as the process is often complex and expensive <sup>74</sup>
Cost score		190	110	
Overall scores		383	350	

<sup>a</sup> Note: all materials were evaluated for each factor using a scale ranging from 1 to 5 (where 1 corresponds to "very bad," 2 to "bad," 3 to "suitable," 4 to "good," and 5 to "very good").

large, which is the result of inconsistencies in the experimental conditions that include the heating rates and atmospheres. As an example, the reported  $T_d$  values for MOF-5 range from 400 to 500 °C, whereas normally UiO-66 decomposes within the temperature range of 425–500 °C, and HKUST-1 shows  $T_d$  values between 250 and 300 °C. These are some of the factors that influence the nature and location of functional groups, the hardness of metal ions, and coordinated solvent molecules.<sup>215</sup> MOFs with harder metal ions, such as lithium-based UL-MOF-1, showed the highest stability with  $T_d$  values as high as about 600 °C due to an increased ionic character of the metal–oxygen bonds compared to Zn or Zr-based MOFs. For example, Mg-

MOF-74 has extremely high thermal stability with a  $T_d$  of *ca.* 400 °C under a nitrogen atmosphere.<sup>215</sup>

Another large problem is their chemical stability, which is easily influenced by moisture and, therefore, significantly limits their usability for industrial processes. Many MOFs have been reported to decompose above 300 °C or under humid conditions, which thus bounds their practical applications. Their syntheses are often complicated, requiring pricey reagents; large-scale production is economically challenging. For instance, the price for the production of MOFs can be as high as \$50 per gram, which is very expensive compared with conventional porous materials like activated carbon with a price of around \$1 per kilogram.<sup>216</sup> Moreover, while some MOFs have



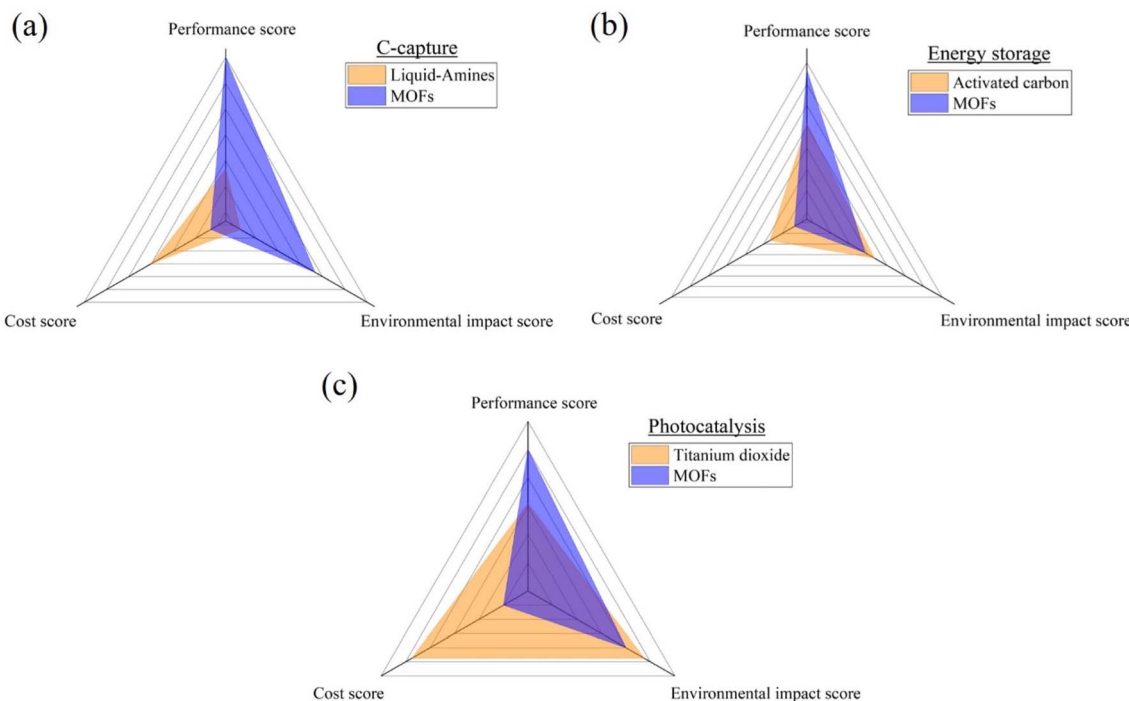


Fig. 10 Radar graph showing 3 factor comparison between MOFs and other conventional materials for; (a) C-capture, (b) energy storage, and (c) photocatalysis applications.

very high methane storage capacities, for example, HKUST-1, impurities can reduce their actual performance by a large extent, significantly diminishing real application.

Another challenge is that it is somehow difficult to scale up the production of MOFs sustainably. Traditional methods of synthesis typically utilize highly toxic solvents under harsh conditions, therefore posing associated environmental and health risks, but usually at high production costs. With more than 99 075 synthetic variants, the enormous number of possible MOF structures makes it challenging and cumbersome to identify and optimize MOFs for a given application with certain desired properties. This leads to long experimental cycles and a high R&D cost.<sup>217</sup> Even for very promising materials like CALF-20 and MIL-100(Fe), multi-ton scale syntheses were achieved only recently, which clearly shows the slow transformation from lab scale to industrial scale production.<sup>218</sup> This is further frustrated by raw material costs and synthesis processes, which themselves are costly, often using highly toxic solvents like DMF that add to the cost and energy requirement of purification methods necessary to maintain the quality of the MOF product.

## 6.2 Future research directions

Future research in MOF technologies has to be directed toward the enhancement of stability, precise characterization of catalytic sites, effective regeneration techniques, and controlled defect engineering. Current MOFs typically show stability up to 300 °C, but future developments must take it further beyond 500 °C through the incorporation of more thermally stable inorganic components and improvement of the node-linker bonds.<sup>219</sup> Improvement in chemical stability to less than 10%

degradation in catalytic activity over 100 hours in an aqueous environment must also be attained. Advanced spectroscopic techniques and computational modelling shall quantify active catalytic sites with an error margin of less than 5% and predict reaction rates to within 10% accuracy of the experimental values. Effective regeneration protocols restore at least 90% of the original catalytic activity after each deactivation cycles, and this performance is maintained over long-term studies. This type of controlled defect synthesis thus should give a standard deviation of less than 10% in defect concentration from batch to batch, while for defect-free MOFs it has to be below 1% of total sites.<sup>219</sup>

One major challenge lies in the naturally very low ionic conductivity of most MOFs, typically much below the level of  $10^{-10}$  S/cm. Nearly liquid electrolyte conductivities are hard to attain with solid electrolytes because of the limited carrier mobility and lack of low-energy pathways for ionic conduction.<sup>220</sup> Future efforts, therefore, need to build on these limitations and focus on strategies that involve improved density of mobile ions and uninterrupted ionic conduction pathways. Additionally, it requires the development of MOFs with stable and high ionic conductivities toward changes in both temperature and humidity. Advancement in synthesis and functionalization approaches with the design of corresponding theoretical models is highly imperative for bringing solutions to the above challenges. The inclusion of flexible frameworks and phase transition mechanisms may yield MOFs with conductivities above  $10^{-2}$  S/cm and may thus render them applicable in the new class of the next-generation energy storage and conversion devices.<sup>220</sup>



Critical is the reduction in the number of steps involved in the synthesis process to reduce production costs to less than \$10 per gram. This can be realized by developing more efficient and up-scaled synthesis methods where applicability is maximally enhanced, such as solvent-free synthesis or the adoption of cheaper and more abundant raw materials.<sup>221</sup> In the future, research should also focus on green synthesis methods with non-toxic, biocompatible linking agents and eco-friendly solvents, along with techniques that apply either no use of solvents at all or solid-state synthesis. High-throughput computation screening and data mining will greatly accelerate the assessment of MOF properties to find promising candidates more efficiently.<sup>222</sup> Separation and recovery processes relating to vacuum filtration and continuous centrifugation, for example, need to be optimized in the scale-up of production. It may potentially also provide more sustainable and cost-effective solutions with respect to reduced energy use and improvement in scalability.<sup>223</sup> This could provide more sustainable and cost-effective solutions due to less energy consumption and efficient scaling of microwave-assisted and mechanochemical synthesis methods.

It is with strategies in creative structural modification and composite material preparation that, finally, such MOF materials could be fabricated with enhanced stability and durability to real-world working conditions. Comprehensive techno-economic analyses and life cycle assessment (LCA) are required concerning an evaluation of the feasibility and environmental impact of large-scale production of MOFs.<sup>224</sup> These assessments will set targets for the development of green and sustainable economically viable MOF technologies whose industrial applications would not contradict their environmental benefits. By taking into consideration these points, there will be a chance for the synthesization of MOFs with improved thermal and chemical stability, reduced production cost, increased scalability, and finally making them practical in much more extended temperature range applications and industrial uses.<sup>225</sup>

## 7 Conclusion

In conclusion, this study provides a comprehensive comparative assessment of Metal-Organic Frameworks (MOFs) and conventional materials across the domains of energy storage, environmental remediation, and photocatalysis. The results underscore the remarkable potential of MOFs as versatile and innovative materials in these critical areas, backed by empirical data.

In energy storage, MOFs consistently outperform conventional activated carbons (ACs) with a performance score of 128, significantly surpassing them. Their exceptional specific surface areas, often exceeding 3000 m<sup>2</sup>/g, enable efficient charge adsorption, rapid charge transfer, and easy ion diffusion within their porous structures. These characteristics, along with their chemical, thermal, and mechanical stability, and the ability to be hybridized with conductive materials, position MOFs as promising contenders for advanced energy storage devices like supercapacitors. Regarding environmental concerns, MOFs excel as effective carbon capture agents, scoring 329 compared

to 275 for liquid amines. Exposed surface areas and high pore volumes further increase their potential for the adsorption capacity toward pollutants. Additionally, besides the presence of functional groups that act specifically toward interactions with the contaminants, the stability under environmental conditions and recyclability underline their effectiveness for environmental clean-up and, therefore, in the promotion of environmental sustainability. In the field of photocatalysis, MOFs exhibit substantial potential with a total score of 304. They showcase extended light harvesting capabilities into the visible and near-infrared regions due to their tunable bandgap, allowing for effective utilization of visible light. They have high surface areas that offer high active sites, while the mechanisms of charge separation do provide a platform for the prevention of recombination of electron–hole pairs, therefore enhancing the catalytic activity. Moreover, their photochemical stability and surface functionalization further enhance their applicability as efficient photocatalysts. However, it's crucial to acknowledge the cost challenges faced by MOFs, with an overall cost score of 110 for supercapacitors and 94 for photocatalysis. High production costs due to complex synthesis processes can act as barriers to widespread technology deployment in these domains. Some challenges, however, remain, such as stability issues, conductivity, and very high production costs. It is a problem of stability and poor electrical conductivity that hampers their potency in energy storage and photocatalysis. Future research should focus on the development of MOF structures with improved stability and conductivity, integration of MOFs with other materials to enhance their performance, and expansion of their applications in environmental remediation. This would have to be supplemented by enhanced environmental adaptability, low-toxicity development of variants to avoid secondary pollution and a deeper study of the pathways and kinetics of charge transfer. Computation design of more effective photocatalysts is probably going to provide the answer. Hence, these issues will be resolved through focused research and innovative solutions for MOFs to achieve their full potential. These empirical data underscore MOFs' promising future in energy storage, environmental remediation, and photocatalysis, showcasing their adaptability and high performance. As the world seeks sustainable technologies, MOFs emerge as pivotal materials, paving the way for a more eco-conscious future.

## Data availability

The data that support the findings of this study are available from the corresponding author, upon reasonable request.

## Conflicts of interest

There are no conflicts to declare.

## Acknowledgements

The authors are grateful to the International Society of Engineering Science and Technology (ISEST) UK. This research is



also supported by "Pioneer" and "Leading Goose" R&D Program of Zhejiang (2024C04049), China. The authors are also thankful for financial support from the Ministry of Research, Innovation and Digitalization (MCID) under Romanian National Core Program LAPLAS VII-Contract No. 30N/2023.

## References

- 1 A. Magfirah, M. M. Ilmi, A. T. N. Fajar and G. T. M. Kadja, *Mater. Today Chem.*, 2020, **17**, 100348.
- 2 A. El Guerraf, W. Zeng, A. Mantel, E. Benhsina, J. M. Chin and H. Shiozawa, *Adv. Electron. Mater.*, 2024, 2300854.
- 3 M. Ding, X. Cai and H.-L. Jiang, *Chem. Sci.*, 2019, **10**, 10209–10230.
- 4 H. C. J. Zhou and S. Kitagawa, *Chem. Soc. Rev.*, 2014, **43**, 5415–5418.
- 5 S. Akhtar, P. Singha, A. De, K. S. Das, S. Saha, S. Bala and R. Mondal, *New J. Chem.*, 2021, **45**, 6438–6449.
- 6 L. R. Redfern and O. K. Farha, *Chem. Sci.*, 2019, **10**, 10666–10679.
- 7 C. Yue, L. Wu, Y. Lin, Y. Lu, C. Shang, R. Ma, X. Zhang, X. Wang, W. D. Wu and X. D. Chen, *ACS Appl. Mater. Interfaces*, 2021, **13**, 26264–26277.
- 8 R. Shah, S. Ali, F. Raziq, S. Ali, P. M. Ismail, S. Shah, R. Iqbal, X. Wu, W. He and X. Zu, *Coord. Chem. Rev.*, 2023, **477**, 214968.
- 9 G. Song, Y. Shi, S. Jiang and H. Pang, *Adv. Funct. Mater.*, 2023, **33**, 2303121.
- 10 N. F. Suremann, B. D. McCarthy, W. Gschwind, A. Kumar, B. A. Johnson, L. Hammarström and S. Ott, *Chem. Rev.*, 2023, **123**, 6545–6611.
- 11 J. Chen and Y. Li, *Chem. Rec.*, 2016, **16**, 1456–1476.
- 12 M. U. Shahid, T. Najam, M. H. Helal, I. Hossain, S. M. El-Bahy, Z. M. El-Bahy, A. ur Rehman, S. S. A. Shah and M. A. Nazir, *Int. J. Hydrogen Energy*, 2024, **62**, 1113–1138.
- 13 T. Wu, X. Liu, Y. Liu, M. Cheng, Z. Liu, G. Zeng, B. Shao, Q. Liang, W. Zhang, Q. He and W. Zhang, *Coord. Chem. Rev.*, 2020, **403**, 213097.
- 14 N. C. Burtch, J. Heinen, T. D. Bennett, D. Dubbeldam and M. D. Allendorf, *Adv. Mater.*, 2018, **30**, 1704124.
- 15 D. Senthil Raja and D.-H. Tsai, *Chem. Commun.*, 2024, **60**, 8497–8515.
- 16 C. Lamiel, I. Hussain, H. Rabiee, O. R. Ogunsakin and K. Zhang, *Coord. Chem. Rev.*, 2023, **480**, 215030.
- 17 L. Zhang and Y. Hou, *Adv. Energy Mater.*, 2023, **13**, 2204378.
- 18 A. Mukherjee, J. A. Okolie, A. Abdelrasoul, C. Niu and A. K. Dalai, *J. Environ. Sci.*, 2019, **83**, 46–63.
- 19 S. Ghosh, *Metal-Organic Frameworks (MOFs) for Environmental Applications*, 2019.
- 20 S. Horike, S. Shimomura and S. Kitagawa, *Nat. Chem.*, 2009, **1**, 695–704.
- 21 T. Ghanbari, F. Abnisa and W. M. A. Wan Daud, *Sci. Total Environ.*, 2020, **707**, 135090.
- 22 Y. Zhao, Z. Song, X. Li, Q. Sun, N. Cheng, S. Lawes and X. Sun, *Energy Storage Mater.*, 2016, **2**, 35–62.
- 23 Y. Li, H. Xu, S. Ouyang and J. Ye, *Phys. Chem. Chem. Phys.*, 2016, **18**, 7563–7572.
- 24 H. Furukawa, K. E. Cordova, M. O'Keeffe and O. M. Yaghi, *Science*, 2013, **341**(6149), 1230444.
- 25 F. Vega, M. Cano, S. Camino, L. M. G. Fernández, E. Portillo and B. Navarrete, *Carbon Dioxide Chemistry, Capture and Oil Recovery*, DOI: **10.5772/INTECHOPEN.71443**.
- 26 M. Bui, C. S. Adjiman, A. Bardow, E. J. Anthony, A. Boston, S. Brown, P. S. Fennell, S. Fuss, A. Galindo, L. A. Hackett, J. P. Hallett, H. J. Herzog, G. Jackson, J. Kemper, S. Krevor, G. C. Maitland, M. Matuszewski, I. S. Metcalfe, C. Petit, G. Puxty, J. Reimer, D. M. Reiner, E. S. Rubin, S. A. Scott, N. Shah, B. Smit, J. P. M. Trusler, P. Webley, J. Wilcox and N. Mac Dowell, *Energy Environ. Sci.*, 2018, **11**, 1062–1176.
- 27 A. I. Osman, M. Hefny, M. I. A. Abdel Maksoud, A. M. Elgarahy and D. W. Rooney, *Environ. Chem. Lett.*, 2021, **19**, 797–849.
- 28 X. Li, X. Zhou, J. Wei, Y. Fan, L. Liao and H. Wang, *Sep. Purif. Technol.*, 2021, **265**, 118481.
- 29 J. J. Vericella, S. E. Baker, J. K. Stolaroff, E. B. Duoss, J. O. Hardin, J. Lewicki, E. Glogowski, W. C. Floyd, C. A. Valdez, W. L. Smith, J. H. Satcher, W. L. Bourcier, C. M. Spadaccini, J. A. Lewis and R. D. Aines, *Nat. Commun.*, 2015, **6**, 6124.
- 30 M. Stec, A. Tatarczuk, L. Więcław-Solny, A. Krótki, T. Spietz, A. Wilk and D. Śpiewak, *Clean Technol. Environ. Policy*, 2016, **18**, 151–160.
- 31 C. A. Grande, R. Blom, A. Spjelkavik, V. Moreau and J. Payet, *Sustainable Mater. Technol.*, 2017, **14**, 11–18.
- 32 Z. Zhang, Z.-Z. Yao, S. Xiang and B. Chen, *Energy Environ. Sci.*, 2014, **7**, 2868.
- 33 N. Williams and R. Custelcean, *Carbon Capture*, 2019, **68**, 4–6.
- 34 Energy technologies Institute, *Reducing the Cost of CCS Developments in Capture Plant Technology*, 2016.
- 35 S. Budinis, S. Krevor, N. Mac Dowell, N. Brandon and A. Hawkes, *Energy Strategy Rev.*, 2018, **22**, 61–81.
- 36 A. Andersen, S. Divekar, S. Dasgupta, J. H. Cavka, A. Aarti, A. Nanoti, A. Spjelkavik, A. N. Goswami, M. O. Garg and R. Blom, *Energy Procedia*, 2013, **37**, 33–39.
- 37 B. L. Huang, Z. Ni, A. Millward, A. J. H. McGaughey, C. Uher, M. Kaviani and O. Yaghi, *Int. J. Heat Mass Transf.*, 2007, **50**, 405–411.
- 38 N. Iqbal, X. Wang, J. Yu and B. Ding, *Adv. Sustainable Syst.*, 2017, **1**, 1600028.
- 39 Y. Lin, C. Kong, Q. Zhang and L. Chen, *Adv. Energy Mater.*, 2017, **7**, 1601296.
- 40 H. R. Khan, Z. Jahan, M. B. Khan Niazi, T. Noor, H. Hou and S. Rafiq, *Carbon Capture Sci. Technol.*, 2022, **3**, 100048.
- 41 P. M. Bhatt, Y. Belmabkhout, A. Cadiou, K. Adil, O. Shekhah, A. Shkurenko, L. J. Barbour and M. Eddaoudi, *J. Am. Chem. Soc.*, 2016, **138**, 9301–9307.
- 42 L. Hu, W. Wu, L. Jiang, M. Hu, H. Zhu, L. Gong, J. Yang, D. Lin and K. Yang, *ACS Appl. Mater. Interfaces*, 2023, **15**, 43925–43932.
- 43 G. Greene-Diniz, D. Z. Manrique, W. Sennane, Y. Magnin, E. Shishenina, P. Cordier, P. Llewellyn, M. Krompiec,



M. J. Rančić and D. Muñoz Ramo, *EPJ Quantum Technol.*, 2022, **9**, 37.

44 T. Zurrer, K. Wong, J. Horlyck, E. C. Lovell, J. Wright, N. M. Bedford, Z. Han, K. Liang, J. Scott and R. Amal, *Adv. Funct. Mater.*, 2021, **31**(9), 2007624.

45 A. S. Palakkal and R. S. Pillai, *Sep. Purif. Technol.*, 2022, **295**, 121298.

46 L. Lei, Y. Cheng, C. Chen, M. Kosari, Z. Jiang and C. He, *J. Colloid Interface Sci.*, 2022, **612**, 132–145.

47 H. An, W. Tian, X. Lu, H. Yuan, L. Yang, H. Zhang, H. Shen and H. Bai, *Chem. Eng. J.*, 2023, **469**, 144052.

48 T.-H. Bae, M. R. Hudson, J. A. Mason, W. L. Queen, J. J. Dutton, K. Sumida, K. J. Micklash, S. S. Kaye, C. M. Brown and J. R. Long, *Energy Environ. Sci.*, 2013, **6**, 128–138.

49 D. Bahamon and L. F. Vega, *Chem. Eng. J.*, 2016, **284**, 438–447.

50 H. Li, K. Wang, Y. Sun, C. T. Lollar, J. Li and H.-C. Zhou, *Mater. Today*, 2018, **21**, 108–121.

51 Y. He, W. Zhou, G. Qian and B. Chen, *Chem. Soc. Rev.*, 2014, **43**, 5657–5678.

52 E. J. Kim, R. L. Siegelman, H. Z. H. Jiang, A. C. Forse, J.-H. Lee, J. D. Martell, P. J. Milner, J. M. Falkowski, J. B. Neaton, J. A. Reimer, S. C. Weston and J. R. Long, *Science*, 2020, **369**, 392–396.

53 T. M. McDonald, J. A. Mason, X. Kong, E. D. Bloch, D. Gygi, A. Dani, V. Crocellà, F. Giordanino, S. O. Odoh, W. S. Drisdell, B. Vlaisavljevich, A. L. Dzubak, R. Poloni, S. K. Schnell, N. Planas, K. Lee, T. Pascal, L. F. Wan, D. Prendergast, J. B. Neaton, B. Smit, J. B. Kortright, L. Gagliardi, S. Bordiga, J. A. Reimer and J. R. Long, *Nature*, 2015, **519**, 303–308.

54 Y. Huang, W. Qin, Z. Li and Y. Li, *Dalton Trans.*, 2012, **41**, 9283.

55 T. M. McDonald, W. R. Lee, J. A. Mason, B. M. Wiers, C. S. Hong and J. R. Long, *J. Am. Chem. Soc.*, 2012, **134**, 7056–7065.

56 P.-Q. Liao, X.-W. Chen, S.-Y. Liu, X.-Y. Li, Y.-T. Xu, M. Tang, Z. Rui, H. Ji, J.-P. Zhang and X.-M. Chen, *Chem. Sci.*, 2016, **7**, 6528–6533.

57 D. Saha, Z. Bao, F. Jia and S. Deng, *Environ. Sci. Technol.*, 2010, **44**, 1820–1826.

58 M. Mazaj, N. Z. Logar, E. Žagar and S. Kovačić, *J. Mater. Chem. A*, 2017, **5**, 1967–1971.

59 J. Liu, Y. Wang, A. I. Benin, P. Jakubczak, R. R. Willis and M. D. LeVan, *Langmuir*, 2010, **26**, 14301–14307.

60 G. W. Peterson, J. B. DeCoste, T. G. Glover, Y. Huang, H. Jasuja and K. S. Walton, *Microporous Mesoporous Mater.*, 2013, **179**, 48–53.

61 T. Asadi, M. R. Ehsani, A. M. Ribeiro, J. M. Loureiro and A. E. Rodrigues, *Chem. Eng. Technol.*, 2013, **36**, 1231–1239.

62 Z. Hu, Y. Wang, B. B. Shah and D. Zhao, *Adv. Sustainable Syst.*, 2019, **3**(1), 1800080.

63 P. J. Milner, R. L. Siegelman, A. C. Forse, M. I. Gonzalez, T. Runčevski, J. D. Martell, J. A. Reimer and J. R. Long, *J. Am. Chem. Soc.*, 2017, **139**, 13541–13553.

64 V. H. Dalvi and P. J. Rossky, *Proc. Natl. Acad. Sci. U. S. A.*, 2010, **107**, 13603–13607.

65 A. H. Valekar, K.-H. Cho, U.-H. Lee, J. S. Lee, J. W. Yoon, Y. K. Hwang, S. G. Lee, S. J. Cho and J.-S. Chang, *RSC Adv.*, 2017, **7**, 55767–55777.

66 R. Das, D. Muthukumar, R. S. Pillai and C. M. Nagaraja, *Chem.-A Euro. J.*, 2020, **26**, 17445–17454.

67 J. Yan, Y. Sun, T. Ji, Y. Liu, N. Zhang, B. Sun, S. Meng, B. H. Yin, M. Wu, H. Hu and Y. Liu, *Ind. Eng. Chem. Res.*, 2023, **62**, 5973–5983.

68 M. R. Abdul Hamid, Y. Qian, R. Wei, Z. Li, Y. Pan, Z. Lai and H.-K. Jeong, *J. Membr. Sci.*, 2021, **640**, 119802.

69 F. Yang, T. Ge, X. Zhu, J. Wu and R. Wang, *Sep. Purif. Technol.*, 2022, **287**, 120535.

70 J. M. Park, D. K. Yoo and S. H. Jhung, *Chem. Eng. J.*, 2020, **402**, 126254.

71 Y. Liu, Z. Ng, E. A. Khan, H.-K. Jeong, C. Ching and Z. Lai, *Microporous Mesoporous Mater.*, 2009, **118**, 296–301.

72 C. R. Groom, I. J. Bruno, M. P. Lightfoot and S. C. Ward, *Acta Crystallogr., Sect. B: Struct. Sci., Cryst. Eng. Mater.*, 2016, **72**, 171–179.

73 S. Huang, X.-R. Shi, C. Sun, Z. Duan, P. Ma and S. Xu, *Nanomaterials*, 2020, **10**, 2268.

74 S. Sundriyal, H. Kaur, S. K. Bhardwaj, S. Mishra, K.-H. Kim and A. Deep, *Coord. Chem. Rev.*, 2018, **369**, 15–38.

75 P. Forouzandeh, V. Kumaravel and S. C. Pillai, *Catalysts*, 2020, **10**, 969.

76 A. C. Forse, C. Merlet, J. M. Griffin and C. P. Grey, *J. Am. Chem. Soc.*, 2016, **138**, 5731–5744.

77 Y. Wu and C. Cao, *Sci. China Mater.*, 2018, **61**, 1517–1526.

78 S. Kumar, G. Saeed, L. Zhu, K. N. Hui, N. H. Kim and J. H. Lee, *Chem. Eng. J.*, 2021, **403**, 126352.

79 J. Phiri, J. Dou, T. Vuorinen, P. A. C. Gane and T. C. Maloney, *ACS Omega*, 2019, **4**, 18108–18117.

80 L. Weinstein and R. Dash, *Mater. Today*, 2013, **16**, 356–357.

81 P. Pongprayoon and A. Chaimanatsakun, *Acta Mech. Solida Sin.*, 2019, **32**, 81–92.

82 A. Gitipour, A. El Badawy, M. Arambewela, B. Miller, K. Scheckel, M. Elk, H. Ryu, V. Gomez-Alvarez, J. Santo Domingo, S. Thiel and T. Tolaymat, *Environ. Sci. Technol.*, 2013, **47**, 14385–14393.

83 L. Li, X. Wang, S. Wang, Z. Cao, Z. Wu, H. Wang, Y. Gao and J. Liu, *Electroanalysis*, 2016, **28**, 243–248.

84 M. Cossutta, V. Vretenar, T. A. Centeno, P. Kotrusz, J. McKechnie and S. J. Pickering, *J. Cleaner Prod.*, 2020, **242**, 118468.

85 K. M. Ajay and M. N. Dinesh, *IOP Conf. Ser.: Mater. Sci. Eng.*, 2018, **310**, 012083.

86 M. Karnan, A. G. K. Raj, K. Subramani, S. Santhoshkumar and M. Sathish, *Sustainable Energy Fuels*, 2020, **4**, 3029–3041.

87 S. Breitenbach, A. Lumetzberger, M. A. Hobisch, C. Unterweger, S. Spirk, D. Stifter, C. Fürst and A. W. Hassel, *C*, 2020, **6**, 17.

88 A. Arenillas, J. A. Menéndez, G. Reichenauer, A. Celzard, V. Fierro, F. J. Maldonado Hodar, E. Bailón-García and N. Job, *Org. Carbon Gels Lab. Synth. Appl.*, 2019, 1–26.



89 Z. S. Iro, C. Subramani and S. S. Dash, *Int. J. Electrochem. Sci.*, 2016, **11**, 10628–10643.

90 I. I. G. Inal, S. M. Holmes, E. Yagmur, N. Ermumcu, A. Banford and Z. Aktas, *J. Ind. Eng. Chem.*, 2018, **61**, 124–132.

91 J. Chen, J. Xie, C. Q. Jia, C. Song, J. Hu and H. Li, *Chem. Eng. J.*, 2022, **450**, 137938.

92 X. Li, Y. Tang, J. Song, W. Yang, M. Wang, C. Zhu, W. Zhao, J. Zheng and Y. Lin, *Carbon*, 2018, **129**, 236–244.

93 F. Ma, S. Ding, H. Ren and Y. Liu, *RSC Adv.*, 2019, **9**, 2474–2483.

94 R. Mehdi, S. R. Naqvi, A. H. Khoja and R. Hussain, *Fuel*, 2023, **348**, 128529.

95 S. Bhat, U. T. Uthappa, T. Sadhasivam, T. Altalhi, S. Soo Han and M. D. Kurkuri, *Chem. Eng. J.*, 2023, **459**, 141577.

96 Y.-P. Gao, Z.-B. Zhai, K.-J. Huang and Y.-Y. Zhang, *New J. Chem.*, 2017, **41**, 11456–11470.

97 G. Jiang and S. J. Pickering, *Waste Manage.*, 2016, **48**, 465–470.

98 Q. Ke and J. Wang, *J. Materomics*, 2016, **2**, 37–54.

99 V. Ntuli and I. Hapazari, *S. Afr. J. Sci.*, 2013, **109**(1), 1–6.

100 E. Glogic, A. K. Kamali, N. M. Keppetipola, B. Alonge, G. R. A. Kumara, G. Sonnemann, T. Toupanee and L. Cojocaru, *ACS Sustain. Chem. Eng.*, 2022, **10**, 15025–15034.

101 Z. Jiang, Y. Zou, Y. Li, F. Kong and D. Yang, *Biochar*, 2021, **3**, 701–714.

102 V. Ruiz, C. Blanco, M. Granda and R. Santamaría, *Electrochim. Acta*, 2008, **54**, 305–310.

103 C. Li, W. Wu, P. Wang, W. Zhou, J. Wang, Y. Chen, L. Fu, Y. Zhu, Y. Wu and W. Huang, *Advanced Science*, 2019, **6**, 1801665.

104 D. Dong and Y. Xiao, *Chem. Eng. J.*, 2023, 144441.

105 L. M. Grishchenko, G. G. Tsaplyuk, M. Ricco, V. E. Diyuk, O. Y. Boldyrieva, R. Mariychuk, I. P. Matushko, D. Pontiroli, V. V. Lisnyak and S. Scaravonati, in *2020 IEEE 40th International Conference on Electronics and Nanotechnology (ELNANO)*, IEEE, 2020, pp. 173–177.

106 F. Cheng, X. Yang, S. Zhang and W. Lu, *J. Power Sources*, 2020, **450**, 227678.

107 L.-H. Tseng, W.-C. Li and T.-C. Wen, *J. Taiwan Inst. Chem. Eng.*, 2023, **143**, 104684.

108 G. Dhakal, D. R. Kumar, S. Sahoo and J.-J. Shim, *Carbon*, 2023, **208**, 277–289.

109 I. Bordun, V. Pohrebnyk, M. Sadowsa, V. Ptashnyk, A. Klos-Witkowska and V. Martsenyuk, in *2017 9th IEEE International Conference on Intelligent Data Acquisition and Advanced Computing Systems: Technology and Applications (IDAACS)*, IEEE, 2017, pp. 86–90.

110 F. R. Maria Sundar Raj, N. V. Jaya, G. Boopathi, D. Kalpana and A. Pandurangan, *Mater. Chem. Phys.*, 2020, **240**, 122151.

111 I. I. G. Inal, Y. Gokce and Z. Aktas, in *2016 IEEE International Conference on Renewable Energy Research and Applications (ICRERA)*, IEEE, 2016, pp. 458–462.

112 M. A. Yahya, Z. Al-Qodah and C. W. Z. Ngah, *Renewable Sustainable Energy Rev.*, 2015, **46**, 218–235.

113 A. M. Al-Enizi, M. Ubaidullah, J. Ahmed, T. Ahamad, T. Ahmad, S. F. Shaikh and Mu. Naushad, *Composites, Part B*, 2020, **183**, 107655.

114 M. K. Sahoo, P. Mane, B. Chakraborty and J. N. Behera, *Inorg. Chem.*, 2024, **63**, 6383–6395.

115 B. Ramasubramanian, C. Chinglenthoba, X. Huiqing, N. Xiping, H. K. Hui, S. Valiyaveetil, S. Ramakrishna and V. Chellappan, *Surf. Interfaces*, 2022, **34**, 102397.

116 S. Xiong, S. Jiang, J. Wang, H. Lin, M. Lin, S. Weng, S. Liu, Y. Jiao, Y. Xu and J. Chen, *Electrochim. Acta*, 2020, **340**, 135956.

117 M. Shaheen, M. Z. Iqbal, M. W. Khan, S. Siddique, S. Aftab and S. M. Wabaidur, *Energy Fuels*, 2023, **37**, 4000–4009.

118 F. Yi, R. Zhang, H. Wang, L. Chen, L. Han, H. Jiang and Q. Xu, *Small Methods*, 2017, **1**(11), 1700187.

119 M. Gu, M. Wu, S.-C. Wang, C. Chen, D. Xiong and F.-Y. Yi, *Electrochim. Acta*, 2020, **343**, 135617.

120 N. Campagnol, R. Romero-Vara, W. Deleu, L. Stappers, K. Binnemans, D. E. De Vos and J. Fransaer, *ChemElectroChem*, 2014, **1**, 1182–1188.

121 L. Wang, Y. Han, X. Feng, J. Zhou, P. Qi and B. Wang, *Coord. Chem. Rev.*, 2016, **307**, 361–381.

122 R. Ramachandran, W. Xuan, C. Zhao, X. Leng, D. Sun, D. Luo and F. Wang, *RSC Adv.*, 2018, **8**, 3462–3469.

123 D. Y. Lee, S. J. Yoon, N. K. Shrestha, S.-H. Lee, H. Ahn and S.-H. Han, *Microporous Mesoporous Mater.*, 2012, **153**, 163–165.

124 Y. Tan, W. Zhang, Y. Gao, J. Wu and B. Tang, *RSC Adv.*, 2015, **5**, 17601–17605.

125 P. Kumar, B. Anand, Y. F. Tsang, K.-H. Kim, S. Khullar and B. Wang, *Environ. Res.*, 2019, **176**, 108488.

126 Y. Yan, P. Gu, S. Zheng, M. Zheng, H. Pang and H. Xue, *J. Mater. Chem. A*, 2016, **4**, 19078–19085.

127 J. Yang, P. Xiong, C. Zheng, H. Qiu and M. Wei, *J. Mater. Chem. A*, 2014, **2**, 16640–16644.

128 M. S. Rahmanifar, H. Hesari, A. Noori, M. Y. Masoomi, A. Morsali and M. F. Mousavi, *Electrochim. Acta*, 2018, **275**, 76–86.

129 G. Li, H. Cai, X. Li, J. Zhang, D. Zhang, Y. Yang and J. Xiong, *ACS Appl. Mater. Interfaces*, 2019, **11**, 37675–37684.

130 Q. Yang, R. Song, Y. Wang, X. Hu, Z. Chen, Z. Li and W. Tan, *Colloids Surf., A*, 2021, **631**, 127665.

131 R. Sahoo, S. Ghosh, S. Chand, S. Chand Pal, T. Kuila and M. C. Das, *Composites, Part B*, 2022, **245**, 110174.

132 Y.-L. Chang, M.-D. Tsai, C.-H. Shen, C.-W. Huang, Y.-C. Wang and C.-W. Kung, *Mater. Today Sustain.*, 2023, **23**, 100449.

133 S. C. Wechsler and F. Z. Amir, *ChemSusChem*, 2020, **13**, 1491–1495.

134 H. S. Kim, M. S. Kang and W. C. Yoo, *J. Mater. Chem. A*, 2019, **7**, 5561–5574.

135 K. M. Choi, H. M. Jeong, J. H. Park, Y.-B. Zhang, J. K. Kang and O. M. Yaghi, *ACS Nano*, 2014, **8**, 7451–7457.

136 D. Sheberla, L. Sun, M. A. Blood-Forsythe, S. Er, C. R. Wade, C. K. Brozek, A. Aspuru-Guzik and M. Dincă, *J. Am. Chem. Soc.*, 2014, **136**, 8859–8862.



137 M. G. Campbell, D. Sheberla, S. F. Liu, T. M. Swager and M. Dincă, *Angew. Chem., Int. Ed.*, 2015, **54**, 4349–4352.

138 D. Feng, W. Sun and W. Hu, *Opt. Switch. Netw.*, 2018, **29**, 1–14.

139 M. Sajid, *Environ. Sci. Pollut. Res.*, 2016, **23**, 14805–14807.

140 K. M. Choi, H. M. Jeong, J. H. Park, Y.-B. Zhang, J. K. Kang and O. M. Yaghi, *ACS Nano*, 2014, **8**, 7451–7457.

141 T. N. Tu, M. V. Nguyen, H. L. Nguyen, B. Yuliarto, K. E. Cordova and S. Demir, *Coord. Chem. Rev.*, 2018, **364**, 33–50.

142 H. Luo, F. Cheng, L. Huelsenbeck and N. Smith, *J. Environ. Chem. Eng.*, 2021, **9**, 105159.

143 M. Mon, R. Bruno, J. Ferrando-Soria, D. Armentano and E. Pardo, *J. Mater. Chem. A*, 2018, **6**, 4912–4947.

144 Y. Zhao, J. Peng, K. Chen, L. Luo, H. Chen, H. Zhang, S. Chou, X. Feng, W. Chen and R. Cao, *Sci. China: Chem.*, 2023, **66**, 3154–3160.

145 Y. Fang, Y. Zeng, Q. Jin, X. F. Lu, D. Luan, X. Zhang and X. W. Lou, *Angew. Chem., Int. Ed.*, 2021, **60**, 8515–8520.

146 J. Du, J. Chai, Q. Li, W. Zhang and B. Tang, *Colloids Surf., A*, 2022, **632**, 127810.

147 J.-G. Zhao, H.-Y. Zhou, Z. Hu, Y.-W. Wu, H. Jia and X.-M. Liu, *Rare Met.*, 2022, **41**, 1504–1511.

148 Y. Fang, D. Luan, Y. Chen, S. Gao and X. W. Lou, *Angew. Chem., Int. Ed.*, 2020, **59**, 2644–2648.

149 S. Bibi, S. S. A. Shah, M. A. Nazir, M. H. Helal, S. M. El-Bahy, Z. M. El-Bahy, S. Ullah, M. A. Wattoo and A. ur Rehman, *Adv. Sustainable Syst.*, 2024, 2400011.

150 X.-Y. Dao, J.-H. Guo, Y.-P. Wei, F. Guo, Y. Liu and W.-Y. Sun, *Inorg. Chem.*, 2019, **58**, 8517–8524.

151 Y. Wang, Y. Pan, L. Zhu, H. Yu, B. Duan, R. Wang, Z. Zhang and S. Qiu, *Carbon*, 2019, **146**, 671–679.

152 K.-S. Lin, A. K. Adhikari, C.-N. Ku, C.-L. Chiang and H. Kuo, *Int. J. Hydrogen Energy*, 2012, **37**, 13865–13871.

153 M. Y. Zorainy, M. G. Alalm, S. Kaliaguine and D. C. Boffito, *J. Mater. Chem. A*, 2021, **9**, 22159–22217.

154 Q. Zhao, W. Yuan, J. Liang and J. Li, *Int. J. Hydrogen Energy*, 2013, **38**, 13104–13109.

155 Z. Yin, Y.-L. Zhou, M.-H. Zeng and M. Kurmoo, *Dalton Trans.*, 2015, **44**, 5258–5275.

156 T.-H. Chen, I. Popov, W. Kaveevivitchai and O. Š. Miljanić, *Chem. Mater.*, 2014, **26**, 4322–4325.

157 K.-S. Lin, A. K. Adhikari, C.-N. Ku, C.-L. Chiang and H. Kuo, *Int. J. Hydrogen Energy*, 2012, **37**, 13865–13871.

158 Z. Mai and D. Liu, *Cryst. Growth Des.*, 2019, **19**, 7439–7462.

159 M. A. Mohamud and A. B. Yurtcan, *Int. J. Hydrogen Energy*, 2021, **46**, 33782–33800.

160 S. Bibi, S. S. A. Shah, M. A. Nazir, M. H. Helal, S. M. El-Bahy, Z. M. El-Bahy, S. Ullah, M. A. Wattoo and A. ur Rehman, *Adv. Sustainable Syst.*, 2024, 2400011.

161 Z. Hu, Y. Peng, Z. Kang, Y. Qian and D. Zhao, *Inorg. Chem.*, 2015, **54**, 4862–4868.

162 E. M. C. Morales, M. A. Méndez-Rojas, L. M. Torres-Martínez, L. F. Garay-Rodríguez, I. López, I. E. Uflyand and B. I. Kharisov, *Polyhedron*, 2021, **210**, 115517.

163 S. Bibi, S. S. A. Shah, M. A. Nazir, M. H. Helal, S. M. El-Bahy, Z. M. El-Bahy, S. Ullah, M. A. Wattoo and A. ur Rehman, *Adv. Sustainable Syst.*, 2024, 2400011.

164 A. Al Obeidli, H. Ben Salah, M. Al Murisi and R. Sabouni, *Int. J. Hydrogen Energy*, 2022, **47**, 2561–2593.

165 M. Safaei, M. M. Foroughi, N. Ebrahimpoor, S. Jahani, A. Omidi and M. Khatami, *TrAC, Trends Anal. Chem.*, 2019, **118**, 401–425.

166 A. Fujishima and K. Honda, *Nature*, 1972, **238**, 37–38.

167 A. B. Djurišić, Y. He and A. M. C. Ng, *APL Mater.*, 2020, **8**(3), DOI: [10.1063/1.5140497](https://doi.org/10.1063/1.5140497).

168 S. R. Shanmugham, G. B. Jegadeesan and V. Ponnusami, in *Nanotechnology in the Beverage Industry*, Elsevier, 2020, pp. 25–49.

169 A. Dhakshinamoorthy, Z. Li and H. Garcia, *Chem. Soc. Rev.*, 2018, **47**, 8134–8172.

170 M. Pawar, S. Topcu Sendoğdular and P. Gouma, *J. Nanomater.*, 2018, **2018**, 1–13.

171 S. Peiris, H. B. de Silva, K. N. Ranasinghe, S. V. Bandara and I. R. Perera, *J. Chin. Chem. Soc.*, 2021, **68**, 738–769.

172 Z. Li, S. Wang, J. Wu and W. Zhou, *Renewable Sustainable Energy Rev.*, 2022, **156**, 111980.

173 F. Li, G. Liu, F. Liu, J. Wu and S. Yang, *J. Hazard. Mater.*, 2023, **452**, 131237.

174 Y. Jin, W. Tang, J. Wang, F. Ren, Z. Chen, Z. Sun and P.-G. Ren, *J. Alloys Compd.*, 2023, **932**, 167627.

175 A. Meng, L. Zhang, B. Cheng and J. Yu, *Adv. Mater.*, 2019, **31**(30), 1807660.

176 S.-Y. Lee and S.-J. Park, *J. Ind. Eng. Chem.*, 2013, **19**, 1761–1769.

177 S.-N. Zhao, G. Wang, D. Poelman and P. Van Der Voort, *Molecules*, 2018, **23**, 2947.

178 J. Moma and J. Baloyi, *Photocatalysts-Applications and Attributes*, 2019, vol. 18, DOI: [10.5772/intechopen.75848](https://doi.org/10.5772/intechopen.75848).

179 S. Higashimoto, *Catalysts*, 2019, **9**, 201.

180 S. Higashimoto, *Catalysts*, 2019, **9**, 201.

181 X. Chen, S. Shen, L. Guo and S. S. Mao, *Chem. Rev.*, 2010, **110**, 6503–6570.

182 M. Skocaj, M. Filipic, J. Petkovic and S. Novak, *Radiol. Oncol.*, 2011, **45**(4), 227–247.

183 F. Wu, Z. Zhou and A. L. Hicks, *Environ. Sci. Technol.*, 2019, **53**, 4078–4087.

184 A.-I. Gopalan, J.-C. Lee, G. Saianand, K.-P. Lee, W.-Y. Chun, Y. Hou, V. Kannan, S.-S. Park and W.-J. Kim, *Materials*, 2020, **13**, 5072.

185 T. Sansenya, N. Masri, T. Chankhanitha, T. Senasu, J. Piriyanon, S. Mukdasai and S. Nanan, *J. Phys. Chem. Solids*, 2022, **160**, 110353.

186 T. Chankhanitha, N. Komchoo, T. Senasu, J. Piriyanon, S. Youngme, K. Hemavibool and S. Nanan, *Colloids Surf., A*, 2021, **626**, 127034.

187 D. Kim and K. Yong, *Appl. Catal., B*, 2021, **282**, 119538.

188 Z. Li, R. Li, H. Jing, J. Xiao, H. Xie, F. Hong, N. Ta, X. Zhang, J. Zhu and C. Li, *Nat. Catal.*, 2023, **6**, 80–88.

189 N. A. F. Al-Rawashdeh, O. Allabadi and M. T. Aljarrah, *ACS Omega*, 2020, **5**, 28046–28055.



190 K. Chaudhary, M. Aadil, S. Zulfiqar, S. Ullah, S. Haider, P. O. Agboola, M. F. Warsi and I. Shakir, *Fullerenes, Nanotubes Carbon Nanostruct.*, 2021, **29**, 915–928.

191 A. Alshammari, Z. Jiang and K. E. Cordova, in *Semiconductor Photocatalysis – Materials, Mechanisms and Applications*, InTech, 2016.

192 V. García-Salcido, P. Mercado-Oliva, J. L. Guzmán-Mar, B. I. Kharisov and L. Hinojosa-Reyes, *J. Solid State Chem.*, 2022, **307**, 122801.

193 Y. Gao, X.-H. Yi, C.-C. Wang, F. Wang and P. Wang, *Mater. Res. Bull.*, 2023, **158**, 112072.

194 C. Jing, Y. Zhang, J. Zheng, S. Ge, J. Lin, D. Pan, N. Naik and Z. Guo, *Particuology*, 2022, **69**, 111–122.

195 H. Sephrmansourie, H. Alamgholiloo, N. Noroozi Pesyan and M. A. Zolfigol, *Appl. Catal., B*, 2023, **321**, 122082.

196 L. Wang, P. Jin, S. Duan, H. She, J. Huang and Q. Wang, *Sci. Bull.*, 2019, **64**, 926–933.

197 M. Xu, C. Sun, X. Zhao, H. Jiang, H. Wang and P. Huo, *Appl. Surf. Sci.*, 2022, **576**, 151792.

198 F. Drache, V. Bon, I. Senkovska, C. Marschelke, A. Synytska and S. Kaskel, *Inorg. Chem.*, 2016, **55**, 7206–7213.

199 A. J. Howarth, Y. Liu, P. Li, Z. Li, T. C. Wang, J. T. Hupp and O. K. Farha, *Nat. Rev. Mater.*, 2016, **1**, 15018.

200 G. Paille, M. Gomez-Mingot, C. Roch-Marchal, B. Lassalle-Kaiser, P. Mialane, M. Fontecave, C. Mellot-Draznieks and A. Dolbecq, *J. Am. Chem. Soc.*, 2018, **140**, 3613–3618.

201 S. S. A. Shah, M. A. Nazir, K. Khan, I. Hussain, M. Tayyab, S. S. Alarfaji, A. M. Hassan, M. Sohail, M. S. Javed and T. Najam, *J. Energy Storage*, 2024, **75**, 109725.

202 D. Crawford, J. Casaban, R. Haydon, N. Giri, T. McNally and S. L. James, *Chem. Sci.*, 2015, **6**, 1645–1649.

203 J. C. Glier and E. S. Rubin, *Energy Procedia*, 2013, **37**, 65–72.

204 M. Karnan, A. G. K. Raj, K. Subramani, S. Santhoshkumar and M. Sathish, *Sustainable Energy Fuels*, 2020, **4**, 3029–3041.

205 S.-N. Zhao, G. Wang, D. Poelman and P. Van Der Voort, *Molecules*, 2018, **23**, 2947.

206 J. Moma and J. Baloyi, in *Photocatalysts – Applications and Attributes*, IntechOpen, 2019.

207 R. Asahi, T. Morikawa, T. Ohwaki, K. Aoki and Y. Taga, *Science*, 2001, **293**, 269–271.

208 H. Demir, G. O. Aksu, H. C. Gulbalkan and S. Keskin, *Carbon Capture Sci. Technol.*, DOI: [10.1016/j.jcest.2021.100026](https://doi.org/10.1016/j.jcest.2021.100026).

209 S. Ali, P. M. Ismail, F. Wahid, A. Kumar, M. Haneef, F. Raziq, S. Ali, M. Javed, R. U. Khan and X. Wu, *Fuel Process. Technol.*, 2022, **236**, 107427.

210 S. Ali, P. M. Ismail, M. Humayun, M. Bououdina and L. Qiao, *Fuel Process. Technol.*, 2024, **255**, 108049.

211 M. Khan, Z. Akmal, M. Tayyab, S. Mansoor, A. Zeb, Z. Ye, J. Zhang, S. Wu and L. Wang, *Carbon Capture Sci. Technol.*, 2024, **11**, 100191.

212 P. Dubey, V. Shrivastav, P. H. Maheshwari, M. Hołdynski, A. Krawczyńska and S. Sundriyal, *J. Energy Storage*, 2023, **68**, 107828.

213 Y. Cao, W. Yang, M. Wang, N. Wu, L. Zhang, Q. Guan and H. Guo, *Int. J. Hydrogen Energy*, 2021, **46**, 18179–18206.

214 J. Khan, A. Khan, B. Rubab, F. Jamshaid, A. A. Al-Kahtani and A. Dahshan, *Appl. Mater. Today*, 2023, **34**, 101906.

215 C. Healy, K. M. Patil, B. H. Wilson, L. Hermanspahn, N. C. Harvey-Reid, B. I. Howard, C. Kleinjan, J. Kolien, F. Payet and S. G. Telfer, *Coord. Chem. Rev.*, 2020, **419**, 213388.

216 S. Bhattacharyya and T. K. Maji, *Coord. Chem. Rev.*, 2022, **469**, 214645.

217 Q. He, F. Zhan, H. Wang, W. Xu, H. Wang and L. Chen, *Mater. Today Sustain.*, 2022, **17**, 100104.

218 D. Chakraborty, A. Yurdusen, G. Mouchaham, F. Nouar and C. Serre, *Adv. Funct. Mater.*, 2023, 2309089.

219 D. Yang and B. C. Gates, *ACS Catal.*, 2019, **9**, 1779–1798.

220 W. Xue, C. D. Sewell, Q. Zhou and Z. Lin, *Angew. Chem., Int. Ed.*, 2022, **61**, e202206512.

221 R. Freund, O. Zaremba, G. Arnauts, R. Ameloot, G. Skorupskii, M. Dincă, A. Bavykina, J. Gascon, A. Ejsmont and J. Goscianska, *Angew. Chem., Int. Ed.*, 2021, **60**, 23975–24001.

222 A. Bavykina, N. Kolobov, I. S. Khan, J. A. Bau, A. Ramirez and J. Gascon, *Chem. Rev.*, 2020, **120**, 8468–8535.

223 P. Falcaro, R. Ricco, C. M. Doherty, K. Liang, A. J. Hill and M. J. Styles, *Chem. Soc. Rev.*, 2014, **43**, 5513–5560.

224 E.-S. M. El-Sayed and D. Yuan, *Green Chem.*, 2020, **22**, 4082–4104.

225 X. Song, Y. Wang, C. Wang, D. Wang, G. Zhuang, K. O. Kirlikovali, P. Li and O. K. Farha, *J. Am. Chem. Soc.*, 2022, **144**, 10663–10687.

